

## **Abstract**

The Qumushan (QMS) syn-collisional granodiorite, which is located in the eastern section of the North Qilian Orogen at the northern margin of the Greater Tibetan Plateau, has typical adakitic characteristics and also contains abundant mafic magmatic enclaves (MMEs). This recognition offers an unprecedented insight into the petrogenesis of both the adakitic host granodiorite and the enclosed MMEs. The MMEs and their host granodiorites share many characteristics in common, including identical crystallization age (~430 Ma), same mineralogy, similar mineral chemistry and whole-rock isotopic compositions, indicating their genetic link. The MMEs are most consistent with being of cumulate origin formed at earlier stages of the same magmatic system that produced the QMS adakitic granodiorite. Subsequent replenishment of adakitic magmas could have disturbed the cumulate piles as “MMEs” dispersed in the adakitic granodiorite host during emplacement. The geochemical data and petrogenetic modeling of trace elements suggest that the QMS adakitic host granodiorite is most consistent with fractional crystallization dominated by the mineral assemblage of the MMEs. The parental magma for the QMS granodiorite is best explained as resulting from partial melting of the ocean crust together with recycled terrigenous sediments during continental collision, which may have also experienced interaction with mantle peridotite during ascent.

Highlights:

1. The QMS adakitic granodiorites and their MMEs formed at ~430 Ma.
2. The MMEs are cumulate rocks formed at earlier stages of the same magmatic systems.
3. The QMS adakitic granodiorites resulted from fractional crystallization dominated by mineral assemblages represented by the MMEs.
4. The parental magma for the QMS granodiorite is best explained as resulting from partial melting of the ocean crust together with recycled terrigenous sediments during continental collision, which may have also experienced interaction with mantle peridotite during ascent.

1 **Syn-collisional adakitic granodiorites formed by fractional crystallization:**  
2 **insights from their enclosed mafic magmatic enclaves (MMEs) in the Qumushan**  
3 **pluton, North Qilian Orogen at the northern margin of the Tibetan Plateau**

4 Shuo Chen <sup>a,b\*</sup>, Yaoling Niu <sup>a,c\*</sup>, Jiyong Li <sup>a,b</sup>, Wenli Sun <sup>a</sup>, Yu Zhang <sup>d</sup>, Yan Hu <sup>a,b</sup>, Fengli Shao <sup>a,b</sup>

5

6 <sup>a</sup> Institute of Oceanology, Chinese Academy of Sciences, Qingdao 266071, China.

7 <sup>b</sup> University of Chinese Academy of Sciences, Beijing 100049, China

8 <sup>c</sup> Department of Earth Sciences, Durham University, Durham DH1 3LE, UK

9 <sup>d</sup> School of Earth Sciences, Lanzhou University, Lanzhou 730000, China

10

11

12

13

14

15 **\*Corresponding authors:**

16 **Mr. Shuo Chen (chenshuo528@foxmail.com)**

17 **Professor Yaoling Niu (yaoling.niu@foxmail.com)**

18

19

20

21

22

23 **Abstract**

24 The Qumushan (QMS) syn-collisional granodiorite, which is located in the eastern section of the  
25 North Qilian Orogen at the northern margin of the Greater Tibetan Plateau, has typical adakitic  
26 characteristics and also contains abundant mafic magmatic enclaves (MMEs). This recognition offers  
27 an unprecedented insight into the petrogenesis of both the adakitic host granodiorite and the enclosed  
28 MMEs. The MMEs and their host granodiorites share many characteristics in common, including  
29 identical crystallization age (~430 Ma), same mineralogy, similar mineral chemistry and whole-rock  
30 isotopic compositions, indicating their genetic link. The MMEs are most consistent with being of  
31 cumulate origin formed at earlier stages of the same magmatic system that produced the QMS adakitic  
32 granodiorite. Subsequent replenishment of adakitic magmas could have disturbed the cumulate piles as  
33 “MMEs” dispersed in the adakitic granodiorite host during emplacement. The geochemical data and  
34 petrogenetic modeling of trace elements suggest that the QMS adakitic host granodiorite is most  
35 consistent with fractional crystallization dominated by the mineral assemblage of the MMEs. The  
36 parental magma for the QMS granodiorite is best explained as resulting from partial melting of the  
37 ocean crust together with recycled terrigenous sediments during continental collision, which may have  
38 also experienced interaction with mantle peridotite during ascent.

39 **Keywords:** Adakitic rocks; Mafic magmatic enclaves; Cumulate; Syn-collisional granodiorite; North  
40 Qilian Orogen

## 41 1. Introduction

42 “Adakite” was introduced by Defant and Drummond (1990) after the name of Adak Island in the  
43 Aleutian arc. It refers to a group of intermediate-felsic igneous rocks observed in modern oceanic and  
44 continental arcs genetically associated with seafloor subduction. They are characterized by high Sr,  
45 light rare earth elements (REEs), Sr/Y (>40) and La/Yb (>20), low Y and heavy REEs, and lack of  
46 obvious Eu anomalies. It was initially considered that adakites were derived by partial melting of  
47 young ( $\leq 25$ Myrs) and warm subducting/subducted ocean crust in subduction zones (Defant and  
48 Drummond, 1990). The origin of adakite has since been one of the most popular subjects of research in  
49 igneous petrology due to its use for tectonic finger-printing (see Castillo, 2006, 2012), yet recent  
50 studies have shown that adakite or rocks with adakitic compositions can be produced in various ways  
51 and in different settings (Castillo et al., 1999; Xu et al., 2002; Chung et al., 2003, 2005; Wang et al.,  
52 2005, 2007; Macpherson et al., 2006; RodrIguuez et al., 2007; Streck et al., 2007; He et al., 2013; Chen  
53 et al., 2013a; Song et al., 2014a). Because adakite is defined on the basis of certain trace element  
54 characteristics as detailed above, geochemistry in combination with experimental geochemistry has  
55 been widely used to discuss the petrogenesis of adakites and adakitic rocks (e.g., Defant and  
56 Drummond, 1990; Sen and Dunn, 1994; Castillo et al., 1999; Xu et al., 2002; Wang et al., 2005; Xiong  
57 et al., 2005; Castillo, 2006, 2012). However, a petrological approach is essential for petrological  
58 problems and is expected to offer insights into the petrogenesis of adakites and adakitic rocks. Indeed,  
59 mafic magmatic enclaves (MMEs) hosted in adakitic rocks have been recently recognized, and the  
60 processes of the MME formation may offer a fresh perspective on the petrogenesis of the adakitic host  
61 (e.g., RodrIguuez et al., 2007; Chen et al., 2013b).

62 In this paper, we report our petrological, mineralogical and geochemical analyses and

63 trace-element modeling on an MME-bearing adakitic pluton well exposed in the eastern section of the  
64 North Qilian orogenic belt (NQOB) (Fig. 1a). This pluton was previously studied using the “standard”  
65 geochemical method with the MMEs being overlooked (e.g., Wang et al., 2006a; Tseng et al., 2009; Yu  
66 et al., 2015). Here we present a simple but effective model of fractional crystallization to successfully  
67 address both the origin of MMEs and their host adakitic granodiorite.

## 68 **2. Geological setting**

69 The NW-SE-trending NQOB is located between the Alashan Block to the northeast and the Qilian  
70 Block to the southwest, and is offset to the northwest by the Altyn-Tagh Fault (Fig.1a). It is made up of  
71 Early Paleozoic subduction-zone complexes including ophiolitic melanges, blueschists and eclogites,  
72 Silurian flysch formations, Devonian molasse, and Carboniferous to Triassic sedimentary cover  
73 sequences (Fig. 1a) (Song et al., 2007, 2013; Zhang et al., 2007). It is composed of three subunits, i.e.,  
74 (1) the southern ophiolite belt, (2) the middle arc magmatic belt and (3) the northern back-arc basin  
75 ophiolite-volcanic belt (Fig. 1a) (Song et al., 2007, 2013; Zhang et al., 2007; Chen et al., 2014). It is  
76 generally accepted that the NQOB is an Early Paleozoic suture zone, which records a long tectonic  
77 history from seafloor spreading/subduction to the ultimate continental collision and mountain-building  
78 (see Song et al., 2013). The Qumushan (QMS) pluton we studied is about 60km<sup>2</sup> in outcrop located in  
79 the eastern section of the NQOB. It lies approximately 10 km southeast of the Baojishan (BJS) pluton  
80 (Fig.1b). The QMS pluton intruded the Ordovician sedimentary and metamorphic rocks of Yingou  
81 group (Fig.1b). MMEs are widespread in the host granodiorite (Fig. 2a).

## 82 **3. Analytical methods**

### 83 *3.1. Zircon U–Pb ages*

84 Zircons were separated by using combined methods of heavy liquid and magnetic techniques  
85 before hand-picking under a binocular microscope. The selected zircons were set in an epoxy mount  
86 that was polished to expose zircon interiors. Cathodoluminescence (CL) images were taken at China  
87 University of Geosciences in Wuhan (CUGW) to examine the internal structure of individual zircon  
88 grains. The zircon U-Pb dating was done using LA-ICP-MS at China University of Geosciences in  
89 Beijing (CUGB). The instrument consists of an Agilent 7500a quadrupole inductively coupled plasma  
90 mass spectrometry (ICP-MS) coupled with a UP-193 Solid-State laser (193 nm, New Wave Research  
91 Inc.). Laser spot size was set to be ~30µm. Zircon 91500 (Wiedenbeck et al., 1995) and a secondary  
92 standard zircon TEMORA (417 Ma) (Black et al., 2003) was used as an external standard. The  
93 analytical procedure is given in Song et al. (2010a). Isotopic ratios and element concentrations of  
94 zircons were calculated using GLITTER (ver. 4.4, Macquarie University). Common Pb correction was  
95 applied using the method of Andersen (2002). Results are given in Appendix 1.

### 96 *3.2. Mineral compositions*

97 Mineral chemistry was determined using a JXA-8100 microprobe at Chang'an University, China.  
98 The operating conditions were a 15 kV accelerating potential with a probe current of 10 nA and the  
99 electron beam diameter of 1µm. Results are given in Appendix 2 and Appendix 3.

### 100 *3.3. Major and trace elements*

101 The bulk-rock major and trace elements were analyzed using Leeman Prodigy inductively coupled

102 plasma-optical emission spectroscopy (ICP-OES) and Agilent-7500a inductively coupled plasma mass  
103 spectrometry (ICP-MS) at CUGB, respectively. The analytical uncertainties are generally less than 1%  
104 for most major elements with the exception of  $\text{TiO}_2$  (~1.5%) and  $\text{P}_2\text{O}_5$  (~2.0%). The loss on ignition  
105 was measured by placing 1 g of sample powder in the furnace at 1000°C for several hours before  
106 cooling in a desiccator and reweighing. The analytical details are given in Song et al. (2010b). The  
107 data are presented in Appendix 4.

#### 108 *3.4. Whole-rock Sr-Nd-Hf isotopes*

109 Whole-rock Sr-Nd-Hf isotopic analyses were done in Guangzhou Institute of Geochemistry,  
110 Chinese Academy of Sciences (GIG-CAS). The rock powders were digested and dissolved in  
111 HF-HNO<sub>3</sub> acid mixtures and dried on a hot-plate. Sr-Nd-Hf fractions were separated using small Sr  
112 Spec resin columns to obtain Sr and Nd-Hf bearing fractions. Sr isotopic compositions were  
113 determined using a Neptune Plus multi-collector ICP-MS (MC-ICP-MS) following Ma et al. (2013a).  
114 Nd fractions were then separated by passing through cation columns followed by HDEHP columns.  
115 Separation of Hf from the matrix and rare earth elements was carried out using a combined method of  
116 Eichrom RE and HDEHP columns. Nd and Hf isotopic compositions were determined using a  
117 Micromass Isoprobe MC-ICP-MS following Li et al. (2009) and Ma et al. (2013b). Repeated analysis  
118 of NBS-987 run during the same period of sample analysis gave  $^{87}\text{Sr}/^{86}\text{Sr}=0.710283\pm 27$  ( $2\sigma$ ,  $n=13$ ).  
119 Repeated analysis of BHVO-2 and JB-3 during the same period of sample analysis yielded  $^{143}\text{Nd}/^{144}\text{Nd}$   
120  $0.512977\pm 14$  ( $2\sigma$ ,  $n=8$ ) and  $0.513053\pm 18$  ( $2\sigma$ ,  $n=13$ ), respectively. During the course of this study, the  
121 mean  $^{176}\text{Hf}/^{177}\text{Hf}$  ratios for BHVO-2 and JB-3 are respectively  $0.283099\pm 15$  ( $2\sigma$ ,  $n = 13$ ) and  $0.283216$   
122  $\pm 15$  ( $2\sigma$ ,  $n=6$ ). All measured  $^{87}\text{Sr}/^{86}\text{Sr}$ ,  $^{143}\text{Nd}/^{144}\text{Nd}$  and  $^{176}\text{Hf}/^{177}\text{Hf}$  ratios were normalized to  $^{86}\text{Sr}/^{88}\text{Sr}$



123 = 0.1194,  $^{146}\text{Nd}/^{144}\text{Nd} = 0.7219$  and  $^{179}\text{Hf}/^{177}\text{Hf} = 0.7325$ , respectively. The USGS rock standards JB-3  
124 and BHVO-2 run with our samples give values consistent with the reported reference values (GeoREM,  
125 <http://georem.mpch-mainz.gwdg.de/>). Results are given in Appendix 5.

## 126 **4. Petrography and mineral chemistry**

### 127 *4.1. Granodiorite*

128 The QMS pluton is of granodioritic composition with a mineral assemblage of plagioclase (45  
129 vol. %-50 vol. %), quartz (35 vol. %-42 vol. %), amphibole (3 vol. %-10 vol. %), biotite (2 vol. %-10  
130 vol. %), minor K-feldspar, and accessory minerals such as apatite, sphene, zircon and Fe-Ti oxides (Fig.  
131 2d). Plagioclase crystals are euhedral to subhedral, and are of oligoclase composition with  $\text{An}_{12-24}$  (Fig.  
132 3a). Zoned-plagioclase crystals display normal zoning with more anorthitic cores rimmed by less calcic  
133 compositions (Fig. 3a). Amphibole is always present as euhedral to subhedral crystals despite the  
134 variably small abundances (Fig. 2d). Amphibole grains are usually homogeneous and rarely display  
135 disequilibrium textures. Amphiboles from the host granodiorite can be classified as edenite (Appendix  
136 3, Fig. 4) following Leake et al. (1997). They have medium  $\text{SiO}_2$ , and low  $\text{TiO}_2$  (0.37-1.24 wt. %),  
137  $\text{Na}_2\text{O}$  (0.87-1.48 wt. %) and  $\text{K}_2\text{O}$  (0.29-1.69 wt. %).

### 138 *4.2. Mafic magmatic enclave*

139 MMEs are abundant in the QMS pluton (Fig. 2a), showing varying shape and size from  
140 centimeters to tens of centimeters in diameter (Fig. 2a). They differ from the host by having finer  
141 grain-size (Figs. 2a-c), but have the same mineralogy albeit with greater mafic modes (e.g., 35-50 vol.%  
142 amphibole, 5-15 vol.% biotite, 40-50 vol.% plagioclase, minor quartz, K-feldspar, along with accessory

143 minerals such as apatite, sphene, zircon and Fe-Ti oxides), thus giving a dioritic bulk composition.  
144 Plagioclase mostly occurs as subhedral grains with compositions similar to those in the host  
145 granodiorite. Zoned-plagioclase in the MMEs shows a compositional continuum with cores slightly  
146 more anorthitic than the rims (Fig. 3b). Amphibole in the MMEs is compositionally identical to that in  
147 the host granodiorite (Fig. 4). Biotite is yellow brown with subhedral to euhedral forms. The MMEs  
148 show no chilled margins nor textures of crystal resorption or reactive overgrowth. These rocks mainly  
149 exhibit porphyritic-like textures.

## 150 **5. Results**

### 151 *5.1. Zircon U–Pb ages*

152 Four samples (2 host-MME pairs) were chosen for dating. In CL images (Figs. 5a, c), zircons from  
153 the host granodiorites (QMS12-04host and QMS12-10host) are transparent, colorless, and mostly  
154 euhedral columnar crystals of varying size (~150-300 $\mu$ m long with length/width ratio of 1:1-3:1) with  
155 well-developed oscillatory zoning. The zircons have varying U (~ 28-386 ppm) and Th (~ 69-423 ppm)  
156 with Th/U ratio of 0.3-1.4. All these characteristics are consistent with the zircons being of magmatic  
157 origin (Hoskin and Schaltegger, 2003). After excluding discordant ages, zircons from the two host  
158 granodiorite samples yielded weighted mean  $^{206}\text{Pb}/^{238}\text{U}$  ages of  $429.7 \pm 2.5$  Ma (1 $\sigma$ , MSWD=0.15, n=23)  
159 and  $431.5 \pm 2.6$  Ma (1 $\sigma$ , MSWD=0.19, n=20), respectively (Figs. 5a, c), representing the crystallization  
160 age (~430 Ma) of the host granodiorite. These age data are in agreement with those in the literature  
161 (Tseng et al., 2009; Yu et al., 2015).

162 Zircons from the MMEs (QMS12-04MME and QMS12-10MME) show similar optical properties  
163 to those in the host with oscillatory zoning (Figs. 5b, d) and varying size (~150-200 $\mu$ m in length

164 length/width ratio of ~ 1:1-2:1). They have varying Th (27-548 ppm), U (50-541 ppm), and Th/U  
165 (0.1-2.4). They are also of magmatic origin. Zircons in the 2 MMEs yielded the same weighted mean  
166 ages as zircons in the host within error, i.e.  $429.6 \pm 2.8$  Ma ( $1\sigma$ , MSWD=0.48, n=18) and  $431.2 \pm 2.8$  Ma  
167 ( $1\sigma$ , MSWD=0.2, n=19), respectively (Figs. 5b, d).

## 168 5.2. Major and trace elements

169 Eleven representative QMS granodiorite samples and their hosted MMEs (including 5 host-MME  
170 pairs) were analyzed for whole-rock major and trace element compositions (Appendix 4). The  
171 granodiorite samples have high SiO<sub>2</sub> (64.37-65.49 wt.%), Al<sub>2</sub>O<sub>3</sub> (16.09-17.61 wt.%), Na<sub>2</sub>O (4.86-5.12  
172 wt.%) and Na<sub>2</sub>O/K<sub>2</sub>O (2.11-3.82) with medium total alkalis (Na<sub>2</sub>O+K<sub>2</sub>O = 6.46-7.25 wt.%), and plot in  
173 the granodiorite field (Fig. 6a). They have low Fe<sub>2</sub>O<sub>3</sub><sup>T</sup> (2.86-3.43 wt.%), MgO (2.14-2.60 wt.%) and  
174 CaO (3.60-4.10 wt.%). They are calc-alkaline (Fig. 6b) and metaluminous to weakly peraluminous  
175 (A/CNK= 0.93 to 1.03) (Fig. 6c), which is typical for I-type granitoids (Chappell and White, 1992). In  
176 contrast, the MMEs plot in the fields of diorite, monzodiorite and monzonite (Fig. 6a). They are  
177 compositionally high-K calc-alkaline to calc-alkaline (Fig. 6b), and metaluminous with A/CNK ranging  
178 from 0.74 to 0.84 (Fig. 6c). They have lower SiO<sub>2</sub> (52.06-58.59 wt.%), higher Fe<sub>2</sub>O<sub>3</sub><sup>T</sup> (6.12-8.50 wt.%),  
179 MgO (5.09-7.22 wt.%), CaO (4.99-6.57 wt.%), P<sub>2</sub>O<sub>5</sub> (0.49-1.01 wt.%), and slightly higher Mg<sup>#</sup>  
180 (0.63-0.68; Mg<sup>#</sup>=Mg/[Mg+Fe<sup>2+</sup>]) than the host granodiorites.

181 In the chondrite-normalized REE diagram, the QMS granodiorite samples are characterized by a  
182 relatively flat heavy REE (HREE) pattern ( $[Dy/Yb]_N = 1.32-1.54$ ), slightly negative to positive Eu  
183 anomalies (Eu/Eu\*=0.88-1.13), and lower total REE contents ( $\Sigma REE=76-134$  ppm) than the hosted  
184 MMEs. The REE patterns of the QMS granodiorites are similar to the field defined by the BJS

185 granodiorites (cf. Chen et al., 2015) (Fig. 7), but display greater light REE (LREE) enrichment  
186 ( $[\text{La}/\text{Sm}]_N = 4.77\text{-}5.36$ ). The MMEs show similar REE patterns, but have significantly higher HREEs  
187 (Fig. 7a, b), which is consistent with greater modes of REE-enriched minerals (e.g., amphibole, apatite  
188 and zircon). They have negative Eu anomalies ( $\text{Eu}/\text{Eu}^* = 0.6\text{-}0.8$ ).

189 In the multi-element spider diagram (Fig. 8), the host granodiorite and MMEs both show  
190 enrichment of large ion lithophile elements (LILE, e.g., P, K, Pb) and depletion in high field strength  
191 elements (HFSE, e.g., Nb, Ta and Ti). Sr appears to have a positive anomaly in the host  
192 ( $\text{Sr}/\text{Sr}^* = 1.66\text{-}2.96$ ), but varying anomalies for the MMEs ( $\text{Sr}/\text{Sr}^* = 0.5\text{-}1.19$ ). In particular, compared to  
193 the BJS granodiorites (Chen et al., 2015), the QMS granodiorite samples have adakitic signatures with  
194 high Sr/Y and La/Yb ratios, and lower Y and Yb abundances, thus plotting in the adakite fields in the  
195 discrimination diagrams (Figs. 9a-b), while most MMEs plot in the normal arc rock field.

### 196 5.3. Sr-Nd-Hf isotopic geochemistry

197 Whole-rock Sr-Nd-Hf isotopic compositions for the MMEs and their host granodiorite are given in  
198 Appendix 5. The initial  $^{87}\text{Sr}/^{86}\text{Sr}_{(t)}$ ,  $\epsilon_{\text{Nd}}(t)$  and  $\epsilon_{\text{Hf}}(t)$  values are calculated at 430 Ma using the zircon  
199 age data (see Fig. 5 above). On the plots of  $^{87}\text{Sr}/^{86}\text{Sr}_{(t)}$ ,  $\epsilon_{\text{Nd}}(t)$  and  $\epsilon_{\text{Hf}}(t)$  against  $\text{SiO}_2$  (Figs. 10j-l), both  
200 host granodiorite and MME samples are indistinguishable and overlapping within a narrow range (also  
201 see Appendix 5).

202 On  $\text{SiO}_2$ -variation diagrams (Fig. 10), the MMEs and their host granodiorite define linear trends  
203 for most elements (e.g.,  $\text{TiO}_2$ ,  $\text{Fe}_2\text{O}_3^T$ , MnO, MgO, CaO,  $\text{P}_2\text{O}_5$ , Eu and Hf abundances) and trace  
204 element ratio (e.g., Hf/Sm) (Figs. 10a-i), but show no correlations of initial Sr, Nd, and Hf isotopic  
205 compositions with  $\text{SiO}_2$  (Figs. 10j-l).

206 **6. Discussion**

207 *6.1. Petrogenesis of the mafic magmatic enclaves*

208 Several models have been proposed for the origin of MMEs in the literature, including foreign  
209 xenoliths (usually country rocks; e.g., Vernon, 1983; Xu et al., 2006), refractory and residual phase  
210 assemblages derived from granitoid sources (e.g., the restite model; Chappell et al., 1987; Chappell and  
211 White, 1991), chilled material or cumulate of early-formed co-genetic crystals (e.g., Dodge and Kistler,  
212 1990; Dahlquist, 2002; Donaire et al., 2005; Rodríguez et al., 2007; Niu et al., 2013; Huang et al., 2014;  
213 Chen et al., 2015), and basaltic melt material incompletely digested and homogenized during a magma  
214 mixing process (e.g., Vernon, 1983; Didier, 1987; Castro et al., 1990; Dorais et al., 1990; Barbarin and  
215 Didier, 1991; Chappell and White, 1991; Barbarin, 2005; Chen et al., 2009a, 2013b; Wang et al., 2013).  
216 We critically evaluate these interpretations below.

217 *6.1.1. Textural and chemical relationships of the MMEs and their hosts*

218 The textural and chemical relationships of the QMS MMEs and their host granodiorite concur  
219 with the findings for the BJS pluton (Chen et al., 2015), and are summarized as follows: (1) the MMEs  
220 in the QMS granodiorites are ellipsoidal, or elongate, show no chilled margins, no textures of crystal  
221 resorption nor reactive overgrowth, but exhibit typical magmatic texture (Figs. 2a-f); (2) they have a  
222 mineral assemblage identical to, and more mafic phases than, their host granodiorite (Figs. 2c-f); (3)  
223 they have mineral compositions (e.g., amphibole and plagioclase) identical to those of their host (Fig.  
224 3-4); (4) they have the same age (~430 Ma) as their host (Fig. 5); (5) their different major and trace  
225 element abundances from their hosts are controlled largely by mineral modal proportions, i.e., MMEs

226 have greater modes of REE-enriched minerals (amphibole, apatite and zircon) and thus have higher  
227 MgO, Fe<sub>2</sub>O<sub>3</sub>, CaO and trace elements easily incorporated into these phases (e.g., TiO<sub>2</sub>, P<sub>2</sub>O<sub>5</sub>, Hf and  
228 HREEs) (Figs. 10a-i); and (6) more importantly, they have overlapping and indistinguishable Sr-Nd-Hf  
229 isotopes with their host granodiorite (Figs. 10j-l).

230 Any successful models for the origin of MMEs must be consistent with these observations.  
231 Models for MMEs as foreign xenoliths from country rocks (e.g., Xu et al., 2006) can be readily rejected,  
232 as there is no evidence of reaction textures for the MMEs. Likewise, the identical age (~430 Ma) of the  
233 MMEs and their host as well as the magmatic textures, constitute a strong argument against the restite  
234 origin (e.g., Chappell et al., 1987). In addition, the MMEs do not contain peraluminous minerals and  
235 their metaluminous composition (Fig. 6c) also excludes their derivation by melting of peraluminous  
236 restites (Barbarin, 2005). Therefore, the most straightforward interpretation is that the MMEs and their  
237 hosts formed as different products of a common magmatic system.

#### 238 *6.1.2. Assessing the origin of magma mixing*

239 Similar observations mentioned above between the MMEs and their host granitoids have been  
240 identified first by Pabst (1928) and by many others since then. The MMEs were thus described as  
241 “autoliths”, referring to “cogenetic” or part of the same system. Despite the “autoliths” nature of the  
242 MMEs with the host, this interpretation has been questioned: (1) Why are isotopic values of some  
243 MMEs intermediate between those of crustal and mantle materials (e.g., DePaolo, 1981; Barbarin,  
244 2005)? (2) Why are the MMEs fine-grained (e.g., Barbarin and Didier, 1991)? Because of these  
245 questions, a model of magma mixing between mantle-derived mafic magma and crust-derived felsic  
246 magma was proposed to address the above issues: (1) the intermediate isotopic values of the MMEs

247 were commonly interpreted as the result of magma mixing between a mantle-derived mafic magma and  
248 a crust-derived felsic magma, because a mafic magma derived from upper mantle provides not only  
249 material but also the heat necessary for melting and subsequently mixing with the crustal rocks (e.g.,  
250 Barbarin, 2005); (2) the fine-grained MMEs were interpreted as due to quenching against host felsic  
251 magmas (e.g., Vernon, 1984; Furman and Spera, 1985; Barbarin, 2005), owing to their higher liquidus  
252 and solidus temperatures compared to felsic magmas. As a result, the magma mixing model has been  
253 the most popular interpretation for the petrogenesis of the MMEs (see critical review by Niu et al.,  
254 2013).

255       Actually, there are many compelling lines of evidence for magma mixing in many granitoids,  
256 especially (1) where a clear isotopic contrast exists between the MMEs and the hosts (e.g., Holden et  
257 al., 1987; Chen et al., 2009b; Liu et al., 2013); and (or) (2) where disequilibrium features occur in the  
258 MMEs, e.g., complex zoning of clinopyroxene crystals that have distinctly low-MgO cores surrounded  
259 by high-MgO rims (e.g., Chen et al., 2013a; Wang et al., 2013), or resorption textures or reversed  
260 zoning of plagioclase (Pietranik et al., 2006; Chen et al., 2009a, 2009b). In the case of our study,  
261 however, none of the above has been observed. Instead, many lines of evidence argue against the  
262 magma mixing origin.

263       First, the MMEs and their host granodiorites in the QMS pluton have overlapping and  
264 indistinguishable Sr-Nd-Hf isotopes (vs. isotopic contrast in magma mixing model). In spite of this,  
265 some authors would still argue that the isotopic and mineral compositional similarity between the  
266 enclaves and the host could result from chemical and isotopic equilibration during magma mixing, (e.g.,  
267 Dorais et al., 1990; Barbarin, 2005; Chen et al., 2009b; Zhang et al., 2010) using some experimental  
268 interpretations that isotopic equilibration is generally more easily achieved than chemical equilibration

269 (Leshner, 1990). However, we emphasize that it is physically unlikely that isotopes become  
270 homogenized whereas major and trace elements are not (Niu et al., 2013), because isotopes are “carried”  
271 by the relevant chemical elements and isotopic diffusion cannot take place without the diffusion of the  
272 “carrying” elements (Chen et al., 2015). In fact, there are two forceful arguments against thermal and  
273 chemical equilibration: (1) the MMEs exhibit no textures of crystal resorption or reactive overgrowth  
274 (Figs. 2b-c), and (2) plagioclase in the MMEs and their host granodiorite shows no compositional or  
275 textural disequilibrium (Fig. 3). In addition, although the fine-grained texture of the MMEs could be  
276 interpreted as resulting from quenching in the magma mixing model, quenching of the mafic magma  
277 would lead to a significantly high viscosity contrast between the solidified enclaves and the felsic host  
278 magma, thereby inhibiting deformation, mechanical mixing (Caricchi et al., 2012; Farner et al., 2014)  
279 and isotope homogenization between the MMEs and the host.

280       Second, strongly correlated variations between major and trace elements (Figs. 10a-i) are  
281 consistent with modal mineralogy control, as the result of magma evolution (i.e., the MMEs are  
282 cumulate and the host represents residual melt) rather than mixing of two magmas with entirely  
283 different origins because magma mixing is a complex, multi-stage process in which linear trends can be  
284 disturbed (e.g., Clemens, 1989; Donaire et al., 2005; Chen et al., 2015). Moreover, the distinctive high  
285 abundances of some elements in the MMEs, such as Zr and P (Fig. 11), cannot be explained by magma  
286 mixing because these elements are controlled by the presence of accessory phases, such as zircon and  
287 apatite. As shown in Fig. 11, mantle derived basaltic magmas would have much lower Zr and P<sub>2</sub>O<sub>5</sub> than  
288 in the QMS MMEs. For example, quantitative calculations by Lee and Bachmann (2014) suggested that  
289 10-20% melting of an upper mantle with 5 ppm Zr and 0.019 wt.% P<sub>2</sub>O<sub>5</sub> (equivalent to that estimated  
290 for depleted mid-ocean ridge basalt mantle), would yield primary liquids with 25-50 ppm Zr and



291 0.1-0.2 wt.% P<sub>2</sub>O<sub>5</sub>. These concentrations are much lower than in the QMS MMEs. Additionally,  
292 boninites are thought to result from partial melting of highly depleted harzburgitic mantle peridotites  
293 induced by subduction-zone slab dehydration (Niu, 2005), but they also have lower Zr and P<sub>2</sub>O<sub>5</sub>  
294 contents (Fig. 11). More importantly, magma mixing between a basalt with any silicic end-member  
295 (e.g., rhyolite) would generate a mixing array (Figs. 11a-b, the dash lines) totally different from the  
296 linear trend (Figs. 11a-b, the solid lines) defined by the QMS granodiorite and their MMEs. In contrast,  
297 all of these observations are consistent with the interpretation that the MMEs represent earlier cumulate  
298 with greater amounts of zircon and apatite than their hosts (e.g., Donaire et al., 2005).

### 299 *6.1.3. Formation of the mafic magmatic enclaves*

300 The foregoing observations, illustrations and discussion leave us with the best interpretation that  
301 the MMEs represent the earlier crystallized cumulate that were later disturbed by subsequent melt  
302 replenishment and induced magma convection in the magma chamber. As illustrated in Fig. 12, when a  
303 primitive magma body is emplaced into a cold environment (e.g., developing a magma chamber) with  
304 the wall-rock having temperatures below the liquidus of the magma, magma quench and rapid  
305 crystallization are inevitable because of the thermal contrast. For an andesitic primitive magma parental  
306 to the syn-collisional granitoids (Niu et al., 2013), the first major liquidus phases would be amphibole,  
307 biotite, plagioclase and accessory minerals such as zircon and apatite, and rapid quench will facilitate  
308 abundant nucleation without between-nuclei space for rapid growth, thus resulting in the formation of  
309 fine-grained cumulate (Chen et al., 2015). This is a fundamentally important petrologic concept with  
310 which any interpretation must comply. This early formed fine-grained mafic cumulate piles (largely  
311 plastic before complete solidification) can be readily disturbed by subsequent magma replenishment

312 and induced convection, resulting in the dispersion of the MMEs in the host granodiorite.

## 313 *6.2 Petrogenesis of QMS adakitic granodiorite*

### 314 *6.2.1 Implication from the MMEs*

315 Recently, mixing of basaltic and felsic magmas was proposed for the genesis of some high-Mg  
316 and low SiO<sub>2</sub> adakitic rocks from Mount Shasta and the North China Craton using the presence of  
317 ubiquitous MMEs as evidence (Chen et al., 2013b) and also based on the disequilibrium petrographic  
318 characteristics in high-Mg andesites (Streck et al., 2007; Chen et al., 2013a). This interpretation could  
319 be reasonable, but it is not the case here because there is no petrographic and compositional evidence  
320 for magma mixing as elaborated above. That is, the MMEs in the QMS adakitic granodiorite are not  
321 evidence for magma mixing, but rather they are of cumulate origin without direct asthenospheric  
322 mantle participation (e.g., Dahlquist, 2002). More importantly, the MMEs comprise dominantly  
323 amphibole and plagioclase, which are common cumulate minerals of andesitic melts. If the parental  
324 melts were basaltic, the typical cumulate from such evolved basaltic melt would be gabbro dominated  
325 by clinopyroxene and plagioclase (Chen et al., 2015). It can be inferred from this important petrological  
326 concept that the parental magmas of the MMEs and their host granodiorite was mafic andesitic (Niu et  
327 al., 2013; Chen et al., 2015).

### 328 *6.2.2 Assessing the model of melting of mafic lower continental crust*

329 To date, some intra-continental high-MgO or -Mg<sup>#</sup> (also high Cr and Ni contents) adakitic rocks  
330 have been considered to originate from melting of delaminated lower crust (e.g., Xu et al., 2002; Gao et  
331 al., 2004; Wang et al., 2006b). By accepting and applying this model, it has been previously interpreted

332 that the QMS adakitic rocks were derived from delaminated lower crust, and they subsequently  
333 interacted with mantle peridotite during ascent (Tseng et al., 2009; Yu et al., 2015). Although this  
334 model seems plausible and applicable to the QMS adakitic rocks, it has more difficulties than  
335 certainties. First, the QMS adakitic granodiorites have lower  $(Dy/Yb)_N$ ,  $(La/Yb)_N$ , and distinctive low  
336  $K_2O/Na_2O$  ratios (Fig. 13b), which are significantly different from the composition of adakitic rocks  
337 inferred to be derived from partial melting of the thickened or delaminated lower continental crust.  
338 Second, the Nd and Hf isotopic data of the QMS adakitic granodiorite indicate a significant mantle  
339 input, which is also inconsistent with those of lower continental crust origin (Fig. 14a). Finally, the  
340 existence of the Paleo-Qilian ocean is manifested by the ophiolites and eclogites in the North Qilian  
341 orogenic belt; the ocean basin started its subduction at ~520 Ma, and was eventually closed at the end  
342 of the Ordovician (~445 Ma) followed by continental collision (see Song et al., 2013). Accordingly,  
343 the coeval (~430 Ma) MMEs and their adakitic host granodiorite of the QMS pluton are best  
344 interpreted as a magmatic response to the collision between the Qilian-Qaidam block and Alashan  
345 block, thereby being contrary to the environment of crustal extension required by a delaminated lower  
346 crustal origin. In fact, continuous lithosphere extension and delamination in the NQOB occurred at  
347 <400 Ma, which resulted in strong magmatic activity and formed a number of  
348 diorite-granodiorite-granite plutons with ages of ~400–360 Ma (Song et al., 2013, 2014b).

### 349 *6.2.3 A fractional crystallization model for the petrogenesis of the QMS adakitic granodiorites*

350 An origin of adakitic rocks by fractional crystallization has been proposed in the literature.  
351 However, it should be noted that all these crystallization models require basaltic parental magmas  
352 derived from the metasomatized mantle wedge in arc settings, such as in the complex Philippine arc

353 (Castillo et al., 1999; Macpherson et al., 2006) and Ecuadorian Andes (Chiaradia et al., 2004). It is  
354 important to note that our crystallization model differs from the basaltic magma crystallization model  
355 of arc magmas in the literature.

356 In our model, the magmas parental to the MMEs and their host granodiorite are the same mafic  
357 andesitic magmas in a syn-collisional setting, rather than basaltic magmas in an arc setting of active  
358 seafloor subduction advocated in the literature (e.g., Macpherson et al., 2006). That is, the QMS  
359 adakitic granodiorites are products of fractional crystallization dominated by the mineral assemblage  
360 indicated by the MMEs from mafic andesitic magmas. We can further consider two fractional  
361 crystallization models to elucidate the effect of crystallization of the observed mineralogy on trace  
362 elements using closed-system Rayleigh fractionation equation: (1) Model A, in reasonable agreement  
363 with observed mineral proportions of the MMEs, 50% amphibole, 40% plagioclase, 7.52% biotite, 2.2%  
364 apatite, 0.2% zircon and 0.03% sphene; (2) Model B, which incorporates fractionation of garnet, 50%  
365 amphibole, 40% plagioclase, 7.6% biotite, 2.4% garnet. The partition coefficients used in the  
366 calculations are for intermediate-felsic magmas (Appendix 6). For convenience (see below), the  
367 assumed parental magma (Appendix 6) is very similar to the bulk continental crust (BCC) composition  
368 (Rudnick and Gao, 2003) (Fig. 15), which is the same as the ~ 60 Ma Linzizong andesite in southern  
369 Tibet (Mo et al., 2008; Niu et al., 2013), in terms of major and trace element abundances.

370 Notably, removal of garnet would yield a smooth decrease of LREE-to-HREE pattern (Richards  
371 and Kerrich, 2007) with elevated  $(Dy/Yb)_N$  and  $(La/Yb)_N$  in the evolving melt (Fig. 9c). However, the  
372  $(Dy/Yb)_N$  ratio in the QMS adakitic granodiorites remain constant with increasing  $(La/Yb)_N$  (Fig. 9c),  
373 which indicate that the effect of garnet fractionation in generating the QMS adakitic granodiorites is  
374 unimportant. Simple modal calculation of fractional crystallization using Model B indicates that the

375 participation of garnet is no more than 3% (Fig. 9), but the low garnet proportion in combination with a  
376 large amount of amphibole-plagioclase fractionation can hardly generate the adakitic signature shown  
377 in the QMS pluton (Figs. 9a-b). Besides, mineralogically, garnet has been observed neither in the QMS  
378 MMEs and their host adakitic granodiorite, nor in the coeval igneous rocks in the eastern section of the  
379 NQOB. In addition, our preferred source for the QMS MMEs and their host adakitic granodiorite is  
380 partial melting of the ocean crust at amphibolite facies conditions (<40km) (Mo et al., 2008; Niu and  
381 O'Hara, 2009; Niu et al., 2013) (see below), rather than the presence of garnet as a residual phase at  
382 garnet amphibolite or eclogite conditions.

383 It is also impossible to generate QMS adakitic granodiorites by fractionation of  
384 amphibole-plagioclase alone, because they tend to produce concave-upwards patterns between the  
385 MREE and HREE and lead to decreasing  $(Dy/Yb)_N$  with increasing  $(La/Yb)_N$  (Fig. 9c), owing to the  
386 affinity of calcic amphiboles for MREEs over the HREEs (Klein et al., 1997). Additionally, removal of  
387 amphibole-plagioclase would result in negative Eu anomalies in the residual melts, which is  
388 inconsistent with QMS adakitic granodiorites (Fig. 9d). In the case of our study, we emphasize that the  
389 widespread accessory minerals such as zircons and apatites in both QMS host adakitic granodiorite and  
390 particularly their cumulate MMEs played a significant role in generating QMS adakitic granodiorites.  
391 For example, zircon fractionation would increase  $(Dy/Yb)_N$  (Fig. 9c) and the La/Yb and Sr/Y ratios of  
392 residue magmas (Figs. 9a-b), because  $Kd_{zircon}^{Dy/Yb} = 0.140$ , and  $Kd_{zircon}^{La/Yb} = 0.005$  (Bea et al., 1994).  
393 Apatite fractionation can also increase the Sr/Y ratio (Figs. 9a-b), but decrease  $(Dy/Yb)_N$  (Fig. 9c).  
394 Importantly, apatite fractionation would increase Eu/Eu\* (Fig. 9d), because  $Kd_{apatite}^{Sm} = 46$  ,  
395  $Kd_{apatite}^{Eu} = 25.5$  ,  $Kd_{apatite}^{Gd} = 43.9$  (Fujimaki et al., 1984). Note that the simple calculation of Model A  
396 (Appendix 6; Figs. 9 and 15), which involves a small proportion of zircon, apatite and sphene in

397 combination with amphibole, biotite and plagioclase to form the fractionation assemblage can explain  
398 the characteristics of the QMS adakitic granodiorites. Although uncertainties exist for mineral partition  
399 coefficients, our model offers insights into the petrogenesis of the adakitic granodiorite as well as the  
400 enclosed MMEs in syn-collisional environments.

### 401 *6.3 Constraints on the source*

402 As discussed above, the primary magmas parental to the MMEs and their host granodiorite are  
403 most consistent with mafic andesitic magmas of ocean crust origin during continental collision. In  
404 addition, our new data and the whole-rock Sr-Nd and zircon Hf isotopic data in the literature on the  
405 QMS pluton (Tseng et al., 2009; Yu et al., 2015) exhibit quite uniform Sr-Nd-Hf composition (Figs.  
406 10j-l). Though the radiogenic Sr and slightly unradiogenic Nd isotopes indicate the input of crustal  
407 materials, the whole-rock  $\epsilon_{\text{Hf}}(t)$  values (+5.5 to +8.4) of this study and the zircon  $\epsilon_{\text{Hf}}(t)$  values (+4.2 to  
408 +7.7) in the literature (Yu et al., 2015) are indicative of significant mantle input or juvenile mafic  
409 continental crust derived from the mantle in no distant past (Zhang et al., 2015). As noted above, many  
410 adakitic rocks can be generated from the lower continental crust, but this is not applicable in our study  
411 (see above). In our case, the most likely source for the andesitic magmas with inherited mantle isotopic  
412 signatures parental to the QMS pluton is partial melting of the remaining part of the North Qilian ocean  
413 crust (Chen et al., 2015). On the other hand, contribution from continental crust is also required. This  
414 may occur in the melting region or in an evolving magma chamber rather than simple crustal level  
415 assimilation, because the Sr-Nd-Hf isotopes for the MMEs and their host granodiorites are closely  
416 similar and show a respectively narrow range of variation, and they do not show correlated variations  
417 with  $\text{SiO}_2$  (Figs. 10j-l). Melting of recycled terrigenous sediments of upper continental crust and

418 remaining part of the North Qilian oceanic crust in the melting region is more likely (Mo et al. 2008;  
419 Niu and O'Hara 2009; Chen et al., 2015).

420 In the broad context of the continental collision, the model of partial melting of the remaining part  
421 of the ocean crust and the recycled terrigenous sediments has been proposed and tested by Niu and  
422 co-workers in southern Tibet, East Kunlun and Qilian Orogenic Belts (e.g., Mo et al., 2008; Niu and  
423 O'Hara, 2009; Niu et al., 2013; Huang et al., 2014; Chen et al., 2015; Zhang et al., 2015). In their model,  
424 during collision, the underthrusting North Qilian ocean crust would subduct/underthrust slowly, tend to  
425 attain thermal equilibrium with the superjacent warm active continental margin, and evolve along a  
426 high T/P path in P-T space as a result of retarded subduction and enhanced heating (Appendix Fig. S1).  
427 The warm hydrated ocean crust of basaltic composition and sediments of felsic composition with rather  
428 similar solidi would melt together under the amphibolite facies conditions (for details see Niu et al.,  
429 2013; also see Appendix Fig. S1).

430 Importantly, this model can generate andesitic magmas not only with inherited mantle  
431 isotopic signatures but also compositions similar to the bulk continental crust (BCC), except for  
432 notable depletion in highly compatible elements like Mg, Cr and Ni (Mo et al., 2008). This model  
433 together with experimental results of melting of metabasalt and eclogite (Fig. 13a) implies that the  
434 relatively high  $Mg^{\#}$  (also high Cr and Ni ) contents in QMS adakitic granodiorites may indeed  
435 reflect melt interaction with mantle peridotite during ascent. Although magmas produced through  
436 the above process lack the adakitic signature, it can be the ideal source that generates QMS  
437 adakitic granodiorites through fractional crystallization dominated by mineral assemblages  
438 represented by the MMEs. Note that this interpretation is consistent with binary isotope mixing  
439 calculations as proposed by Chen et al. (2015) (Figs. 14a-b), and with trace element model

440 calculations (see above) (Figs. 9 and 15). As illustrated by these mass balance calculations, ~95%  
441 ocean crust and ~5% continental materials contribute to the source of the QMS pluton (Fig. 14),  
442 and 30%-50% fractional crystallization dominated by mineralogy and modes of the MMEs can  
443 lead to the highly evolved granodioritic composition of the QMS pluton with the adakitic  
444 signature (Figs. 9 and 15).

## 445 **7. Conclusions**

446 (1) The zircon U-Pb dating of the QMS pluton yields the same age (~430 Ma) for both the MMEs  
447 and their host granodiorite, which is the same as the closure time of the Qilian ocean and continental  
448 collision at ~440-420Ma.

449 (2) The MMEs and their host granodiorite also share the same mineralogy with indistinguishable  
450 isotopic compositions, all of which indicate that the MMEs are cumulate formed at earlier stages of the  
451 same magmatic system rather than representing mantle melt required by the popular magma mixing  
452 model.

453 (3) The QMS host granodiorite has adakite-like major and trace element features, including high Sr,  
454 Sr/Y and La/Yb, but low Y and Yb. By accepting our model for the petrogenesis of the MMEs, it  
455 follows that the QMS adakitic granodiorite resulted from fractional crystallization dominated by  
456 mineral assemblages represented by the MMEs.

457 (4) The parental magma for the QMS pluton is best explained as resulting from partial melting of the  
458 remaining part of ocean crust together with recycled terrigenous sediments during continental collision.  
459 The resulting magma may have also experienced interaction with mantle peridotite during ascent.



460 **Acknowledgments**

461 We thank Li Su for the assistance with whole rock major, trace elements and zircon U-Pb age  
462 analysis, Minwu Liu with electron microprobe analysis, and Jinlong Ma, Xirong Liang and Zhongyuan  
463 Ren with whole rock Sr-Nd-Hf isotope analysis. Pu Sun, Huixiang Cui and Yuxing Ma are thanked for  
464 their help with sample preparation. This work was supported by the National Natural Science  
465 Foundation of China (NSFC: 91014003, 41130314), Chinese Academy of Sciences (Innovation Grant  
466 Y42217101L) and grants from regional and local authorities (Shandong Province and City of Qingdao),  
467 two projects of Chinese Geological Survey Departments and Offices (1212011121092,  
468 1212011220928), and supported by National Oceanography Laboratory in Qingdao.

469

470 **References**

- 471 Andersen, T., 2002. Correction of common lead in U-Pb analyses that do not report <sup>204</sup>Pb. *Chemical*  
472 *Geology* 192, 59-79.
- 473 Bachmann, O., Dungan, M.A., Bussy, F., 2005. Insights into shallow magmatic processes in large  
474 silicic magma bodies: the trace element record in the Fish Canyon magma body, Colorado.  
475 *Contributions to Mineralogy and Petrology* 149, 338-349.
- 476 Barbarin, B., 2005. Mafic magmatic enclaves and mafic rocks associated with some granitoids of the  
477 central Sierra Nevada batholith, California: nature, origin, and relations with the hosts. *Lithos* 80,  
478 155-177.
- 479 Barbarin, B., Didier, J., 1991. Enclaves of the Mesozoic calc-alkaline granitoids of the Sierra Nevada  
480 Batholith, California. *Enclaves and granite petrology*. Elsevier, Amsterdam 135, 153.

481 Bea, F., Pereira, M., Stroh, A., 1994. Mineral/leucosome trace-element partitioning in a peraluminous  
482 migmatite (a laser ablation-ICP-MS study). *Chemical Geology* 117, 291-312.

483 Black, L.P., Kamo, S.L., Allen, C.M., Aleinikoff, J.N., Davis, D.W., Korsch, R.J., Foudoulis, C., 2003.  
484 TEMORA 1: a new zircon standard for Phanerozoic U–Pb geochronology. *Chemical Geology* 200,  
485 155-170.

486 Caricchi, L., Annen, C., Rust, A., Blundy, J., 2012. Insights into the mechanisms and timescales of  
487 pluton assembly from deformation patterns of mafic enclaves. *Journal of Geophysical Research:*  
488 *Solid Earth* (1978–2012) 117.

489 Castillo, P.R., 2006. An overview of adakite petrogenesis. *Chinese Science Bulletin* 51, 257-268.

490 Castillo, P.R., 2012. Adakite petrogenesis. *Lithos* 134-135, 304-316.

491 Castillo, P.R., Janney, P.E., Solidum, R.U., 1999. Petrology and geochemistry of Camiguin Island,  
492 southern Philippines: insights to the source of adakites and other lavas in a complex arc setting.  
493 *Contributions to Mineralogy and Petrology* 134, 33-51.

494 Castro, A., Moreno - Ventas, I., De la Rosa, J., 1990. Microgranular enclaves as indicators of  
495 hybridization processes in granitoid rocks, Hercynian Belt, Spain. *Geological Journal* 25, 391-404.

496 Chappell, B., White, A., 1991. Restite enclaves and the restite model, *Enclaves and granite petrology*.  
497 Elsevier Amsterdam, pp. 479-492.

498 Chappell, B., White, A., 1992. I- and S-type granites in the Lachlan Fold Belt. *Geological Society of*  
499 *America Special Papers* 272, 1-26.

500 Chappell, B., White, A., Wyborn, D., 1987. The importance of residual source material (restite) in  
501 granite petrogenesis. *Journal of Petrology* 28, 1111-1138.

502 Chen, B., He, J., Ma, X., 2009a. Petrogenesis of mafic enclaves from the north Taihang Yanshanian

503 intermediate to felsic plutons: Evidence from petrological, geochemical, and zircon Hf-O isotopic  
504 data. *Science in China Series D: Earth Sciences* 52, 1331-1344.

505 Chen, B., Chen, Z.C., Jahn, B.M., 2009b. Origin of mafic enclaves from the Taihang Mesozoic orogen,  
506 north China craton. *Lithos* 110, 343-358.

507 Chen, B., Jahn, B.M., Suzuki, K., 2013a. Petrological and Nd-Sr-Os isotopic constraints on the origin  
508 of high-Mg adakitic rocks from the North China Craton: Tectonic implications. *Geology* 41,  
509 91-94.

510 Chen, B., Chen, C., He, J., Liu, A., 2013b. Origin of Mesozoic high-Mg adakitic rocks from  
511 northeastern China: Petrological and Nd-Sr-Os isotopic constraints. *Chinese Science Bulletin* 58,  
512 1941-1953.

513 Chen, S., Niu, Y., Sun, W., Zhang, Y., Li, J., Guo, P., Sun, P., 2015. On the origin of mafic magmatic  
514 enclaves (MMEs) in syn-collisional granitoids: evidence from the Baojishan pluton in the North  
515 Qilian Orogen, China. *Mineralogy and Petrology* 109, 577-596.

516 Chen, Y., Song, S., Niu, Y., Wei, C., 2014. Melting of continental crust during subduction initiation: A  
517 case study from the Chaidanuo peraluminous granite in the North Qilian suture zone. *Geochimica  
518 et Cosmochimica Acta* 132, 311-336.

519 Chiaradia, M., Fontbote, L., Beate, B., 2004. Cenozoic continental arc magmatism and associated  
520 mineralization in Ecuador. *Mineralium Deposita* 39, 204-222.

521 Chung, S.L., Liu, D., Ji, J., Chu, M. F., Lee, H.Y., Wen, D.J., Lo, C.H., Lee, T.Y., Qian, Q., Zhang, Q.,  
522 2003. Adakites from continental collision zones: Melting of thickened lower crust beneath  
523 southern Tibet. *Geology* 31, 1021.

524 Chung, S.L., Chu, M.F., Zhang, Y., Xie, Y., Lo, C.H., Lee, T.Y., Lan, C.Y., Li, X., Zhang, Q., Wang, Y.,

525 2005. Tibetan tectonic evolution inferred from spatial and temporal variations in post-collisional  
526 magmatism. *Earth-Science Reviews* 68, 173-196.

527 Clemens, J., 1989. The importance of residual source material (restite) in granite petrogenesis: a  
528 comment. *Journal of Petrology* 30, 1313-1316.

529 Dahlquist, J., 2002. Mafic microgranular enclaves: early segregation from metaluminous magma  
530 (Sierra de Chepes), Pampean Ranges, NW Argentina. *Journal of South American Earth Sciences*  
531 15, 643-655.

532 Defant, M.J., Drummond, M.S., 1990. Derivation of some modern arc magmas by melting of young  
533 subducted lithosphere. *Nature* 347, 662-665.

534 DePaolo, D.J., 1981. A neodymium and strontium isotopic study of the Mesozoic calc-alkaline granitic  
535 batholiths of the Sierra Nevada and Peninsular Ranges, California. *Journal of Geophysical*  
536 *Research* 86, 10470.

537 Didier, J., 1987. Contribution of enclave studies to the understanding of origin and evolution of granitic  
538 magmas. *Geologische Rundschau* 76, 41-50.

539 Dodge, F.C.W., Kistler, R.W., 1990. Some additional observations on inclusions in the granitic rocks of  
540 the Sierra Nevada. *Journal of Geophysical Research* 95, 17841.

541 Donaire, T., Pascual, E., Pin, C., Duthou, J.L., 2005. Microgranular enclaves as evidence of rapid  
542 cooling in granitoid rocks: the case of the Los Pedroches granodiorite, Iberian Massif, Spain.  
543 *Contributions to Mineralogy and Petrology* 149, 247-265.

544 Dorais, M.J., Whitney, J.A., Roden, M.F., 1990. Origin of mafic enclaves in the Dinkey Creek pluton,  
545 central Sierra Nevada batholith, California. *Journal of Petrology* 31, 853-881.

546 Ewart, A., Griffin, W., 1994. Application of proton-microprobe data to trace-element partitioning in

547 volcanic rocks. *Chemical Geology* 117, 251-284.

548 Farner, M.J., Lee, C.T.A., Putirka, K.D., 2014. Mafic–felsic magma mixing limited by reactive  
549 processes: A case study of biotite-rich rinds on mafic enclaves. *Earth and Planetary Science*  
550 *Letters* 393, 49-59.

551 Fujimaki, H., Tatsumoto, M., Aoki, K.I., 1984. Partition coefficients of Hf, Zr, and ree between  
552 phenocrysts and groundmasses. *Journal of Geophysical Research* 89, B662.

553 Furman, T., Spera, F.J., 1985. Co-mingling of acid and basic magma with implications for the origin of  
554 mafic I-type xenoliths: field and petrochemical relations of an unusual dike complex at Eagle Lake,  
555 Sequoia National Park, California, USA. *Journal of Volcanology and Geothermal Research* 24,  
556 151-178.

557 Gao, S., Rudnick, R.L., Yuan, H.L., Liu, X.M., Liu, Y.S., Xu, W.L., Ling, W.L., Ayers, J., Wang, X.C.,  
558 Wang, Q.H., 2004. Recycling lower continental crust in the North China Craton. *Nature* 432,  
559 892–897.

560 Green, T., Blundy, J., Adam, J., Yaxley, G., 2000. SIMS determination of trace element partition  
561 coefficients between garnet, clinopyroxene and hydrous basaltic liquids at 2–7.5 GPa and  
562 1080–1200 C. *Lithos* 53, 165-187.

563 He, Y., Li, S., Hoefs, J., Kleinhanns, I.C., 2013. Sr-Nd-Pb isotopic compositions of Early Cretaceous  
564 granitoids from the Dabie orogen: Constraints on the recycled lower continental crust. *Lithos*  
565 156-159, 204-217.

566 Holden, P., Halliday, A., Stephens, W., 1987. Neodymium and strontium isotope content of microdiorite  
567 enclaves points to mantle input to granitoid production. *Nature* 330, 53-56.

568 Hoskin, P.W., Schaltegger, U., 2003. The composition of zircon and igneous and metamorphic

569 petrogenesis. *Reviews in mineralogy and geochemistry* 53, 27-62.

570 Huang, H., Niu, Y., Nowell, G., Zhao, Z., Yu, X., Zhu, D.C., Mo, X., Ding, S., 2014. Geochemical  
571 constraints on the petrogenesis of granitoids in the East Kunlun Orogenic belt, northern Tibetan  
572 Plateau: Implications for continental crust growth through syn-collisional felsic magmatism.  
573 *Chemical Geology* 370, 1-18.

574 Irving, A.J., Frey, F.A., 1984. Trace element abundances in megacrysts and their host basalts:  
575 constraints on partition coefficients and megacryst genesis. *Geochimica et Cosmochimica Acta* 48,  
576 1201-1221.

577 Klein, M., Stosch, H.G., Seck, H., 1997. Partitioning of high field-strength and rare-earth elements  
578 between amphibole and quartz-dioritic to tonalitic melts: an experimental study. *Chemical*  
579 *Geology* 138, 257-271.

580 Le Maitre, R.W., Bateman, P., Dudek, A., Keller, J., Lameyre, J., Le Bas, M., Sabine, P., Schmid, R.,  
581 Sorensen, H., Streckeisen, A., 1989. A classification of igneous rocks and glossary of terms:  
582 Recommendations of the International Union of Geological Sciences Subcommittee on the  
583 Systematics of Igneous Rocks. Blackwell Oxford.

584 Leake, B., Arps, C., Birch, W., Gilbert, M., Grice, J., Hawthorne, F., Kato, A., Kisch, H., Krivovichev,  
585 V., Linthout, K., 1997. Nomenclature of Amphiboles: Report of the Subcommittee on Amphiboles  
586 of the International Mineralogical Association, Commission on New Minerals and Mineral  
587 Names. *The Canadian Mineralogist* 35, 219-246.

588 Lee, C.T., Bachmann, O., 2014. How important is the role of crystal fractionation in making  
589 intermediate magmas? Insights from Zr and P systematics. *Earth and Planetary Science Letters*  
590 393, 266-274.

591 Leshner, C.E., 1990. Decoupling of chemical and isotopic exchange during magma mixing. *Nature* 344,  
592 235-237.

593 Li, X.H., Li, W.X., Li, Z.X., Lo, C.H., Wang, J., Ye, M.F., Yang, Y.H., 2009. Amalgamation between  
594 the Yangtze and Cathaysia Blocks in South China: Constraints from SHRIMP U–Pb zircon ages,  
595 geochemistry and Nd–Hf isotopes of the Shuangxiwu volcanic rocks. *Precambrian Research* 174,  
596 117-128.

597 Liu, L., Qiu, J.S., Li, Z., 2013. Origin of mafic microgranular enclaves (MMEs) and their host quartz  
598 monzonites from the Muchen pluton in Zhejiang Province, Southeast China: Implications for  
599 magma mixing and crust–mantle interaction. *Lithos* 160-161, 145-163.

600 Ma, J., Wei, G., Liu, Y., Ren, Z., Xu, Y., Yang, Y., 2013a. Precise measurement of stable ( $\delta^{88/86}\text{Sr}$ ) and  
601 radiogenic ( $^{87}\text{Sr}/^{86}\text{Sr}$ ) strontium isotope ratios in geological standard reference materials using  
602 MC-ICP-MS. *Chinese Science Bulletin* 58, 3111-3118.

603 Ma, J., Wei, G., Liu, Y., Ren, Z., Xu, Y., Yang, Y., 2013b. Precise measurement of stable neodymium  
604 isotopes of geological materials by using MC-ICP-MS. *Journal of Analytical Atomic Spectrometry*  
605 28, 1926.

606 Ma, Q., Zheng, J.P., Xu, Y.G., Griffin, W.L., Zhang, R.S., 2015. Are continental “adakites” derived  
607 from thickened or foundered lower crust? *Earth and Planetary Science Letters* 419, 125-133.

608 Macpherson, C.G., Dreher, S.T., Thirlwall, M.F., 2006. Adakites without slab melting: High pressure  
609 differentiation of island arc magma, Mindanao, the Philippines. *Earth and Planetary Science*  
610 *Letters* 243, 581-593.

611 Mahood, G., Hildreth, W., 1983. Large partition coefficients for trace elements in high-silica rhyolites.  
612 *Geochimica et Cosmochimica Acta* 47, 11-30.

613 Matsui, Y., Onuma, N., Nagasawa, H., Higuchi, H. and Banno, S., 1977. Crystal structure control in  
614 trace element partition between crystal and magma. *Tectonics* 100, 315-324.

615 Mo, X., Niu, Y., Dong, G., Zhao, Z., Hou, Z., Zhou, S., Ke, S., 2008. Contribution of syncollisional  
616 felsic magmatism to continental crust growth: A case study of the Paleogene Linzizong volcanic  
617 Succession in southern Tibet. *Chemical Geology* 250, 49-67.

618 Nash, W., Crecraft, H., 1985. Partition coefficients for trace elements in silicic magmas. *Geochimica et*  
619 *Cosmochimica Acta* 49, 2309-2322.

620 Niu, Y., Batiza, R., 1997. Trace element evidence from seamounts for recycled oceanic crust in the  
621 Eastern Pacific mantle. *Earth and Planetary Science Letters* 148, 471-483.

622 Niu, Y., Regelous, M., Wendt, I.J., Batiza, R., O'Hara, M.J., 2002. Geochemistry of near-EPR  
623 seamounts: importance of source vs. process and the origin of enriched mantle component. *Earth*  
624 *and Planetary Science Letters* 199, 327-345.

625 Niu, Y., O'Hara, M.J., 2003. Origin of ocean island basalts: A new perspective from petrology,  
626 geochemistry, and mineral physics considerations. *Journal of Geophysical Research: Solid Earth*  
627 (1978–2012) 108.

628 Niu, Y., 2005. Generation and evolution of basaltic magmas: some basic concepts and a new view on  
629 the origin of Mesozoic–Cenozoic basaltic volcanism in eastern China. *Geological Journal of*  
630 *China Universities* 11, 9-46.

631 Niu, Y., O'Hara, M.J., 2009. MORB mantle hosts the missing Eu (Sr, Nb, Ta and Ti) in the continental  
632 crust: New perspectives on crustal growth, crust–mantle differentiation and chemical structure of  
633 oceanic upper mantle. *Lithos* 112, 1-17.

634 Niu, Y., Zhao, Z., Zhu, D.C., Mo, X., 2013. Continental collision zones are primary sites for net



635 continental crust growth — A testable hypothesis. *Earth-Science Reviews* 127, 96-110.

636 Pabst, A., 1928. Observations on inclusions in the granitic rocks of the Sierra Nevada. University of  
637 California Publications in Geological Sciences 17, 325-386.

638 Pearce, J.A., Norry, M.J., 1979. Petrogenetic implications of Ti, Zr, Y, and Nb variations in volcanic  
639 rocks. *Contributions to mineralogy and petrology* 69, 33-47.

640 Pietranik, A., Koepke, J., Puziewicz, J., 2006. Crystallization and resorption in plutonic plagioclase:  
641 Implications on the evolution of granodiorite magma (Gęsiniec granodiorite, Strzelin Crystalline  
642 Massif, SW Poland). *Lithos* 86, 260-280.

643 Prowatke, S., Klemme, S., 2006. Trace element partitioning between apatite and silicate melts.  
644 *Geochimica et Cosmochimica Acta* 70, 4513-4527.

645 Qian, Q., Hermann, J., 2013. Partial melting of lower crust at 10–15 kbar: constraints on adakite and  
646 TTG formation. *Contributions to Mineralogy and Petrology* 165, 1195-1224.

647 Rapp, R.P., Watson, E.B., 1995. Dehydration melting of metabasalt at 8–32 kbar: implications for  
648 continental growth and crust-mantle recycling. *Journal of Petrology* 36, 891-931.

649 Richards, J.P., Kerrich, R., 2007. Special paper: adakite-like rocks: their diverse origins and  
650 questionable role in metallogenesis. *Economic Geology* 102, 537-576.

651 Rodriguez, C., Selles, D., Dungan, M., Langmuir, C., Leeman, W., 2007. Adakitic dacites formed by  
652 intracrustal crystal fractionation of water-rich parent magmas at Nevado de Longavi Volcano  
653 (36.2° S; Andean Southern Volcanic Zone, Central Chile). *Journal of Petrology* 48, 2033-2061.

654 Ronov, A., Yaroshevsky, A., 1976. A new model for the chemical structure of the Earth's crust.  
655 *Geochemistry International* 13, 89-121.

656 Rudnick, R., Gao, S., 2003. Composition of the continental crust. *Treatise on geochemistry* 3, 1-64.

657 Schnetzler, C., Philpotts, J.A., 1970. Partition coefficients of rare-earth elements between igneous  
658 matrix material and rock-forming mineral phenocrysts—II. *Geochimica et Cosmochimica Acta* 34,  
659 331-340.

660 Sen, C., Dunn, T., 1994. Dehydration melting of a basaltic composition amphibolite at 1.5 and 2.0 GPa:  
661 implications for the origin of adakites. *Contributions to Mineralogy and Petrology* 117, 394-409.

662 Song, S., Su, L., Niu, Y., Zhang, L., Zhang, G., 2007. Petrological and geochemical constraints on the  
663 origin of garnet peridotite in the North Qaidam ultrahigh-pressure metamorphic belt, northwestern  
664 China. *Lithos* 96, 243-265.

665 Song, S., Niu, Y., Wei, C., Ji, J., Su, L., 2010a. Metamorphism, anatexis, zircon ages and tectonic  
666 evolution of the Gongshan block in the northern Indochina continent—An eastern extension of the  
667 Lhasa Block. *Lithos* 120, 327-346.

668 Song, S., Su, L., Li, X.H., Zhang, G., Niu, Y., Zhang, L., 2010b. Tracing the 850-Ma continental flood  
669 basalts from a piece of subducted continental crust in the North Qaidam UHPM belt, NW China.  
670 *Precambrian Research* 183, 805-816.

671 Song, S., Niu, Y., Su, L., Xia, X., 2013. Tectonics of the North Qilian orogen, NW China. *Gondwana*  
672 *Research* 23, 1378-1401.

673 Song, S., Niu, Y., Su, L., Wei, C., Zhang, L., 2014a. Adakitic (tonalitic-trondhjemitic) magmas  
674 resulting from eclogite decompression and dehydration melting during exhumation in response to  
675 continental collision. *Geochimica et Cosmochimica Acta* 130, 42-62.

676 Song, S., Niu, Y., Su, L., Zhang, C., Zhang, L., 2014b. Continental orogenesis from ocean subduction,  
677 continent collision/subduction, to orogen collapse, and orogen recycling: The example of the  
678 North Qaidam UHPM belt, NW China. *Earth-Science Reviews* 129, 59-84.

679 Streck, M.J., Leeman, W.P., Chesley, J., 2007. High-magnesian andesite from Mount Shasta: A product  
680 of magma mixing and contamination, not a primitive mantle melt. *Geology* 35, 351.

681 Sun, S.S., McDonough, W., 1989. Chemical and isotopic systematics of oceanic basalts: implications  
682 for mantle composition and processes. Geological Society, London, Special Publications 42,  
683 313-345.

684 Thomas, J., Bodnar, R., Shimizu, N., Sinha, A., 2002. Determination of zircon/melt trace element  
685 partition coefficients from SIMS analysis of melt inclusions in zircon. *Geochimica et*  
686 *Cosmochimica Acta* 66, 2887-2901.

687 Tseng, C.Y., Yang, H.J., Yang, H.Y., Liu, D., Wu, C., Cheng, C.K., Chen, C.H., Ker, C.M., 2009.  
688 Continuity of the North Qilian and North Qinling orogenic belts, Central Orogenic System of  
689 China: Evidence from newly discovered Paleozoic adakitic rocks. *Gondwana Research* 16,  
690 285-293.

691 Vernon, R., 1984. Microgranitoid enclaves in granites—globules of hybrid magma quenched in a  
692 plutonic environment. *Nature* 309, 438-439.

693 Vernon, R.H., 1983. Restite, xenoliths and microgranitoid enclaves in granites. *Journal and Proceedings*  
694 *of the Royal Society of New South Wales* 116, 77–103.

695 Wang, J., Wu, C., Cai, Z., Guo, Y., Wu, J., Liu, X., 2006a. Early Paleozoic high-Mg adakite from  
696 Yindongliang in the eastern section of the North Qilian: Implications for geodynamics and Cu-Au  
697 mineralization. *Acta Petrol Sinica* 22, 2655–2664. (in Chinese with English abstract)

698 Wang, Q., McDermott, F., Xu, J.F., Bellon, H., Zhu, Y.T., 2005. Cenozoic K-rich adakitic volcanic  
699 rocks in the Hohxil area, northern Tibet: Lower-crustal melting in an intracontinental setting.  
700 *Geology* 33, 465.

701 Wang, Q., Wyman, D.A., Xu, J.F., Zhao, Z.H., Jian, P., Xiong, X.L., Bao, Z.W., Li, C.F., Bai, Z.H.,  
702 2006b. Petrogenesis of Cretaceous adakitic and shoshonitic igneous rocks in the Luzong area,  
703 Anhui Province (eastern China): Implications for geodynamics and Cu–Au mineralization. *Lithos*  
704 89, 424-446.

705 Wang, Q., Wyman, D.A., Xu, J., Jian, P., Zhao, Z., Li, C., Xu, W., Ma, J., He, B., 2007. Early  
706 Cretaceous adakitic granites in the Northern Dabie Complex, central China: Implications for  
707 partial melting and delamination of thickened lower crust. *Geochimica et Cosmochimica Acta* 71,  
708 2609-2636.

709 Wang, Q., Wyman, D.A., Xu, J., Dong, Y., Vasconcelos, P.M., Pearson, N., Wan, Y., Dong, H., Li, C.,  
710 Yu, Y., Zhu, T., Feng, X., Zhang, Q., Zi, F., Chu, Z., 2008. Eocene melting of subducting  
711 continental crust and early uplifting of central Tibet: Evidence from central-western Qiangtang  
712 high-K calc-alkaline andesites, dacites and rhyolites. *Earth and Planetary Science Letters* 272,  
713 158-171.

714 Wang, Q., Li, X.H., Jia, X.H., Wyman, D., Tang, G.J., Li, Z.X., Ma, L., Yang, Y.H., Jiang, Z.Q., Gou,  
715 G.N., 2013. Late Early Cretaceous adakitic granitoids and associated magnesian and potassium -  
716 rich mafic enclaves and dikes in the Tunchang–Fengmu area, Hainan Province (South China):  
717 Partial melting of lower crust and mantle, and magma hybridization. *Chemical Geology* 328,  
718 222-243.

719 Wiedenbeck, M., Alle, P., Corfu, F., Griffin, W., Meier, M., Oberli, F., Quadt, A.v., Roddick, J., Spiegel,  
720 W., 1995. Three natural zircon standards for U-Th-Pb, Lu-Hf, trace element and REE analyses.  
721 *Geostandards newsletter* 19, 1-23.

722 Xiong, X.L., Adam, J., Green, T.H., 2005. Rutile stability and rutile/melt HFSE partitioning during

723 partial melting of hydrous basalt: Implications for TTG genesis. *Chemical Geology* 218, 339-359.

724 Xu, J.F., Shinjo, R., Defant, M.J., Wang, Q., Rapp, R.P., 2002. Origin of Mesozoic adakitic intrusive  
725 rocks in the Ningzhen area of east China: Partial melting of delaminated lower continental crust?  
726 *Geology* 30, 1111.

727 Xu, W., Gao, S., Wang, Q., Wang, D., Liu, Y., 2006. Mesozoic crustal thickening of the eastern North  
728 China craton: Evidence from eclogite xenoliths and petrologic implications. *Geology* 34, 721-724.

729 Yu, S., Zhang, J., Qin, H., Sun, D., Zhao, X., Cong, F., Li, Y., 2015. Petrogenesis of the early Paleozoic  
730 low-Mg and high-Mg adakitic rocks in the North Qilian orogenic belt, NW China: Implications for  
731 transition from crustal thickening to extension thinning. *Journal of Asian Earth Sciences* 107,  
732 122-139.

733 Zhang, C., Ma, C., Holtz, F., 2010. Origin of high-Mg adakitic magmatic enclaves from the Meichuan  
734 pluton, southern Dabie orogen (central China): Implications for delamination of the lower  
735 continental crust and melt-mantle interaction. *Lithos* 119, 467-484.

736 Zhang, J., Meng, F., Wan, Y., 2007. A cold Early Palaeozoic subduction zone in the North Qilian  
737 Mountains, NW China: petrological and U-Pb geochronological constraints. *Journal of*  
738 *Metamorphic Geology* 25, 285-304.

739 Zhang, Y., Niu, Y., Hu, Y., Liu, J., Ye, L., Kong, J., Duan, M., 2015. The syncollisional granitoid  
740 magmatism and continental crust growth in the West Kunlun Orogen, China - Evidence from  
741 geochronology and geochemistry of the Arkarz pluton. *Lithos*. [doi: 10.1016/j.lithos.2015.05.007](https://doi.org/10.1016/j.lithos.2015.05.007)  
742 (in press).

743

744 **Figure captions:**

745 **Fig.1:** (a) Simplified geological map of the North Qilian Orogen showing distributions of the main  
746 tectonic units (modified after Song et al., 2013; Chen et al., 2015). (b) Simplified map of the Qumushan  
747 (QMS) and Baojishan (BJS) area in the eastern section of the North Qilian Orogen. U-Pb ages are  
748 shown for granodiorite and MMEs in the BJS and QMS plutons from Chen et al. (2015), Yu et al.  
749 (2015) and this study as indicated.

750 **Fig. 2:** Photographs of the adakitic granodiorite and the MMEs in the field and in thin-sections. (a), (b)  
751 and (c) showing the sharp contact of MMEs of varying size with their host granodiorite with MMEs  
752 being finer-grained than the host; (d) showing the mineral assemblage of the adakitic host granodiorite  
753 (QMS12-02host) and (e), (f) showing the mineral assemblage of MMEs (QMS12-02MME,  
754 QMS12-06MME). Amp = amphibole; Bt = biotite; Pl= plagioclase; Qz = quartz; Ap = apatite; Zrn=  
755 zircon. Plates c-f are taken under cross-polarized light.

756 **Fig. 3:** Photomicrographs showing a plagioclase crystal with a high-Ca core rimmed by a euhedral  
757 overgrowth of low-Ca plagioclase in both (a) adakitic rocks (e.g., QMS12-04host) and (b) MMEs (e.g.,  
758 QMS12-04MME). Numerals are the An contents. See Appendix 2 for compositional data.

759 **Fig. 4:** Chemical compositions of amphiboles from the host granodiorite and MMEs in the amphibole  
760 classification diagram (Leake et al., 1997). Data from the host granodiorites and the MMEs of BJS  
761 pluton (Chen et al., 2015) are also shown for comparison.

762 **Fig. 5:** Concordia diagrams of LA-ICP-MS U-Pb zircon age data and representative CL images of  
763 zircon grains showing spots for the host adakitic granodiorites (a, c) and the MMEs (b, d) in the QMS  
764 pluton.

765 **Fig. 6:** Classification diagrams of the host granodiorites and the MMEs in the QMS pluton. (a) Total  
766 alkalis vs. SiO<sub>2</sub> (Le Maitre et al., 1989), (b) K<sub>2</sub>O vs. SiO<sub>2</sub>, and (c) A/NK vs. A/CNK. The blue circles  
767 and squares are data from BJS granodiorites and their MMEs (Chen et al., 2015), and the open circles  
768 are literature data on the QMS granodiorites (Wang et al., 2006a; Tseng et al., 2009; Yu et al., 2015).

769 **Fig. 7:** (a) Chondrite normalized REE patterns for the QMS host adakitic granodiorites and the MMEs;  
770 (b) host rock-normalized REE patterns of MMEs. Chondrite REE values and bulk continental crust  
771 (BCC) are from Sun and McDonough (1989) and Rudnick and Gao (2003), respectively. Shaded fields  
772 of BJS granodiorite and the MMEs are from Chen et al. (2015).

773 **Fig. 8:** Average ocean crust-normalized (OC; Niu and O'Hara, 2003) trace element patterns for the  
774 QMS host adakitic granodiorites and the MMEs.

775 **Fig. 9:** Plots of (a) Sr/Y vs. Y, where fields of adakite, and normal arc andesite-dacite-rhyolite are from  
776 Defant and Drummond (1990); (b) La/Yb vs. Yb, discrimination lines are from Richards and Kerrich  
777 (2007); (c) (Dy/Yb)<sub>N</sub> vs (La/Yb)<sub>N</sub>, and (d) Eu/Eu\* vs. Sr. Results in a-d using Rayleigh fractional  
778 crystallization models indicate the effects of garnet, amphibole, plagioclase, zircon and apatite  
779 fractionation on Sr/Y and Y (a), on La/Yb and Yb (b), on (Dy/Yb)<sub>N</sub> and (La/Yb)<sub>N</sub> (c), and on Eu/Eu\*  
780 and Sr (d). The partition coefficients used and modeling details are given in Appendix 6. Two  
781 crystallization models were designed to elucidate the effect of crystallization on bulk-rock (assumed to  
782 approximate melt) trace element systematics: (1) Model A, in reasonable agreement with observed  
783 mineral proportions of the MMEs, 50% amphibole, 40% plagioclase, 7.52% biotite, 2.2% apatite, 0.2%  
784 zircon and 0.03% sphene; (2) Model B, 50% amphibole, 40% plagioclase, 7.6% biotite, 2.4% garnet.  
785 Data sources for the QMS and BJS plutons are the same as in Fig. 6. Amp = amphibole; Bt = biotite;  
786 Pl= plagioclase; Ap = apatite; Zrn=zircon; Grt = garnet; Spn=sphene.

787 **Fig. 10:** SiO<sub>2</sub> variation diagrams of (a) MgO, (b) Fe<sub>2</sub>O<sub>3</sub><sup>T</sup>, (c) TiO<sub>2</sub>, (d) CaO, (e) MnO, (f) P<sub>2</sub>O<sub>5</sub>, (g) Eu,  
788 (h) Hf, (i) La/Sm, (j) <sup>87</sup>Sr/<sup>86</sup>Sr<sub>(t)</sub>, (k) ε<sub>Nd</sub>(t) and (l) ε<sub>Hf</sub>(t). Fractional crystallization trends in g–i: the  
789 inverse linear trend of SiO<sub>2</sub> versus Eu and Hf indicate the effects of plagioclase and zircon fractional  
790 crystallization, respectively. Because Sm is incorporated more easily than Hf in amphibole (Fujimaki et  
791 al., 1984; Klein et al., 1997), amphibole crystallization will cause Hf/Sm increase in residual magmas  
792 (i). Crustal contamination and (or) basalt-rhyolite mixing trend in j–l are after Wang et al. (2008). Data  
793 sources of the QMS and BJS pluton are the same as in Fig. 6. The average zircon ε<sub>Hf</sub>(t) isotopic data  
794 (6.2±2, 2σ) calculated from Yu et al. (2015) is also presented in l.

795 **Fig. 11:** (a) SiO<sub>2</sub> versus P<sub>2</sub>O<sub>5</sub>; (b) SiO<sub>2</sub> versus Zr. Data for Island arc basalt (n=284 for P and 277 for  
796 Zr), boninite (n=37 for P and 34 for Zr) and rhyolite (n=66 for P and 45 for Zr) are from the Georoc  
797 database (<http://georoc.mpch-mainz.gwdg.de/georoc/>). Dashed and solid lines in a-b are hypothetical  
798 mixing lines and linear trend defined the QMS granodiorite and their MMEs, respectively. Data sources  
799 of the QMS and BJS plutons are the same as in Fig. 6.

800 **Fig. 12:** Cartoon illustrating a possible scenario for MME formation. Earlier crystallized cumulate with  
801 the mineral assemblage of amphibole, biotite, plagioclase and accessory minerals such as zircon and  
802 apatite (a), which was later disturbed by subsequent magma replenishment in the magma chamber,  
803 constituting MMEs in the dominant host granodiorite.

804 **Fig. 13:** Plots of (a) SiO<sub>2</sub> versus Mg<sup>#</sup>; (b) Na<sub>2</sub>O versus K<sub>2</sub>O. Data sources: classical adakite, resulting  
805 from partial melting of subducted ocean crust in modern arcs, are from the GeoRoc database  
806 (<http://georoc.mpch-mainz.gwdg.de/georoc/>); Tibet Plateau (Chung et al., 2003; Wang et al., 2005),  
807 Dabie Orogen (He et al., 2013; Wang et al., 2007), Yangtze Craton (Xu et al., 2002; Wang et al.,  
808 2006b); North China Craton (Chen et al., 2013a; Ma et al., 2015) , experimental data (Sen and Dunn,



809 1994; Rapp and Watson, 1995. Data sources of the QMS and BJS plutons are the same as in Fig. 6.

810 **Fig. 14:** (a) Nd–Sr and (b) Nd-Hf isotope diagrams for the QMS adakitic rocks and their MMEs. The  
811 MORB data are from Niu and Batiza (1997) and Niu et al. (2002), other data sources are the same as  
812 Fig. 13. Binary isotope mixing calculations between North Qilian Ocean MORB (average composition:  
813 Sr=159.6 ppm, Nd=10.5 ppm, Hf=2.41,  $^{87}\text{Sr}/^{76}\text{Sr}_{(t)}=0.7054$ ,  $\epsilon_{\text{Nd}}(t)=5.44$ ,  $\epsilon_{\text{Hf}}(t)=9.93$ ) and Mohe  
814 Basement (average composition: Sr=586 ppm, Nd=32.97 ppm, Hf=3.44,  $^{87}\text{Sr}/^{76}\text{Sr}_{(t)}=0.7234$ ,  $\epsilon_{\text{Nd}}$   
815  $(t)=-19.80$ ,  $\epsilon_{\text{Hf}}(t)=-43.65$ ) are after Chen et al. (2015) and references therein.  
816  $K=[(\text{Sr}/\text{Nd})_{\text{MORB}}]/[(\text{Sr}/\text{Nd})_{\text{Mohe basement}}]$ , where  $K_{\text{max}}$ ,  $K_{\text{min}}$ , and  $K_{\text{average}}$  are the maximum, minimum and  
817 average values respectively.

818 **Fig. 15:** Shows 30%, 40%, 50% and 60% fractional crystallization of mineral assemblages of Model A  
819 and Model B from the assumed magma along with the BCC and QMS adakitic granodiorites and their  
820 MMEs on primitive mantle normalized multi-element diagram. The light red and green shaded regions  
821 are the field of QMS adakitic granodiorite and MMEs, respectively.

822 **Appendix Fig. S1:** Simplified phase diagram showing hydrous solidi of basalts and granitic rocks  
823 modified from Niu et al. (2013) (after Niu, 2005). The red line with arrow illustrates the concept of the  
824 underthrusting North Qilian oceanic crust evolve along a high T/P path as a result of retarded  
825 subducting and enhanced heating upon continental collision at a prior active continental margin setting.

826

#### 827 **Appendix tables captions:**

828 Appendix 1: U-Th-Pb analyses by LA-ICP-MS for zircons from host granodiorites (QMS12-04host and  
829 QMS12-10host) and the mafic magmatic enclaves (QMS12-04MME and QMS12-10MME).

830 Appendix 2: Microprobe analysis of representative plagioclase in the host granodiorites and the mafic

831 magmatic enclaves.

832 Appendix 3: Microprobe analysis of representative amphibole in the host granodiorites and the mafic

833 magmatic enclaves.

834 Appendix 4: Whole-rock major and trace elements analysis of the host adakitic granodiorites and the

835 mafic magmatic enclaves in the NQOB.

836 Appendix 5: Whole rock Sr-Nd-Hf isotopic analyses for the host adakitic granodiorites and the mafic

837 magmatic enclaves in the NQOB.

838 Appendix 6: Relevant partition coefficients, assumed melt and model compositions.

839

1 **Syn-collisional adakitic granodiorites formed by fractional crystallization:**  
2 **insights from their enclosed mafic magmatic enclaves (MMEs) in the Qumushan**  
3 **pluton, North Qilian Orogen at the northern margin of the Tibetan Plateau**

4 Shuo Chen <sup>a,b\*</sup>, Yaoling Niu <sup>a,c\*</sup>, Jiyong Li <sup>a,b</sup>, Wenli Sun <sup>a</sup>, Yu Zhang <sup>d</sup>, Yan Hu<sup>a,b</sup>, Fengli Shao <sup>a,b</sup>

5

6 <sup>a</sup> Institute of Oceanology, Chinese Academy of Sciences, Qingdao 266071, China.

7 <sup>b</sup> University of Chinese Academy of Sciences, Beijing 100049, China

8 <sup>c</sup> Department of Earth Sciences, Durham University, Durham DH1 3LE, UK

9 <sup>d</sup> School of Earth Sciences, Lanzhou University, Lanzhou 730000, China

10

11

12

13

14

15 **\*Corresponding authors:**

16 **Mr. Shuo Chen (chenshuo528@foxmail.com)**

17 **Professor Yaoling Niu (yaoling.niu@foxmail.com)**

18

19

20

21

22

23 **Abstract**

24       The Qumushan (QMS) syn-collisional granodiorite, which is located in the eastern section of the  
25 North Qilian Orogen at the northern margin of the Greater Tibetan Plateau, has typical adakitic  
26 characteristics and also contains abundant mafic magmatic enclaves (MMEs). This recognition offers  
27 an unprecedented insight into the petrogenesis of both the adakitic host granodiorite and the enclosed  
28 MMEs. The MMEs and their host granodiorites share many characteristics in common, including  
29 identical crystallization age (~430 Ma), same mineralogy, similar mineral chemistry and whole-rock  
30 isotopic compositions, indicating their genetic link. The MMEs are most consistent with being of  
31 cumulate origin formed at earlier stages of the same magmatic system that produced the QMS adakitic  
32 granodiorite. Subsequent replenishment of adakitic magmas could have disturbed the cumulate piles as  
33 “MMEs” dispersed in the adakitic granodiorite host during emplacement. The geochemical data and  
34 petrogenetic modeling of trace elements suggest that the QMS adakitic host granodiorite is most  
35 consistent with fractional crystallization dominated by the mineral assemblage of the MMEs. The  
36 parental magma for the QMS granodiorite is best explained as resulting from partial melting of the  
37 ocean crust together with recycled terrigenous sediments during continental collision, which may have  
38 also experienced interaction with mantle peridotite during ascent.

39 **Keywords:** Adakitic rocks; Mafic magmatic enclaves; Cumulate; Syn-collisional granodiorite; North  
40 Qilian Orogen

## 41 1. Introduction

42 “Adakite” was introduced by Defant and Drummond (1990) after the name of Adak Island in the  
43 Aleutian arc. It refers to a group of intermediate-felsic igneous rocks observed in modern oceanic and  
44 continental arcs genetically associated with seafloor subduction. They are characterized by high Sr,  
45 light rare earth elements (REEs), Sr/Y (>40) and La/Yb (>20), low Y and heavy REEs, and lack of  
46 obvious Eu anomalies. It was initially considered that adakites were derived by partial melting of  
47 young ( $\leq 25$ Myrs) and warm subducting/subducted ocean crust in subduction zones (Defant and  
48 Drummond, 1990). The origin of adakite has since been one of the most popular subjects of research in  
49 igneous petrology due to its use for tectonic finger-printing (see Castillo, 2006, 2012), yet recent  
50 studies have shown that adakite or rocks with adakitic compositions can be produced in various ways  
51 and in different settings (Castillo et al., 1999; Xu et al., 2002; Chung et al., 2003, 2005; Wang et al.,  
52 2005, 2007; Macpherson et al., 2006; RodrIguuez et al., 2007; Streck et al., 2007; He et al., 2013; Chen  
53 et al., 2013a; Song et al., 2014a). Because adakite is defined on the basis of certain trace element  
54 characteristics as detailed above, geochemistry in combination with experimental geochemistry has  
55 been widely used to discuss the petrogenesis of adakites and adakitic rocks (e.g., Defant and  
56 Drummond, 1990; Sen and Dunn, 1994; Castillo et al., 1999; Xu et al., 2002; Wang et al., 2005; Xiong  
57 et al., 2005; Castillo, 2006, 2012). However, a petrological approach is essential for petrological  
58 problems and is expected to offer insights into the petrogenesis of adakites and adakitic rocks. Indeed,  
59 mafic magmatic enclaves (MMEs) hosted in adakitic rocks have been recently recognized, and the  
60 processes of the MME formation may offer a fresh perspective on the petrogenesis of the adakitic host  
61 (e.g., RodrIguuez et al., 2007; Chen et al., 2013b).

62 In this paper, we report our petrological, mineralogical and geochemical analyses and

63 trace-element modeling on an MME-bearing adakitic pluton well exposed in the eastern section of the  
64 North Qilian orogenic belt (NQOB) (Fig. 1a). This pluton was previously studied using the “standard”  
65 geochemical method with the MMEs being overlooked (e.g., Wang et al., 2006a; Tseng et al., 2009; Yu  
66 et al., 2015). Here we present a simple but effective model of fractional crystallization to successfully  
67 address both the origin of MMEs and their host adakitic granodiorite.

## 68 **2. Geological setting**

69 The NW-SE-trending NQOB is located between the Alashan Block to the northeast and the Qilian  
70 Block to the southwest, and is offset to the northwest by the Altyn-Tagh Fault (Fig.1a). It is made up of  
71 Early Paleozoic subduction-zone complexes including ophiolitic melanges, blueschists and eclogites,  
72 Silurian flysch formations, Devonian molasse, and Carboniferous to Triassic sedimentary cover  
73 sequences (Fig. 1a) (Song et al., 2007, 2013; Zhang et al., 2007). It is composed of three subunits, i.e.,  
74 (1) the southern ophiolite belt, (2) the middle arc magmatic belt and (3) the northern back-arc basin  
75 ophiolite-volcanic belt (Fig. 1a) (Song et al., 2007, 2013; Zhang et al., 2007; Chen et al., 2014). It is  
76 generally accepted that the NQOB is an Early Paleozoic suture zone, which records a long tectonic  
77 history from seafloor spreading/subduction to the ultimate continental collision and mountain-building  
78 (see Song et al., 2013). The Qumushan (QMS) pluton we studied is about 60km<sup>2</sup> in outcrop located in  
79 the eastern section of the NQOB. It lies approximately 10 km southeast of the Baojishan (BJS) pluton  
80 (Fig.1b). The QMS pluton intruded the Ordovician sedimentary and metamorphic rocks of Yingou  
81 group (Fig.1b). MMEs are widespread in the host granodiorite (Fig. 2a).

## 82 **3. Analytical methods**

### 83 *3.1. Zircon U–Pb ages*

84 Zircons were separated by using combined methods of heavy liquid and magnetic techniques  
85 before hand-picking under a binocular microscope. The selected zircons were set in an epoxy mount  
86 that was polished to expose zircon interiors. Cathodoluminescence (CL) images were taken at China  
87 University of Geosciences in Wuhan (CUGW) to examine the internal structure of individual zircon  
88 grains. The zircon U-Pb dating was done using LA-ICP-MS at China University of Geosciences in  
89 Beijing (CUGB). The instrument consists of an Agilent 7500a quadrupole inductively coupled plasma  
90 mass spectrometry (ICP-MS) coupled with a UP-193 Solid-State laser (193 nm, New Wave Research  
91 Inc.). Laser spot size was set to be ~30µm. Zircon 91500 (Wiedenbeck et al., 1995) and a secondary  
92 standard zircon TEMORA (417 Ma) (Black et al., 2003) was used as an external standard. The  
93 analytical procedure is given in Song et al. (2010a). Isotopic ratios and element concentrations of  
94 zircons were calculated using GLITTER (ver. 4.4, Macquarie University). Common Pb correction was  
95 applied using the method of Andersen (2002). Results are given in ~~Appendix A~~[Appendix 1](#).

### 96 *3.2. Mineral compositions*

97 Mineral chemistry was determined using a JXA-8100 microprobe at Chang'an University, China.  
98 The operating conditions were a 15 kV accelerating potential with a probe current of 10 nA and the  
99 electron beam diameter of 1µm. Results are given in ~~Appendix B~~[Appendix 2](#) and ~~Appendix C~~[Appendix](#)  
100 [3](#).

101 *3.3. Major and trace elements*

102 The bulk-rock major and trace elements were analyzed using Leeman Prodigy inductively coupled  
103 plasma-optical emission spectroscopy (ICP-OES) and Agilent-7500a inductively coupled plasma mass  
104 spectrometry (ICP-MS) at CUGB, respectively. The analytical uncertainties are generally less than 1%  
105 for most major elements with the exception of TiO<sub>2</sub> (~1.5%) and P<sub>2</sub>O<sub>5</sub> (~2.0%). The loss on ignition  
106 was measured by placing 1 g of sample powder in the furnace at 1000°C for several hours before  
107 cooling in a desiccator and reweighing. The analytical details are given in Song et al. (2010b). The  
108 data are presented in [Table 1 Appendix 4](#).

109 *3.4. Whole-rock Sr-Nd-Hf isotopes*

110 Whole-rock Sr-Nd-Hf isotopic analyses were done in Guangzhou Institute of Geochemistry,  
111 Chinese Academy of Sciences (GIG-CAS). The rock powders were digested and dissolved in  
112 HF-HNO<sub>3</sub> acid mixtures and dried on a hot-plate. Sr-Nd-Hf fractions were separated using small Sr  
113 Spec resin columns to obtain Sr and Nd-Hf bearing fractions. Sr isotopic compositions were  
114 determined using a Neptune Plus multi-collector ICP-MS (MC-ICP-MS) following Ma et al. (2013a).  
115 Nd fractions were then separated by passing through cation columns followed by HDEHP columns.  
116 Separation of Hf from the matrix and rare earth elements was carried out using a combined method of  
117 Eichrom RE and HDEHP columns. Nd and Hf isotopic compositions were determined using a  
118 Micromass Isoprobe MC-ICP-MS following Li et al. (2009) and Ma et al. (2013b). Repeated analysis  
119 of NBS-987 run during the same period of sample analysis gave  $^{87}\text{Sr}/^{86}\text{Sr}=0.710283\pm 27$  (2 $\sigma$ , n=13).  
120 Repeated analysis of BHVO-2 and JB-3 during the same period of sample analysis yielded  $^{143}\text{Nd}/^{144}\text{Nd}$   
121  $0.512977\pm 14$  (2 $\sigma$ , n=8) and  $0.513053\pm 18$  (2 $\sigma$ , n=13), respectively. During the course of this study, the



122 mean  $^{176}\text{Hf}/^{177}\text{Hf}$  ratios for BHVO-2 and JB-3 are respectively  $0.283099 \pm 15$  ( $2\sigma$ ,  $n = 13$ ) and  $0.283216$   
123  $\pm 15$  ( $2\sigma$ ,  $n=6$ ). All measured  $^{87}\text{Sr}/^{86}\text{Sr}$ ,  $^{143}\text{Nd}/^{144}\text{Nd}$  and  $^{176}\text{Hf}/^{177}\text{Hf}$  ratios were normalized to  $^{86}\text{Sr}/^{88}\text{Sr}$   
124  $= 0.1194$ ,  $^{146}\text{Nd}/^{144}\text{Nd} = 0.7219$  and  $^{179}\text{Hf}/^{177}\text{Hf} = 0.7325$ , respectively. The USGS rock standards JB-3  
125 and BHVO-2 run with our samples give values consistent with the reported reference values (GeoREM,  
126 <http://georem.mpch-mainz.gwdg.de/>). Results are given in [Table 2 Appendix 5](#).

## 127 4. Petrography and mineral chemistry

### 128 4.1. Granodiorite

129 The QMS pluton is of granodioritic composition with a mineral assemblage of plagioclase (45  
130 vol. %–50 vol. %), quartz (35 vol. %–42 vol. %), amphibole (3 vol. %–10 vol. %), biotite (2 vol. %–10  
131 vol. %), minor K-feldspar, and accessory minerals such as apatite, sphene, zircon and Fe-Ti oxides (Fig.  
132 2d). Plagioclase crystals are euhedral to subhedral, and are of oligoclase composition with  $\text{An}_{12-24}$  (Fig.  
133 3a). Zoned-plagioclase crystals display normal zoning with more anorthitic cores rimmed by less calcic  
134 compositions (Fig. 3a). Amphibole is always present as euhedral to subhedral crystals despite the  
135 variably small abundances (Fig. 2d). Amphibole grains are usually homogeneous and rarely display  
136 disequilibrium textures. Amphiboles from the host granodiorite can be classified as edenite ([Appendix](#)  
137 [Appendix 3](#), Fig. 4) following Leake et al. (1997). They have medium  $\text{SiO}_2$ , and low  $\text{TiO}_2$  (0.37–1.24  
138 wt. %),  $\text{Na}_2\text{O}$  (0.87–1.48 wt. %) and  $\text{K}_2\text{O}$  (0.29–1.69 wt. %).

### 139 4.2. Mafic magmatic enclave

140 MMEs are abundant in the QMS pluton (Fig. 2a), showing varying shape and size from  
141 centimeters to tens of centimeters in diameter (Fig. 2a). They differ from the host by having finer

142 grain-size (Figs. 2a-c), but have the same mineralogy albeit with greater mafic modes (e.g., 35-50 vol.%  
143 amphibole, 5-15 vol.% biotite, 40-50 vol.% plagioclase, minor quartz, K-feldspar, along with accessory  
144 minerals such as apatite, sphene, zircon and Fe-Ti oxides), thus giving a dioritic bulk composition.  
145 Plagioclase mostly occurs as subhedral grains with compositions similar to those in the host  
146 granodiorite. Zoned-plagioclase in the MMEs shows a compositional continuum with cores slightly  
147 more anorthitic than the rims (Fig. 3b). Amphibole in the MMEs is compositionally identical to that in  
148 the host granodiorite (Fig. 4). Biotite is yellow brown with subhedral to euhedral forms. The MMEs  
149 show no chilled margins nor textures of crystal resorption or reactive overgrowth. These rocks mainly  
150 exhibit porphyritic-like textures.

## 151 **5. Results**

### 152 *5.1. Zircon U–Pb ages*

153 Four samples (2 host-MME pairs) were chosen for dating. In CL images (Figs. 5a, c), zircons from  
154 the host granodiorites (QMS12-04host and QMS12-10host) are transparent, colorless, and mostly  
155 euhedral columnar crystals of varying size (~150-300µm long with length/width ratio of 1:1-3:1) with  
156 well-developed oscillatory zoning. The zircons have varying U (~ 28-386 ppm) and Th (~ 69-423 ppm)  
157 with Th/U ratio of 0.3-1.4. All these characteristics are consistent with the zircons being of magmatic  
158 origin (Hoskin and Schaltegger, 2003). After excluding discordant ages, zircons from the two host  
159 granodiorite samples yielded weighted mean  $^{206}\text{Pb}/^{238}\text{U}$  ages of  $429.7 \pm 2.5$  Ma ( $1\sigma$ , MSWD=0.15, n=23)  
160 and  $431.5 \pm 2.6$  Ma ( $1\sigma$ , MSWD=0.19, n=20), respectively (Figs. 5a, c), representing the crystallization  
161 age (~430 Ma) of the host granodiorite. These age data are in agreement with those in the literature  
162 (Tseng et al., 2009; Yu et al., 2015).

163 Zircons from the MMEs (QMS12-04MME and QMS12-10MME) show similar optical properties  
164 to those in the host with oscillatory zoning (Figs. 5b, d) and varying size (~150-200µm in length  
165 length/width ratio of ~ 1:1-2:1). They have varying Th (27-548 ppm), U (50-541 ppm), and Th/U  
166 (0.1-2.4). They are also of magmatic origin. Zircons in the 2 MMEs yielded the same weighted mean  
167 ages as zircons in the host within error, i.e. 429.6 ±2.8 Ma (1σ, MSWD=0.48, n=18) and 431.2 ±2.8 Ma  
168 (1σ, MSWD=0.2, n=19), respectively (Figs. 5b, d).

## 169 5.2. Major and trace elements

170 Eleven representative QMS granodiorite samples and their hosted MMEs (including 5 host-MME  
171 pairs) were analyzed for whole-rock major and trace element compositions ([Table 4 Appendix 4](#)). The  
172 granodiorite samples have high SiO<sub>2</sub> (64.37-65.49 wt.%), Al<sub>2</sub>O<sub>3</sub> (16.09-17.61 wt.%), Na<sub>2</sub>O (4.86-5.12  
173 wt.%) and Na<sub>2</sub>O/K<sub>2</sub>O (2.11-3.82) with medium total alkalis (Na<sub>2</sub>O+K<sub>2</sub>O = 6.46-7.25 wt.%), and plot in  
174 the granodiorite field (Fig. 6a). They have low Fe<sub>2</sub>O<sub>3</sub><sup>T</sup> (2.86-3.43 wt.%), MgO (2.14-2.60 wt.%) and  
175 CaO (3.60-4.10 wt.%). They are calc-alkaline (Fig. 6b) and metaluminous to weakly peraluminous  
176 (A/CNK= 0.93 to 1.03) (Fig. 6c), which is typical for I-type granitoids (Chappell and White, 1992). In  
177 contrast, the MMEs plot in the fields of diorite, monzodiorite and monzonite (Fig. 6a). They are  
178 compositionally high-K calc-alkaline to calc-alkaline (Fig. 6b), and metaluminous with A/CNK ranging  
179 from 0.74 to 0.84 (Fig. 6c). They have lower SiO<sub>2</sub> (52.06-58.59 wt.%), higher Fe<sub>2</sub>O<sub>3</sub><sup>T</sup> (6.12-8.50 wt.%),  
180 MgO (5.09-7.22 wt.%), CaO (4.99-6.57 wt.%), P<sub>2</sub>O<sub>5</sub> (0.49-1.01 wt.%), and slightly higher Mg<sup>#</sup>  
181 (0.63-0.68; Mg<sup>#</sup>=Mg/[Mg+Fe<sup>2+</sup>]) than the host granodiorites.

182 In the chondrite-normalized REE diagram, the QMS granodiorite samples are characterized by a  
183 relatively flat heavy REE (HREE) pattern ([Dy/Yb]<sub>N</sub> = 1.32-1.54), slightly negative to positive Eu

184 anomalies ( $\text{Eu}/\text{Eu}^*=0.88-1.13$ ), and lower total REE contents ( $\Sigma\text{REE}=76-134$  ppm) than the hosted  
185 MMEs. The REE patterns of the QMS granodiorites are similar to the field defined by the BJS  
186 granodiorites (cf. Chen et al., 2015) (Fig. 7), but display greater light REE (LREE) enrichment  
187 ( $[\text{La}/\text{Sm}]_N = 4.77-5.36$ ). The MMEs show similar REE patterns, but have significantly higher HREEs  
188 (Fig. 7a, b), which is consistent with greater modes of REE-enriched minerals (e.g., amphibole, apatite  
189 and zircon). They have negative Eu anomalies ( $\text{Eu}/\text{Eu}^*=0.6-0.8$ ).

190 In the multi-element spider diagram (Fig. 8), the host granodiorite and MMEs both show  
191 enrichment of large ion lithophile elements (LILE, e.g., P, K, Pb) and depletion in high field strength  
192 elements (HFSE, e.g., Nb, Ta and Ti). Sr appears to have a positive anomaly in the host  
193 ( $\text{Sr}/\text{Sr}^*=1.66-2.96$ ), but varying anomalies for the MMEs ( $\text{Sr}/\text{Sr}^*=0.5-1.19$ ). In particular, compared to  
194 the BJS granodiorites (Chen et al., 2015), the QMS granodiorite samples have adakitic signatures with  
195 high Sr/Y and La/Yb ratios, and lower Y and Yb abundances, thus plotting in the adakite fields in the  
196 discrimination diagrams (Figs. 9a-b), while most MMEs plot in the normal arc rock field.

### 197 5.3. Sr-Nd-Hf isotopic geochemistry

198 Whole-rock Sr-Nd-Hf isotopic compositions for the MMEs and their host granodiorite are given in  
199 [Table 2Appendix 5](#). The initial  $^{87}\text{Sr}/^{86}\text{Sr}_{(t)}$ ,  $\epsilon_{\text{Nd}}(t)$  and  $\epsilon_{\text{Hf}}(t)$  values are calculated at 430 Ma using the  
200 zircon age data (see Fig. 5 above). On the plots of  $^{87}\text{Sr}/^{86}\text{Sr}_{(t)}$ ,  $\epsilon_{\text{Nd}}(t)$  and  $\epsilon_{\text{Hf}}(t)$  against  $\text{SiO}_2$  (Figs.  
201 10j-l), both host granodiorite and MME samples are indistinguishable and overlapping within a narrow  
202 range (also see [Table 2Appendix 5](#)).

203 On  $\text{SiO}_2$ -variation diagrams (Fig. 10), the MMEs and their host granodiorite define linear trends  
204 for most elements (e.g.,  $\text{TiO}_2$ ,  $\text{Fe}_2\text{O}_3^T$ , MnO, MgO, CaO,  $\text{P}_2\text{O}_5$ , Eu and Hf abundances) and trace

205 element ratio (e.g., Hf/Sm) (Figs. 10a-i), but show no correlations of initial Sr, Nd, and Hf isotopic  
206 compositions with SiO<sub>2</sub> (Figs. 10j-l).

## 207 **6. Discussion**

### 208 *6.1. Petrogenesis of the mafic magmatic enclaves*

209 Several models have been proposed for the origin of MMEs in the literature, including foreign  
210 xenoliths (usually country rocks; e.g., Vernon, 1983; Xu et al., 2006), refractory and residual phase  
211 assemblages derived from granitoid sources (e.g., the restite model; Chappell et al., 1987; Chappell and  
212 White, 1991), chilled material or cumulate of early-formed co-genetic crystals (e.g., Dodge and Kistler,  
213 1990; Dahlquist, 2002; Donaire et al., 2005; Rodriguez et al., 2007; Niu et al., 2013; Huang et al., 2014;  
214 Chen et al., 2015), and basaltic melt material incompletely digested and homogenized during a magma  
215 mixing process (e.g., Vernon, 1983; Didier, 1987; Castro et al., 1990; Dorais et al., 1990; Barbarin and  
216 Didier, 1991; Chappell and White, 1991; Barbarin, 2005; Chen et al., 2009a, 2013b; Wang et al., 2013).  
217 We critically evaluate these interpretations below.

#### 218 *6.1.1. Textural and chemical relationships of the MMEs and their hosts*

219 The textural and chemical relationships of the QMS MMEs and their host granodiorite concur  
220 with the findings for the BJS pluton (Chen et al., 2015), and are summarized as follows: (1) the MMEs  
221 in the QMS granodiorites are ellipsoidal, or elongate, show no chilled margins, no textures of crystal  
222 resorption nor reactive overgrowth, but exhibit typical magmatic texture (Figs. 2a-f); (2) they have a  
223 mineral assemblage identical to, and more mafic phases than, their host granodiorite (Figs. 2c-f); (3)  
224 they have mineral compositions (e.g., amphibole and plagioclase) identical to those of their host (Fig.

225 3-4); (4) they have the same age (~430 Ma) as their host (Fig. 5); (5) their different major and trace  
226 element abundances from their hosts are controlled largely by mineral modal proportions, i.e., MMEs  
227 have greater modes of REE-enriched minerals (amphibole, apatite and zircon) and thus have higher  
228 MgO, Fe<sub>2</sub>O<sub>3</sub>, CaO and trace elements easily incorporated into these phases (e.g., TiO<sub>2</sub>, P<sub>2</sub>O<sub>5</sub>, Hf and  
229 HREEs) (Figs. 10a-i); and (6) more importantly, they have overlapping and indistinguishable Sr-Nd-Hf  
230 isotopes with their host granodiorite (Figs. 10j-l).

231 Any successful models for the origin of MMEs must be consistent with these observations.  
232 Models for MMEs as foreign xenoliths from country rocks (e.g., Xu et al., 2006) can be readily rejected,  
233 as there is no evidence of reaction textures for the MMEs. Likewise, the identical age (~430 Ma) of the  
234 MMEs and their host as well as the magmatic textures, constitute a strong argument against the restite  
235 origin (e.g., Chappell et al., 1987). In addition, the MMEs do not contain peraluminous minerals and  
236 their metaluminous composition (Fig. 6c) also excludes their derivation by melting of peraluminous  
237 restites (Barbarin, 2005). Therefore, the most straightforward interpretation is that the MMEs and their  
238 hosts formed as different products of a common magmatic system.

#### 239 *6.1.2. Assessing the origin of magma mixing*

240 Similar observations mentioned above between the MMEs and their host granitoids have been  
241 identified first by Pabst (1928) and by many others since then. The MMEs were thus described as  
242 “autoliths”, referring to “cogenetic” or part of the same system. Despite the “autoliths” nature of the  
243 MMEs with the host, this interpretation has been questioned: (1) Why are isotopic values of some  
244 MMEs intermediate between those of crustal and mantle materials (e.g., DePaolo, 1981; Barbarin,  
245 2005)? (2) Why are the MMEs fine-grained (e.g., Barbarin and Didier, 1991)? Because of these

246 questions, a model of magma mixing between mantle-derived mafic magma and crust-derived felsic  
247 magma was proposed to address the above issues: (1) the intermediate isotopic values of the MMEs  
248 were commonly interpreted as the result of magma mixing between a mantle-derived mafic magma and  
249 a crust-derived felsic magma, because a mafic magma derived from upper mantle provides not only  
250 material but also the heat necessary for melting and subsequently mixing with the crustal rocks (e.g.,  
251 Barbarin, 2005); (2) the fine-grained MMEs were interpreted as due to quenching against host felsic  
252 magmas (e.g., Vernon, 1984; Furman and Spera, 1985; Barbarin, 2005), owing to their higher liquidus  
253 and solidus temperatures compared to felsic magmas. As a result, the magma mixing model has been  
254 the most popular interpretation for the petrogenesis of the MMEs (see critical review by Niu et al.,  
255 2013).

256       Actually, there are many compelling lines of evidence for magma mixing in many granitoids,  
257 especially (1) where a clear isotopic contrast exists between the MMEs and the hosts (e.g., Holden et  
258 al., 1987; Chen et al., 2009b; Liu et al., 2013); and (or) (2) where disequilibrium features occur in the  
259 MMEs, e.g., complex zoning of clinopyroxene crystals that have distinctly low-MgO cores surrounded  
260 by high-MgO rims (e.g., Chen et al., 2013a; Wang et al., 2013), or resorption textures or reversed  
261 zoning of plagioclase (Pietranik et al., 2006; Chen et al., 2009a, 2009b). In the case of our study,  
262 however, none of the above has been observed. Instead, many lines of evidence argue against the  
263 magma mixing origin.

264       First, the MMEs and their host granodiorites in the QMS pluton have overlapping and  
265 indistinguishable Sr-Nd-Hf isotopes (vs. isotopic contrast in magma mixing model). In spite of this,  
266 some authors would still argue that the isotopic and mineral compositional similarity between the  
267 enclaves and the host could result from chemical and isotopic equilibration during magma mixing, (e.g.,

268 Dorais et al., 1990; Barbarin, 2005; Chen et al., 2009b; Zhang et al., 2010) using some experimental  
269 interpretations that isotopic equilibration is generally more easily achieved than chemical equilibration  
270 (Leshner, 1990). However, we emphasize that it is physically unlikely that isotopes become  
271 homogenized whereas major and trace elements are not (Niu et al., 2013), because isotopes are “carried”  
272 by the relevant chemical elements and isotopic diffusion cannot take place without the diffusion of the  
273 “carrying” elements (Chen et al., 2015). In fact, there are two forceful arguments against thermal and  
274 chemical equilibration: (1) the MMEs exhibit no textures of crystal resorption or reactive overgrowth  
275 (Figs. 2b-c), and (2) plagioclase in the MMEs and their host granodiorite shows no compositional or  
276 textural disequilibrium (Fig. 3). In addition, although the fine-grained texture of the MMEs could be  
277 interpreted as resulting from quenching in the magma mixing model, quenching of the mafic magma  
278 would lead to a significantly high viscosity contrast between the solidified enclaves and the felsic host  
279 magma, thereby inhibiting deformation, mechanical mixing (Caricchi et al., 2012; Farner et al., 2014)  
280 and isotope homogenization between the MMEs and the host.

281       Second, strongly correlated variations between major and trace elements (Figs. 10a-i) are  
282 consistent with modal mineralogy control, as the result of magma evolution (i.e., the MMEs are  
283 cumulate and the host represents residual melt) rather than mixing of two magmas with entirely  
284 different origins because magma mixing is a complex, multi-stage process in which linear trends can be  
285 disturbed (e.g., Clemens, 1989; Donaire et al., 2005; Chen et al., 2015). Moreover, the distinctive high  
286 abundances of some elements in the MMEs, such as Zr and P (Fig. 11), cannot be explained by magma  
287 mixing because these elements are controlled by the presence of accessory phases, such as zircon and  
288 apatite. As shown in Fig. 11, mantle derived basaltic magmas would have much lower Zr and P<sub>2</sub>O<sub>5</sub> than  
289 in the QMS MMEs. For example, quantitative calculations by Lee and Bachmann (2014) suggested that



290 10-20% melting of an upper mantle with 5 ppm Zr and 0.019 wt.% P<sub>2</sub>O<sub>5</sub> (equivalent to that estimated  
291 for depleted mid-ocean ridge basalt mantle), would yield primary liquids with 25-50 ppm Zr and  
292 0.1-0.2 wt.% P<sub>2</sub>O<sub>5</sub>. These concentrations are much lower than in the QMS MMEs. Additionally,  
293 boninites are thought to result from partial melting of highly depleted harzburgitic mantle peridotites  
294 induced by subduction-zone slab dehydration (Niu, 2005), but they also have lower Zr and P<sub>2</sub>O<sub>5</sub>  
295 contents (Fig. 11). More importantly, magma mixing between a basalt with any silicic end-member  
296 (e.g., rhyolite) would generate a mixing array (Figs. 11a-b, the dash lines) totally different from the  
297 linear trend (Figs. 11a-b, the solid lines) defined by the QMS granodiorite and their MMEs. In contrast,  
298 all of these observations are consistent with the interpretation that the MMEs represent earlier cumulate  
299 with greater amounts of zircon and apatite than their hosts (e.g., Donaire et al., 2005).

### 300 *6.1.3. Formation of the mafic magmatic enclaves*

301 The foregoing observations, illustrations and discussion leave us with the best interpretation that  
302 the MMEs represent the earlier crystallized cumulate that were later disturbed by subsequent melt  
303 replenishment and induced magma convection in the magma chamber. As illustrated in Fig. 12, when a  
304 primitive magma body is emplaced into a cold environment (e.g., developing a magma chamber) with  
305 the wall-rock having temperatures below the liquidus of the magma, magma quench and rapid  
306 crystallization are inevitable because of the thermal contrast. For an andesitic primitive magma parental  
307 to the syn-collisional granitoids (Niu et al., 2013), the first major liquidus phases would be amphibole,  
308 biotite, plagioclase and accessory minerals such as zircon and apatite, and rapid quench will facilitate  
309 abundant nucleation without between-nuclei space for rapid growth, thus resulting in the formation of  
310 fine-grained cumulate (Chen et al., 2015). This is a fundamentally important petrologic concept with

311 which any interpretation must comply. This early formed fine-grained mafic cumulate piles (largely  
312 plastic before complete solidification) can be readily disturbed by subsequent magma replenishment  
313 and induced convection, resulting in the dispersion of the MMEs in the host granodiorite.

## 314 *6.2 Petrogenesis of QMS adakitic granodiorite*

### 315 *6.2.1 Implication from the MMEs*

316 Recently, mixing of basaltic and felsic magmas was proposed for the genesis of some high-Mg  
317 and low SiO<sub>2</sub> adakitic rocks from Mount Shasta and the North China Craton using the presence of  
318 ubiquitous MMEs as evidence (Chen et al., 2013b) and also based on the disequilibrium petrographic  
319 characteristics in high-Mg andesites (Streck et al., 2007; Chen et al., 2013a). This interpretation could  
320 be reasonable, but it is not the case here because there is no petrographic and compositional evidence  
321 for magma mixing as elaborated above. That is, the MMEs in the QMS adakitic granodiorite are not  
322 evidence for magma mixing, but rather they are of cumulate origin without direct asthenospheric  
323 mantle participation (e.g., Dahlquist, 2002). More importantly, the MMEs comprise dominantly  
324 amphibole and plagioclase, which are common cumulate minerals of andesitic melts. If the parental  
325 melts were basaltic, the typical cumulate from such evolved basaltic melt would be gabbro dominated  
326 by clinopyroxene and plagioclase (Chen et al., 2015). It can be inferred from this important petrological  
327 concept that the parental magmas of the MMEs and their host granodiorite was mafic andesitic (Niu et  
328 al., 2013; Chen et al., 2015).

### 329 *6.2.2 Assessing the model of melting of mafic lower continental crust*

330 To date, some intra-continental high-MgO or -Mg<sup>#</sup> (also high Cr and Ni contents) adakitic rocks

331 have been considered to originate from melting of delaminated lower crust (e.g., Xu et al., 2002; Gao et  
332 al., 2004; Wang et al., 2006b). By accepting and applying this model, it has been previously interpreted  
333 that the QMS adakitic rocks were derived from delaminated lower crust, and they subsequently  
334 interacted with mantle peridotite during ascent (Tseng et al., 2009; Yu et al., 2015). Although this  
335 model seems plausible and applicable to the QMS adakitic rocks, it has more difficulties than  
336 certainties. First, the QMS adakitic granodiorites have lower  $(Dy/Yb)_N$ ,  $(La/Yb)_N$ , and distinctive low  
337  $K_2O/Na_2O$  ratios (Fig. 13b), which are significantly different from the composition of adakitic rocks  
338 inferred to be derived from partial melting of the thickened or delaminated lower continental crust.  
339 Second, the Nd and Hf isotopic data of the QMS adakitic granodiorite indicate a significant mantle  
340 input, which is also inconsistent with those of lower continental crust origin (Fig. 14a). Finally, the  
341 existence of the Paleo-Qilian ocean is manifested by the ophiolites and eclogites in the North Qilian  
342 orogenic belt; the ocean basin started its subduction at ~520 Ma, and was eventually closed at the end  
343 of the Ordovician (~445 Ma) followed by continental collision (see Song et al., 2013). Accordingly,  
344 the coeval (~430 Ma) MMEs and their adakitic host granodiorite of the QMS pluton are best  
345 interpreted as a magmatic response to the collision between the Qilian-Qaidam block and Alashan  
346 block, thereby being contrary to the environment of crustal extension required by a delaminated lower  
347 crustal origin. In fact, continuous lithosphere extension and delamination in the NQOB occurred at  
348 <400 Ma, which resulted in strong magmatic activity and formed a number of  
349 diorite-granodiorite-granite plutons with ages of ~400–360 Ma (Song et al., 2013, 2014b).

### 350 6.2.3 A fractional crystallization model for the petrogenesis of the QMS adakitic granodiorites

351 An origin of adakitic rocks by fractional crystallization has been proposed in the literature.

352 However, it should be noted that all these crystallization models require basaltic parental magmas  
353 derived from the metasomatized mantle wedge in arc settings, such as in the complex Philippine arc  
354 (Castillo et al., 1999; Macpherson et al., 2006) and Ecuadorian Andes (Chiaradia et al., 2004). It is  
355 important to note that our crystallization model differs from the basaltic magma crystallization model  
356 of arc magmas in the literature.

357 In our model, the magmas parental to the MMEs and their host granodiorite are the same mafic  
358 andesitic magmas in a syn-collisional setting, rather than basaltic magmas in an arc setting of active  
359 seafloor subduction advocated in the literature (e.g., Macpherson et al., 2006). That is, the QMS  
360 adakitic granodiorites are products of fractional crystallization dominated by the mineral assemblage  
361 indicated by the MMEs from mafic andesitic magmas. We can further consider two fractional  
362 crystallization models to elucidate the effect of crystallization of the observed mineralogy on trace  
363 elements using closed-system Rayleigh fractionation equation: (1) Model A, in reasonable agreement  
364 with observed mineral proportions of the MMEs, 50% amphibole, 40% plagioclase, 7.52% biotite, 2.2%  
365 apatite, 0.2% zircon and 0.03% sphene; (2) Model B, which incorporates fractionation of garnet, 50%  
366 amphibole, 40% plagioclase, 7.6% biotite, 2.4% garnet. The partition coefficients used in the  
367 calculations are for intermediate-felsic magmas ([Table 3Appendix 6](#)). For convenience (see below), the  
368 assumed parental magma ([Table 3Appendix 6](#)) is very similar to the bulk continental crust (BCC)  
369 composition (Rudnick and Gao, 2003) (Fig. 15), which is the same as the ~ 60 Ma Linzizong andesite  
370 in southern Tibet (Mo et al., 2008; Niu et al., 2013), in terms of major and trace element abundances.

371 Notably, removal of garnet would yield a smooth decrease of LREE-to-HREE pattern (Richards  
372 and Kerrich, 2007) with elevated  $(Dy/Yb)_N$  and  $(La/Yb)_N$  in the evolving melt (Fig. 9c). However, the  
373  $(Dy/Yb)_N$  ratio in the QMS adakitic granodiorites remain constant with increasing  $(La/Yb)_N$  (Fig. 9c),

374 which indicate that the effect of garnet fractionation in generating the QMS adakitic granodiorites is  
375 unimportant. Simple modal calculation of fractional crystallization using Model B indicates that the  
376 participation of garnet is no more than 3% (Fig. 9), but the low garnet proportion in combination with a  
377 large amount of amphibole-plagioclase fractionation can hardly generate the adakitic signature shown  
378 in the QMS pluton (Figs. 9a-b). Besides, mineralogically, garnet has been observed neither in the QMS  
379 MMEs and their host adakitic granodiorite, nor in the coeval igneous rocks in the eastern section of the  
380 NQOB. In addition, our preferred source for the QMS MMEs and their host adakitic granodiorite is  
381 partial melting of the ocean crust at amphibolite facies conditions (<40km) (Mo et al., 2008; Niu and  
382 O'Hara, 2009; Niu et al., 2013) (see below), rather than the presence of garnet as a residual phase at  
383 garnet amphibolite or eclogite conditions.

384 It is also impossible to generate QMS adakitic granodiorites by fractionation of  
385 amphibole-plagioclase alone, because they trend to produce concave-upwards patterns between the  
386 MREE and HREE and lead to decreasing  $(Dy/Yb)_N$  with increasing  $(La/Yb)_N$  (Fig. 9c), owing to the  
387 affinity of calcic amphiboles for MREEs over the HREEs (Klein et al., 1997). Additionally, removal of  
388 amphibole-plagioclase would result in negative Eu anomalies in the residual melts, which is  
389 inconsistent with QMS adakitic granodiorites (Fig. 9d). In the case of our study, we emphasize that the  
390 widespread accessory minerals such as zircons and apatites in both QMS host adakitic granodiorite and  
391 particularly their cumulate MMEs played a significant role in generating QMS adakitic granodiorites.  
392 For example, zircon fractionation would increase  $(Dy/Yb)_N$  (Fig. 9c) and the La/Yb and Sr/Y ratios of  
393 residue magmas (Figs. 9a-b), because  $Kd_{zircon}^{Dy/Yb} = 0.140$ , and  $Kd_{zircon}^{La/Yb} = 0.005$  (Bea et al., 1994).  
394 Apatite fractionation can also increase the Sr/Y ratio (Figs. 9a-b), but decrease  $(Dy/Yb)_N$  (Fig. 9c).  
395 Importantly, apatite fractionation would increase Eu/Eu\* (Fig. 9d), because  $Kd_{apatite}^{Sm} = 46$ ,

396  $Kd_{apatite}^{Eu} = 25.5$ ,  $Kd_{apatite}^{Gd} = 43.9$  (Fujimaki et al., 1984). Note that the simple calculation of Model A  
397 (Table 3 Appendix 6; Figs. 9 and 15), which involves a small proportion of zircon, apatite and sphene in  
398 combination with amphibole, biotite and plagioclase to form the fractionation assemblage can explain  
399 the characteristics of the QMS adakitic granodiorites. Although uncertainties exist for mineral partition  
400 coefficients, our model offers insights into the petrogenesis of the adakitic granodiorite as well as the  
401 enclosed MMEs in syn-collisional environments.

### 402 6.3 Constraints on the source

403 As discussed above, the primary magmas parental to the MMEs and their host granodiorite are  
404 most consistent with mafic andesitic magmas of ocean crust origin during continental collision. In  
405 addition, our new data and the whole-rock Sr-Nd and zircon Hf isotopic data in the literature on the  
406 QMS pluton (Tseng et al., 2009; Yu et al., 2015) exhibit quite uniform Sr-Nd-Hf composition (Figs.  
407 10j-l). Though the radiogenic Sr and slightly unradiogenic Nd isotopes indicate the input of crustal  
408 materials, the whole-rock  $\epsilon_{Hf}(t)$  values (+5.5 to +8.4) of this study and the zircon  $\epsilon_{Hf}(t)$  values (+4.2 to  
409 +7.7) in the literature (Yu et al., 2015) are indicative of significant mantle input or juvenile mafic  
410 continental crust derived from the mantle in no distant past (Zhang et al., 2015). As noted above, many  
411 adakitic rocks can be generated from the lower continental crust, but this is not applicable in our study  
412 (see above). In our case, the most likely source for the andesitic magmas with inherited mantle isotopic  
413 signatures parental to the QMS pluton is partial melting of the remaining part of the North Qilian ocean  
414 crust (Chen et al., 2015). On the other hand, contribution from continental crust is also required. This  
415 may occur in the melting region or in an evolving magma chamber rather than simple crustal level  
416 assimilation, because the Sr-Nd-Hf isotopes for the MMEs and their host granodiorites are closely

417 similar and show a respectively narrow range of variation, and they do not show correlated variations  
418 with SiO<sub>2</sub> (Figs. 10j-l). Melting of recycled terrigenous sediments of upper continental crust and  
419 remaining part of the North Qilian oceanic crust in the melting region is more likely (Mo et al. 2008;  
420 Niu and O'Hara 2009; Chen et al., 2015).

421 In the broad context of the continental collision, the model of partial melting of the remaining part  
422 of the ocean crust and the recycled terrigenous sediments has been proposed and tested by Niu and  
423 co-workers in southern Tibet, East Kunlun and Qilian Orogenic Belts (e.g., Mo et al., 2008; Niu and  
424 O'Hara, 2009; Niu et al., 2013; Huang et al., 2014; Chen et al., 2015; Zhang et al., 2015). In their model,  
425 during collision, the underthrusting North Qilian ocean crust would subduct/underthrust slowly, tend to  
426 attain thermal equilibrium with the superjacent warm active continental margin, and evolve along a  
427 high T/P path in P-T space as a result of retarded subduction and enhanced heating (Appendix Fig. S1).  
428 The warm hydrated ocean crust of basaltic composition and sediments of felsic composition with rather  
429 similar solidi would melt together under the amphibolite facies conditions (for details see Niu et al.,  
430 2013; also see Appendix Fig. S1).

431 Importantly, this model can generate andesitic magmas not only with inherited mantle  
432 isotopic signatures but also compositions similar to the bulk continental crust (BCC), except for  
433 notable depletion in highly compatible elements like Mg, Cr and Ni (Mo et al., 2008). This model  
434 together with experimental results of melting of metabasalt and eclogite (Fig. 13a) implies that the  
435 relatively high Mg<sup>#</sup> (also high Cr and Ni ) contents in QMS adakitic granodiorites may indeed  
436 reflect melt interaction with mantle peridotite during ascent. Although magmas produced through  
437 the above process lack the adakitic signature, it can be the ideal source that generates QMS  
438 adakitic granodiorites through fractional crystallization dominated by mineral assemblages

439 represented by the MMEs. Note that this interpretation is consistent with binary isotope mixing  
440 calculations as proposed by Chen et al. (2015) (Figs. 14a-b), and with trace element model  
441 calculations (see above) (Figs. 9 and 15). As illustrated by these mass balance calculations, ~95%  
442 ocean crust and ~5% continental materials contribute to the source of the QMS pluton (Fig. 14),  
443 and 30%-50% fractional crystallization dominated by mineralogy and modes of the MMEs can  
444 lead to the highly evolved granodioritic composition of the QMS pluton with the adakitic  
445 signature (Figs. 9 and 15).

## 446 **7. Conclusions**

447 (1) The zircon U-Pb dating of the QMS pluton yields the same age (~430 Ma) for both the MMEs  
448 and their host granodiorite, which is the same as the closure time of the Qilian ocean and continental  
449 collision at ~440-420Ma.

450 (2) The MMEs and their host granodiorite also share the same mineralogy with indistinguishable  
451 isotopic compositions, all of which indicate that the MMEs are cumulate formed at earlier stages of the  
452 same magmatic system rather than representing mantle melt required by the popular magma mixing  
453 model.

454 (3) The QMS host granodiorite has adakite-like major and trace element features, including high Sr,  
455 Sr/Y and La/Yb, but low Y and Yb. By accepting our model for the petrogenesis of the MMEs, it  
456 follows that the QMS adakitic granodiorite resulted from fractional crystallization dominated by  
457 mineral assemblages represented by the MMEs.

458 (4) The parental magma for the QMS pluton is best explained as resulting from partial melting of the  
459 remaining part of ocean crust together with recycled terrigenous sediments during continental collision.



460 The resulting magma may have also experienced interaction with mantle peridotite during ascent.

#### 461 **Acknowledgments**

462 We thank Li Su for the assistance with whole rock major, trace elements and zircon U-Pb age  
463 analysis, Minwu Liu with electron microprobe analysis, and Jinlong Ma, Xirong Liang and Zhongyuan  
464 Ren with whole rock Sr-Nd-Hf isotope analysis. Pu Sun, Huixiang Cui and Yuxing Ma are thanked for  
465 their help with sample preparation. This work was supported by the National Natural Science  
466 Foundation of China (NSFC: 91014003, 41130314), Chinese Academy of Sciences (Innovation Grant  
467 Y42217101L) and grants from regional and local authorities (Shandong Province and City of Qingdao),  
468 two projects of Chinese Geological Survey Departments and Offices (1212011121092,  
469 1212011220928), and supported by National Oceanography Laboratory in Qingdao.

470

#### 471 **References**

- 472 Andersen, T., 2002. Correction of common lead in U-Pb analyses that do not report <sup>204</sup>Pb. *Chemical*  
473 *Geology* 192, 59-79.
- 474 Bachmann, O., Dungan, M.A., Bussy, F., 2005. Insights into shallow magmatic processes in large  
475 silicic magma bodies: the trace element record in the Fish Canyon magma body, Colorado.  
476 *Contributions to Mineralogy and Petrology* 149, 338-349.
- 477 Barbarin, B., 2005. Mafic magmatic enclaves and mafic rocks associated with some granitoids of the  
478 central Sierra Nevada batholith, California: nature, origin, and relations with the hosts. *Lithos* 80,  
479 155-177.

480 Barbarin, B., Didier, J., 1991. Enclaves of the Mesozoic calc-alkaline granitoids of the Sierra Nevada  
481 Batholith, California. Enclaves and granite petrology. Elsevier, Amsterdam 135, 153.

482 Bea, F., Pereira, M., Stroh, A., 1994. Mineral/leucosome trace-element partitioning in a peraluminous  
483 migmatite (a laser ablation-ICP-MS study). Chemical Geology 117, 291-312.

484 Black, L.P., Kamo, S.L., Allen, C.M., Aleinikoff, J.N., Davis, D.W., Korsch, R.J., Foudoulis, C., 2003.  
485 TEMORA 1: a new zircon standard for Phanerozoic U–Pb geochronology. Chemical Geology 200,  
486 155-170.

487 Caricchi, L., Annen, C., Rust, A., Blundy, J., 2012. Insights into the mechanisms and timescales of  
488 pluton assembly from deformation patterns of mafic enclaves. Journal of Geophysical Research:  
489 Solid Earth (1978–2012) 117.

490 Castillo, P.R., 2006. An overview of adakite petrogenesis. Chinese Science Bulletin 51, 257-268.

491 Castillo, P.R., 2012. Adakite petrogenesis. Lithos 134-135, 304-316.

492 Castillo, P.R., Janney, P.E., Solidum, R.U., 1999. Petrology and geochemistry of Camiguin Island,  
493 southern Philippines: insights to the source of adakites and other lavas in a complex arc setting.  
494 Contributions to Mineralogy and Petrology 134, 33-51.

495 Castro, A., Moreno - Ventas, I., De la Rosa, J., 1990. Microgranular enclaves as indicators of  
496 hybridization processes in granitoid rocks, Hercynian Belt, Spain. Geological Journal 25, 391-404.

497 Chappell, B., White, A., 1991. Restite enclaves and the restite model, Enclaves and granite petrology.  
498 Elsevier Amsterdam, pp. 479-492.

499 Chappell, B., White, A., 1992. I-and S-type granites in the Lachlan Fold Belt. Geological Society of  
500 America Special Papers 272, 1-26.

501 Chappell, B., White, A., Wyborn, D., 1987. The importance of residual source material (restite) in

502 granite petrogenesis. *Journal of Petrology* 28, 1111-1138.

503 Chen, B., He, J., Ma, X., 2009a. Petrogenesis of mafic enclaves from the north Taihang Yanshanian  
504 intermediate to felsic plutons: Evidence from petrological, geochemical, and zircon Hf-O isotopic  
505 data. *Science in China Series D: Earth Sciences* 52, 1331-1344.

506 Chen, B., Chen, Z.C., Jahn, B.M., 2009b. Origin of mafic enclaves from the Taihang Mesozoic orogen,  
507 north China craton. *Lithos* 110, 343-358.

508 Chen, B., Jahn, B.M., Suzuki, K., 2013a. Petrological and Nd-Sr-Os isotopic constraints on the origin  
509 of high-Mg adakitic rocks from the North China Craton: Tectonic implications. *Geology* 41,  
510 91-94.

511 Chen, B., Chen, C., He, J., Liu, A., 2013b. Origin of Mesozoic high-Mg adakitic rocks from  
512 northeastern China: Petrological and Nd-Sr-Os isotopic constraints. *Chinese Science Bulletin* 58,  
513 1941-1953.

514 Chen, S., Niu, Y., Sun, W., Zhang, Y., Li, J., Guo, P., Sun, P., 2015. On the origin of mafic magmatic  
515 enclaves (MMEs) in syn-collisional granitoids: evidence from the Baojishan pluton in the North  
516 Qilian Orogen, China. *Mineralogy and Petrology* 109, 577-596.

517 Chen, Y., Song, S., Niu, Y., Wei, C., 2014. Melting of continental crust during subduction initiation: A  
518 case study from the Chaidanuo peraluminous granite in the North Qilian suture zone. *Geochimica  
519 et Cosmochimica Acta* 132, 311-336.

520 Chiaradia, M., Fontbote, L., Beate, B., 2004. Cenozoic continental arc magmatism and associated  
521 mineralization in Ecuador. *Mineralium Deposita* 39, 204-222.

522 Chung, S.L., Liu, D., Ji, J., Chu, M. F., Lee, H.Y., Wen, D.J., Lo, C.H., Lee, T.Y., Qian, Q., Zhang, Q.,  
523 2003. Adakites from continental collision zones: Melting of thickened lower crust beneath

524 southern Tibet. *Geology* 31, 1021.

525 Chung, S.L., Chu, M.F., Zhang, Y., Xie, Y., Lo, C.H., Lee, T.Y., Lan, C.Y., Li, X., Zhang, Q., Wang, Y.,  
526 2005. Tibetan tectonic evolution inferred from spatial and temporal variations in post-collisional  
527 magmatism. *Earth-Science Reviews* 68, 173-196.

528 Clemens, J., 1989. The importance of residual source material (restite) in granite petrogenesis: a  
529 comment. *Journal of Petrology* 30, 1313-1316.

530 Dahlquist, J., 2002. Mafic microgranular enclaves: early segregation from metaluminous magma  
531 (Sierra de Chepes), Pampean Ranges, NW Argentina. *Journal of South American Earth Sciences*  
532 15, 643-655.

533 Defant, M.J., Drummond, M.S., 1990. Derivation of some modern arc magmas by melting of young  
534 subducted lithosphere. *Nature* 347, 662-665.

535 DePaolo, D.J., 1981. A neodymium and strontium isotopic study of the Mesozoic calc-alkaline granitic  
536 batholiths of the Sierra Nevada and Peninsular Ranges, California. *Journal of Geophysical*  
537 *Research* 86, 10470.

538 Didier, J., 1987. Contribution of enclave studies to the understanding of origin and evolution of granitic  
539 magmas. *Geologische Rundschau* 76, 41-50.

540 Dodge, F.C.W., Kistler, R.W., 1990. Some additional observations on inclusions in the granitic rocks of  
541 the Sierra Nevada. *Journal of Geophysical Research* 95, 17841.

542 Donaire, T., Pascual, E., Pin, C., Duthou, J.L., 2005. Microgranular enclaves as evidence of rapid  
543 cooling in granitoid rocks: the case of the Los Pedroches granodiorite, Iberian Massif, Spain.  
544 *Contributions to Mineralogy and Petrology* 149, 247-265.

545 Dorais, M.J., Whitney, J.A., Roden, M.F., 1990. Origin of mafic enclaves in the Dinkey Creek pluton,

546 central Sierra Nevada batholith, California. *Journal of Petrology* 31, 853-881.

547 Ewart, A., Griffin, W., 1994. Application of proton-microprobe data to trace-element partitioning in  
548 volcanic rocks. *Chemical Geology* 117, 251-284.

549 Farner, M.J., Lee, C.T.A., Putirka, K.D., 2014. Mafic–felsic magma mixing limited by reactive  
550 processes: A case study of biotite-rich rinds on mafic enclaves. *Earth and Planetary Science  
551 Letters* 393, 49-59.

552 Fujimaki, H., Tatsumoto, M., Aoki, K.I., 1984. Partition coefficients of Hf, Zr, and ree between  
553 phenocrysts and groundmasses. *Journal of Geophysical Research* 89, B662.

554 Furman, T., Spera, F.J., 1985. Co-mingling of acid and basic magma with implications for the origin of  
555 mafic I-type xenoliths: field and petrochemical relations of an unusual dike complex at Eagle Lake,  
556 Sequoia National Park, California, USA. *Journal of Volcanology and Geothermal Research* 24,  
557 151-178.

558 Gao, S., Rudnick, R.L., Yuan, H.L., Liu, X.M., Liu, Y.S., Xu, W.L., Ling, W.L., Ayers, J., Wang, X.C.,  
559 Wang, Q.H., 2004. Recycling lower continental crust in the North China Craton. *Nature* 432,  
560 892–897.

561 Green, T., Blundy, J., Adam, J., Yaxley, G., 2000. SIMS determination of trace element partition  
562 coefficients between garnet, clinopyroxene and hydrous basaltic liquids at 2–7.5 GPa and  
563 1080–1200 C. *Lithos* 53, 165-187.

564 He, Y., Li, S., Hoefs, J., Kleinhanns, I.C., 2013. Sr-Nd-Pb isotopic compositions of Early Cretaceous  
565 granitoids from the Dabie orogen: Constraints on the recycled lower continental crust. *Lithos*  
566 156-159, 204-217.

567 Holden, P., Halliday, A., Stephens, W., 1987. Neodymium and strontium isotope content of microdiorite

568 enclaves points to mantle input to granitoid production. *Nature* 330, 53-56.

569 Hoskin, P.W., Schaltegger, U., 2003. The composition of zircon and igneous and metamorphic  
570 petrogenesis. *Reviews in mineralogy and geochemistry* 53, 27-62.

571 Huang, H., Niu, Y., Nowell, G., Zhao, Z., Yu, X., Zhu, D.C., Mo, X., Ding, S., 2014. Geochemical  
572 constraints on the petrogenesis of granitoids in the East Kunlun Orogenic belt, northern Tibetan  
573 Plateau: Implications for continental crust growth through syn-collisional felsic magmatism.  
574 *Chemical Geology* 370, 1-18.

575 Irving, A.J., Frey, F.A., 1984. Trace element abundances in megacrysts and their host basalts:  
576 constraints on partition coefficients and megacryst genesis. *Geochimica et Cosmochimica Acta* 48,  
577 1201-1221.

578 Klein, M., Stosch, H.G., Seck, H., 1997. Partitioning of high field-strength and rare-earth elements  
579 between amphibole and quartz-dioritic to tonalitic melts: an experimental study. *Chemical*  
580 *Geology* 138, 257-271.

581 Le Maitre, R.W., Bateman, P., Dudek, A., Keller, J., Lameyre, J., Le Bas, M., Sabine, P., Schmid, R.,  
582 Sorensen, H., Streckeisen, A., 1989. A classification of igneous rocks and glossary of terms:  
583 Recommendations of the International Union of Geological Sciences Subcommittee on the  
584 Systematics of Igneous Rocks. Blackwell Oxford.

585 Leake, B., Arps, C., Birch, W., Gilbert, M., Grice, J., Hawthorne, F., Kato, A., Kisch, H., Krivovichev,  
586 V., Linthout, K., 1997. Nomenclature of Amphiboles: Report of the Subcommittee on Amphiboles  
587 of the International Mineralogical Association, Commission on New Minerals and Mineral  
588 Names. *The Canadian Mineralogist* 35, 219-246.

589 Lee, C.T., Bachmann, O., 2014. How important is the role of crystal fractionation in making

590 intermediate magmas? Insights from Zr and P systematics. *Earth and Planetary Science Letters*  
591 393, 266-274.

592 Leshner, C.E., 1990. Decoupling of chemical and isotopic exchange during magma mixing. *Nature* 344,  
593 235-237.

594 Li, X.H., Li, W.X., Li, Z.X., Lo, C.H., Wang, J., Ye, M.F., Yang, Y.H., 2009. Amalgamation between  
595 the Yangtze and Cathaysia Blocks in South China: Constraints from SHRIMP U–Pb zircon ages,  
596 geochemistry and Nd–Hf isotopes of the Shuangxiwu volcanic rocks. *Precambrian Research* 174,  
597 117-128.

598 Liu, L., Qiu, J.S., Li, Z., 2013. Origin of mafic microgranular enclaves (MMEs) and their host quartz  
599 monzonites from the Muchen pluton in Zhejiang Province, Southeast China: Implications for  
600 magma mixing and crust–mantle interaction. *Lithos* 160-161, 145-163.

601 Ma, J., Wei, G., Liu, Y., Ren, Z., Xu, Y., Yang, Y., 2013a. Precise measurement of stable ( $\delta^{88/86}\text{Sr}$ ) and  
602 radiogenic ( $^{87}\text{Sr}/^{86}\text{Sr}$ ) strontium isotope ratios in geological standard reference materials using  
603 MC-ICP-MS. *Chinese Science Bulletin* 58, 3111-3118.

604 Ma, J., Wei, G., Liu, Y., Ren, Z., Xu, Y., Yang, Y., 2013b. Precise measurement of stable neodymium  
605 isotopes of geological materials by using MC-ICP-MS. *Journal of Analytical Atomic Spectrometry*  
606 28, 1926.

607 Ma, Q., Zheng, J.P., Xu, Y.G., Griffin, W.L., Zhang, R.S., 2015. Are continental “adakites” derived  
608 from thickened or foundered lower crust? *Earth and Planetary Science Letters* 419, 125-133.

609 Macpherson, C.G., Dreher, S.T., Thirlwall, M.F., 2006. Adakites without slab melting: High pressure  
610 differentiation of island arc magma, Mindanao, the Philippines. *Earth and Planetary Science*  
611 *Letters* 243, 581-593.

612 Mahood, G., Hildreth, W., 1983. Large partition coefficients for trace elements in high-silica rhyolites.  
613 *Geochimica et Cosmochimica Acta* 47, 11-30.

614 Matsui, Y., Onuma, N., Nagasawa, H., Higuchi, H. and Banno, S., 1977. Crystal structure control in  
615 trace element partition between crystal and magma. *Tectonics* 100, 315-324.

616 Mo, X., Niu, Y., Dong, G., Zhao, Z., Hou, Z., Zhou, S., Ke, S., 2008. Contribution of syncollisional  
617 felsic magmatism to continental crust growth: A case study of the Paleogene Linzizong volcanic  
618 Succession in southern Tibet. *Chemical Geology* 250, 49-67.

619 Nash, W., Crecraft, H., 1985. Partition coefficients for trace elements in silicic magmas. *Geochimica et*  
620 *Cosmochimica Acta* 49, 2309-2322.

621 Niu, Y., Batiza, R., 1997. Trace element evidence from seamounts for recycled oceanic crust in the  
622 Eastern Pacific mantle. *Earth and Planetary Science Letters* 148, 471-483.

623 Niu, Y., Regelous, M., Wendt, I.J., Batiza, R., O'Hara, M.J., 2002. Geochemistry of near-EPR  
624 seamounts: importance of source vs. process and the origin of enriched mantle component. *Earth*  
625 *and Planetary Science Letters* 199, 327-345.

626 Niu, Y., O'Hara, M.J., 2003. Origin of ocean island basalts: A new perspective from petrology,  
627 geochemistry, and mineral physics considerations. *Journal of Geophysical Research: Solid Earth*  
628 (1978–2012) 108.

629 Niu, Y., 2005. Generation and evolution of basaltic magmas: some basic concepts and a new view on  
630 the origin of Mesozoic–Cenozoic basaltic volcanism in eastern China. *Geological Journal of*  
631 *China Universities* 11, 9-46.

632 Niu, Y., O'Hara, M.J., 2009. MORB mantle hosts the missing Eu (Sr, Nb, Ta and Ti) in the continental  
633 crust: New perspectives on crustal growth, crust–mantle differentiation and chemical structure of



634 oceanic upper mantle. *Lithos* 112, 1-17.

635 Niu, Y., Zhao, Z., Zhu, D.C., Mo, X., 2013. Continental collision zones are primary sites for net  
636 continental crust growth — A testable hypothesis. *Earth-Science Reviews* 127, 96-110.

637 Pabst, A., 1928. Observations on inclusions in the granitic rocks of the Sierra Nevada. University of  
638 California Publications in Geological Sciences 17, 325-386.

639 Pearce, J.A., Norry, M.J., 1979. Petrogenetic implications of Ti, Zr, Y, and Nb variations in volcanic  
640 rocks. *Contributions to mineralogy and petrology* 69, 33-47.

641 Pietranik, A., Koepke, J., Puziewicz, J., 2006. Crystallization and resorption in plutonic plagioclase:  
642 Implications on the evolution of granodiorite magma (Gęsiniec granodiorite, Strzelin Crystalline  
643 Massif, SW Poland). *Lithos* 86, 260-280.

644 Prowatke, S., Klemme, S., 2006. Trace element partitioning between apatite and silicate melts.  
645 *Geochimica et Cosmochimica Acta* 70, 4513-4527.

646 Qian, Q., Hermann, J., 2013. Partial melting of lower crust at 10–15 kbar: constraints on adakite and  
647 TTG formation. *Contributions to Mineralogy and Petrology* 165, 1195-1224.

648 Rapp, R.P., Watson, E.B., 1995. Dehydration melting of metabasalt at 8–32 kbar: implications for  
649 continental growth and crust-mantle recycling. *Journal of Petrology* 36, 891-931.

650 Richards, J.P., Kerrich, R., 2007. Special paper: adakite-like rocks: their diverse origins and  
651 questionable role in metallogenesis. *Economic Geology* 102, 537-576.

652 Rodriguez, C., Selles, D., Dungan, M., Langmuir, C., Leeman, W., 2007. Adakitic dacites formed by  
653 intracrustal crystal fractionation of water-rich parent magmas at Nevado de Longavi Volcano  
654 (36.2° S; Andean Southern Volcanic Zone, Central Chile). *Journal of Petrology* 48, 2033-2061.

655 Ronov, A., Yaroshevsky, A., 1976. A new model for the chemical structure of the Earth's crust.

656 Geochemistry International 13, 89-121.

657 Rudnick, R., Gao, S., 2003. Composition of the continental crust. *Treatise on geochemistry* 3, 1-64.

658 Schnetzler, C., Philpotts, J.A., 1970. Partition coefficients of rare-earth elements between igneous  
659 matrix material and rock-forming mineral phenocrysts—II. *Geochimica et Cosmochimica Acta* 34,  
660 331-340.

661 Sen, C., Dunn, T., 1994. Dehydration melting of a basaltic composition amphibolite at 1.5 and 2.0 GPa:  
662 implications for the origin of adakites. *Contributions to Mineralogy and Petrology* 117, 394-409.

663 Song, S., Su, L., Niu, Y., Zhang, L., Zhang, G., 2007. Petrological and geochemical constraints on the  
664 origin of garnet peridotite in the North Qaidam ultrahigh-pressure metamorphic belt, northwestern  
665 China. *Lithos* 96, 243-265.

666 Song, S., Niu, Y., Wei, C., Ji, J., Su, L., 2010a. Metamorphism, anatexis, zircon ages and tectonic  
667 evolution of the Gongshan block in the northern Indochina continent—An eastern extension of the  
668 Lhasa Block. *Lithos* 120, 327-346.

669 Song, S., Su, L., Li, X.H., Zhang, G., Niu, Y., Zhang, L., 2010b. Tracing the 850-Ma continental flood  
670 basalts from a piece of subducted continental crust in the North Qaidam UHPM belt, NW China.  
671 *Precambrian Research* 183, 805-816.

672 Song, S., Niu, Y., Su, L., Xia, X., 2013. Tectonics of the North Qilian orogen, NW China. *Gondwana  
673 Research* 23, 1378-1401.

674 Song, S., Niu, Y., Su, L., Wei, C., Zhang, L., 2014a. Adakitic (tonalitic-trondhjemitic) magmas  
675 resulting from eclogite decompression and dehydration melting during exhumation in response to  
676 continental collision. *Geochimica et Cosmochimica Acta* 130, 42-62.

677 Song, S., Niu, Y., Su, L., Zhang, C., Zhang, L., 2014b. Continental orogenesis from ocean subduction,

678 continent collision/subduction, to orogen collapse, and orogen recycling: The example of the  
679 North Qaidam UHPM belt, NW China. *Earth-Science Reviews* 129, 59-84.

680 Streck, M.J., Leeman, W.P., Chesley, J., 2007. High-magnesian andesite from Mount Shasta: A product  
681 of magma mixing and contamination, not a primitive mantle melt. *Geology* 35, 351.

682 Sun, S.S., McDonough, W., 1989. Chemical and isotopic systematics of oceanic basalts: implications  
683 for mantle composition and processes. Geological Society, London, Special Publications 42,  
684 313-345.

685 Thomas, J., Bodnar, R., Shimizu, N., Sinha, A., 2002. Determination of zircon/melt trace element  
686 partition coefficients from SIMS analysis of melt inclusions in zircon. *Geochimica et*  
687 *Cosmochimica Acta* 66, 2887-2901.

688 Tseng, C.Y., Yang, H.J., Yang, H.Y., Liu, D., Wu, C., Cheng, C.K., Chen, C.H., Ker, C.M., 2009.  
689 Continuity of the North Qilian and North Qinling orogenic belts, Central Orogenic System of  
690 China: Evidence from newly discovered Paleozoic adakitic rocks. *Gondwana Research* 16,  
691 285-293.

692 Vernon, R., 1984. Microgranitoid enclaves in granites—globules of hybrid magma quenched in a  
693 plutonic environment. *Nature* 309, 438-439.

694 Vernon, R.H., 1983. Restite, xenoliths and microgranitoid enclaves in granites. *Journal and Proceedings*  
695 *of the Royal Society of New South Wales* 116, 77–103.

696 Wang, J., Wu, C., Cai, Z., Guo, Y., Wu, J., Liu, X., 2006a. Early Paleozoic high-Mg adakite from  
697 Yindongliang in the eastern section of the North Qilian: Implications for geodynamics and Cu-Au  
698 mineralization. *Acta Petrol Sinica* 22, 2655–2664. (in Chinese with English abstract)

699 Wang, Q., McDermott, F., Xu, J.F., Bellon, H., Zhu, Y.T., 2005. Cenozoic K-rich adakitic volcanic

700 rocks in the Hohxil area, northern Tibet: Lower-crustal melting in an intracontinental setting.  
701 *Geology* 33, 465.

702 Wang, Q., Wyman, D.A., Xu, J.F., Zhao, Z.H., Jian, P., Xiong, X.L., Bao, Z.W., Li, C.F., Bai, Z.H.,  
703 2006b. Petrogenesis of Cretaceous adakitic and shoshonitic igneous rocks in the Luzong area,  
704 Anhui Province (eastern China): Implications for geodynamics and Cu–Au mineralization. *Lithos*  
705 89, 424-446.

706 Wang, Q., Wyman, D.A., Xu, J., Jian, P., Zhao, Z., Li, C., Xu, W., Ma, J., He, B., 2007. Early  
707 Cretaceous adakitic granites in the Northern Dabie Complex, central China: Implications for  
708 partial melting and delamination of thickened lower crust. *Geochimica et Cosmochimica Acta* 71,  
709 2609-2636.

710 Wang, Q., Wyman, D.A., Xu, J., Dong, Y., Vasconcelos, P.M., Pearson, N., Wan, Y., Dong, H., Li, C.,  
711 Yu, Y., Zhu, T., Feng, X., Zhang, Q., Zi, F., Chu, Z., 2008. Eocene melting of subducting  
712 continental crust and early uplifting of central Tibet: Evidence from central-western Qiangtang  
713 high-K calc-alkaline andesites, dacites and rhyolites. *Earth and Planetary Science Letters* 272,  
714 158-171.

715 Wang, Q., Li, X.H., Jia, X.H., Wyman, D., Tang, G.J., Li, Z.X., Ma, L., Yang, Y.H., Jiang, Z.Q., Gou,  
716 G.N., 2013. Late Early Cretaceous adakitic granitoids and associated magnesian and potassium -  
717 rich mafic enclaves and dikes in the Tunchang–Fengmu area, Hainan Province (South China):  
718 Partial melting of lower crust and mantle, and magma hybridization. *Chemical Geology* 328,  
719 222-243.

720 Wiedenbeck, M., Alle, P., Corfu, F., Griffin, W., Meier, M., Oberli, F., Quadt, A.v., Roddick, J., Spiegel,  
721 W., 1995. Three natural zircon standards for U-Th-Pb, Lu-Hf, trace element and REE analyses.

722 Geostandards newsletter 19, 1-23.

723 Xiong, X.L., Adam, J., Green, T.H., 2005. Rutile stability and rutile/melt HFSE partitioning during  
724 partial melting of hydrous basalt: Implications for TTG genesis. *Chemical Geology* 218, 339-359.

725 Xu, J.F., Shinjo, R., Defant, M.J., Wang, Q., Rapp, R.P., 2002. Origin of Mesozoic adakitic intrusive  
726 rocks in the Ningzhen area of east China: Partial melting of delaminated lower continental crust?  
727 *Geology* 30, 1111.

728 Xu, W., Gao, S., Wang, Q., Wang, D., Liu, Y., 2006. Mesozoic crustal thickening of the eastern North  
729 China craton: Evidence from eclogite xenoliths and petrologic implications. *Geology* 34, 721-724.

730 Yu, S., Zhang, J., Qin, H., Sun, D., Zhao, X., Cong, F., Li, Y., 2015. Petrogenesis of the early Paleozoic  
731 low-Mg and high-Mg adakitic rocks in the North Qilian orogenic belt, NW China: Implications for  
732 transition from crustal thickening to extension thinning. *Journal of Asian Earth Sciences* 107,  
733 122-139.

734 Zhang, C., Ma, C., Holtz, F., 2010. Origin of high-Mg adakitic magmatic enclaves from the Meichuan  
735 pluton, southern Dabie orogen (central China): Implications for delamination of the lower  
736 continental crust and melt-mantle interaction. *Lithos* 119, 467-484.

737 Zhang, J., Meng, F., Wan, Y., 2007. A cold Early Palaeozoic subduction zone in the North Qilian  
738 Mountains, NW China: petrological and U-Pb geochronological constraints. *Journal of*  
739 *Metamorphic Geology* 25, 285-304.

740 Zhang, Y., Niu, Y., Hu, Y., Liu, J., Ye, L., Kong, J., Duan, M., 2015. The syncollisional granitoid  
741 magmatism and continental crust growth in the West Kunlun Orogen, China - Evidence from  
742 geochronology and geochemistry of the Arkarz pluton. *Lithos.* [doi: 10.1016/j.lithos.2015.05.007](https://doi.org/10.1016/j.lithos.2015.05.007)  
743 (in press).

744

745 **Figure captions:**

746 **Fig.1:** (a) Simplified geological map of the North Qilian Orogen showing distributions of the main  
747 tectonic units (modified after Song et al., 2013; Chen et al., 2015). (b) Simplified map of the Qumushan  
748 (QMS) and Baojishan (BJS) area in the eastern section of the North Qilian Orogen. U-Pb ages are  
749 shown for granodiorite and MMEs in the BJS and QMS plutons from Chen et al. (2015), Yu et al.  
750 (2015) and this study as indicated.

751 **Fig. 2:** Photographs of the adakitic granodiorite and the MMEs in the field and in thin-sections. (a), (b)  
752 and (c) showing the sharp contact of MMEs of varying size with their host granodiorite with MMEs  
753 being finer-grained than the host; (d) showing the mineral assemblage of the adakitic host granodiorite  
754 (QMS12-02host) and (e), (f) showing the mineral assemblage of MMEs (QMS12-02MME,  
755 QMS12-06MME). Amp = amphibole; Bt = biotite; Pl= plagioclase; Qz = quartz; Ap = apatite; Zrn=  
756 zircon. Plates c-f are taken under cross-polarized light.

757 **Fig. 3:** Photomicrographs showing a plagioclase crystal with a high-Ca core rimmed by a euhedral  
758 overgrowth of low-Ca plagioclase in both (a) adakitic rocks (e.g., QMS12-04host) and (b) MMEs (e.g.,  
759 QMS12-04MME). Numerals are the An contents. See [Appendix B Appendix 2](#) for compositional data.

760 **Fig. 4:** Chemical compositions of amphiboles from the host granodiorite and MMEs in the amphibole  
761 classification diagram (Leake et al., 1997). Data from the host granodiorites and the MMEs of BJS  
762 pluton (Chen et al., 2015) are also shown for comparison.

763 **Fig. 5:** Concordia diagrams of LA-ICP-MS U-Pb zircon age data and representative CL images of  
764 zircon grains showing spots for the host adakitic granodiorites (a, c) and the MMEs (b, d) in the QMS

765 pluton.

766 **Fig. 6:** Classification diagrams of the host granodiorites and the MMEs in the QMS pluton. (a) Total  
767 alkalis vs. SiO<sub>2</sub> (Le Maitre et al., 1989), (b) K<sub>2</sub>O vs. SiO<sub>2</sub>, and (c) A/NK vs. A/CNK. The blue circles  
768 and squares are data from BJS granodiorites and their MMEs (Chen et al., 2015), and the open circles  
769 are literature data on the QMS granodiorites (Wang et al., 2006a; Tseng et al., 2009; Yu et al., 2015).

770 **Fig. 7:** (a) Chondrite normalized REE patterns for the QMS host adakitic granodiorites and the MMEs;  
771 (b) host rock-normalized REE patterns of MMEs. Chondrite REE values and bulk continental crust  
772 (BCC) are from Sun and McDonough (1989) and Rudnick and Gao (2003), respectively. Shaded fields  
773 of BJS granodiorite and the MMEs are from Chen et al. (2015).

774 **Fig. 8:** Average ocean crust-normalized (OC; Niu and O'Hara, 2003) trace element patterns for the  
775 QMS host adakitic granodiorites and the MMEs.

776 **Fig. 9:** Plots of (a) Sr/Y vs. Y, where fields of adakite, and normal arc andesite-dacite-rhyolite are from  
777 Defant and Drummond (1990); (b) La/Yb vs. Yb, discrimination lines are from Richards and Kerrich  
778 (2007); (c) (Dy/Yb)<sub>N</sub> vs (La/Yb)<sub>N</sub>, and (d) Eu/Eu\* vs. Sr. Results in a-d using Rayleigh fractional  
779 crystallization models indicate the effects of garnet, amphibole, plagioclase, zircon and apatite  
780 fractionation on Sr/Y and Y (a), on La/Yb and Yb (b), on (Dy/Yb)<sub>N</sub> and (La/Yb)<sub>N</sub> (c), and on Eu/Eu\*  
781 and Sr (d). The partition coefficients used and modeling details are given in [Table 3 Appendix 6](#). Two  
782 crystallization models were designed to elucidate the effect of crystallization on bulk-rock (assumed to  
783 approximate melt) trace element systematics: (1) Model A, in reasonable agreement with observed  
784 mineral proportions of the MMEs, 50% amphibole, 40% plagioclase, 7.52% biotite, 2.2% apatite, 0.2%  
785 zircon and 0.03% sphene; (2) Model B, 50% amphibole, 40% plagioclase, 7.6% biotite, 2.4% garnet.  
786 Data sources for the QMS and BJS plutons are the same as in Fig. 6. Amp = amphibole; Bt = biotite;

787 Pl= plagioclase; Ap = apatite; Zrn=zircon; Grt = garnet; Spn=sphene.

788 **Fig. 10:** SiO<sub>2</sub> variation diagrams of (a) MgO, (b) Fe<sub>2</sub>O<sub>3</sub><sup>T</sup>, (c) TiO<sub>2</sub>, (d) CaO, (e) MnO, (f) P<sub>2</sub>O<sub>5</sub>, (g) Eu,  
789 (h) Hf, (i) La/Sm, (j) <sup>87</sup>Sr/<sup>86</sup>Sr<sub>(t)</sub>, (k) ε<sub>Nd</sub>(t) and (l) ε<sub>Hf</sub>(t). Fractional crystallization trends in g–i: the  
790 inverse linear trend of SiO<sub>2</sub> versus Eu and Hf indicate the effects of plagioclase and zircon fractional  
791 crystallization, respectively. Because Sm is incorporated more easily than Hf in amphibole (Fujimaki et  
792 al., 1984; Klein et al., 1997), amphibole crystallization will cause Hf/Sm increase in residual magmas  
793 (i). Crustal contamination and (or) basalt-rhyolite mixing trend in j–l are after Wang et al. (2008). Data  
794 sources of the QMS and BJS pluton are the same as in Fig. 6. The average zircon ε<sub>Hf</sub>(t) isotopic data  
795 (6.2±2, 2σ) calculated from Yu et al. (2015) is also presented in l.

796 **Fig. 11:** (a) SiO<sub>2</sub> versus P<sub>2</sub>O<sub>5</sub>; (b) SiO<sub>2</sub> versus Zr. Data for Island arc basalt (n=284 for P and 277 for  
797 Zr), boninite (n=37 for P and 34 for Zr) and rhyolite (n=66 for P and 45 for Zr) are from the Georoc  
798 database (<http://georoc.mpch-mainz.gwdg.de/georoc/>). Dashed and solid lines in a-b are hypothetical  
799 mixing lines and linear trend defined the QMS granodiorite and their MMEs, respectively. Data sources  
800 of the QMS and BJS plutons are the same as in Fig. 6.

801 **Fig. 12:** Cartoon illustrating a possible scenario for MME formation. Earlier crystallized cumulate with  
802 the mineral assemblage of amphibole, biotite, plagioclase and accessory minerals such as zircon and  
803 apatite (a), which was later disturbed by subsequent magma replenishment in the magma chamber,  
804 constituting MMEs in the dominant host granodiorite.

805 **Fig. 13:** Plots of (a) SiO<sub>2</sub> versus Mg<sup>#</sup>; (b) Na<sub>2</sub>O versus K<sub>2</sub>O. Data sources: classical adakite, resulting  
806 from partial melting of subducted ocean crust in modern arcs, are from the GeoRoc database  
807 (<http://georoc.mpch-mainz.gwdg.de/georoc/>); Tibet Plateau (Chung et al., 2003; Wang et al., 2005),  
808 Dabie Orogen (He et al., 2013; Wang et al., 2007), Yangtze Craton (Xu et al., 2002; Wang et al.,



809 2006b); North China Craton (Chen et al., 2013a; Ma et al., 2015) , experimental data (Sen and Dunn,  
810 1994; Rapp and Watson, 1995. Data sources of the QMS and BJS plutons are the same as in Fig. 6.

811 **Fig. 14:** (a) Nd–Sr and (b) Nd-Hf isotope diagrams for the QMS adakitic rocks and their MMEs. The  
812 MORB data are from Niu and Batiza (1997) and Niu et al. (2002), other data sources are the same as  
813 Fig. 13. Binary isotope mixing calculations between North Qilian Ocean MORB (average composition:  
814 Sr=159.6 ppm, Nd=10.5 ppm, Hf=2.41,  $^{87}\text{Sr}/^{76}\text{Sr}_{(t)}=0.7054$ ,  $\epsilon_{\text{Nd}}(t)=5.44$ ,  $\epsilon_{\text{Hf}}(t)=9.93$ ) and Mohe  
815 Basement (average composition: Sr=586 ppm, Nd=32.97 ppm, Hf=3.44,  $^{87}\text{Sr}/^{76}\text{Sr}_{(t)}=0.7234$ ,  $\epsilon_{\text{Nd}}$   
816 (t)=-19.80,  $\epsilon_{\text{Hf}}(t)=-43.65$ ) are after Chen et al. (2015) and references therein.  
817  $K=[(\text{Sr}/\text{Nd})_{\text{MORB}}]/[(\text{Sr}/\text{Nd})_{\text{Mohe basement}}]$ , where  $K_{\text{max}}$ ,  $K_{\text{min}}$ , and  $K_{\text{average}}$  are the maximum, minimum and  
818 average values respectively.

819 **Fig. 15:** Shows 30%, 40%, 50% and 60% fractional crystallization of mineral assemblages of Model A  
820 and Model B from the assumed magma along with the BCC and QMS adakitic granodiorites and their  
821 MMEs on primitive mantle normalized multi-element diagram. The light red and green shaded regions  
822 are the field of QMS adakitic granodiorite and MMEs, respectively.

823 **Appendix Fig. S1:** Simplified phase diagram showing hydrous solidi of basalts and granitic rocks  
824 modified from Niu et al. (2013) (after Niu, 2005). The red line with arrow illustrates the concept of the  
825 underthrusting North Qilian oceanic crust evolve along a high T/P path as a result of retarded  
826 subducting and enhanced heating upon continental collision at a prior active continental margin setting.

827

828 **Table captions:**

829 ~~Table 1: Whole rock major and trace elements analysis of the host adakitic granodiorites and the mafic~~

830 ~~magmatic enclaves in the NQOB.~~

831 ~~Table 2: Whole rock Sr Nd Hf isotopic analyses for the host adakitic granodiorites and the mafic~~

832 ~~magmatic enclaves in the NQOB.~~

833 ~~Table 3: Relevant partition coefficients, assumed melt and model compositions.~~

834 ~~Appendix A~~Appendix 1: U-Th-Pb analyses by LA-ICP-MS for zircons from host granodiorites

835 (QMS12-04host and QMS12-10host) and the mafic magmatic enclaves (QMS12-04MME and

836 QMS12-10MME).

837 ~~Appendix B~~Appendix 2: Microprobe analysis of representative plagioclase in the host granodiorites

838 and the mafic magmatic enclaves.

839 ~~Appendix C~~Appendix 3: Microprobe analysis of representative amphibole in the host granodiorites and

840 the mafic magmatic enclaves.

841 Appendix 4: Whole-rock major and trace elements analysis of the host adakitic granodiorites and the

842 mafic magmatic enclaves in the NQOB.

843 Appendix 5: Whole rock Sr-Nd-Hf isotopic analyses for the host adakitic granodiorites and the mafic

844 magmatic enclaves in the NQOB.

845 Appendix 6: Relevant partition coefficients, assumed melt and model compositions.

846

Figure 1  
[Click here to download high resolution image](#)

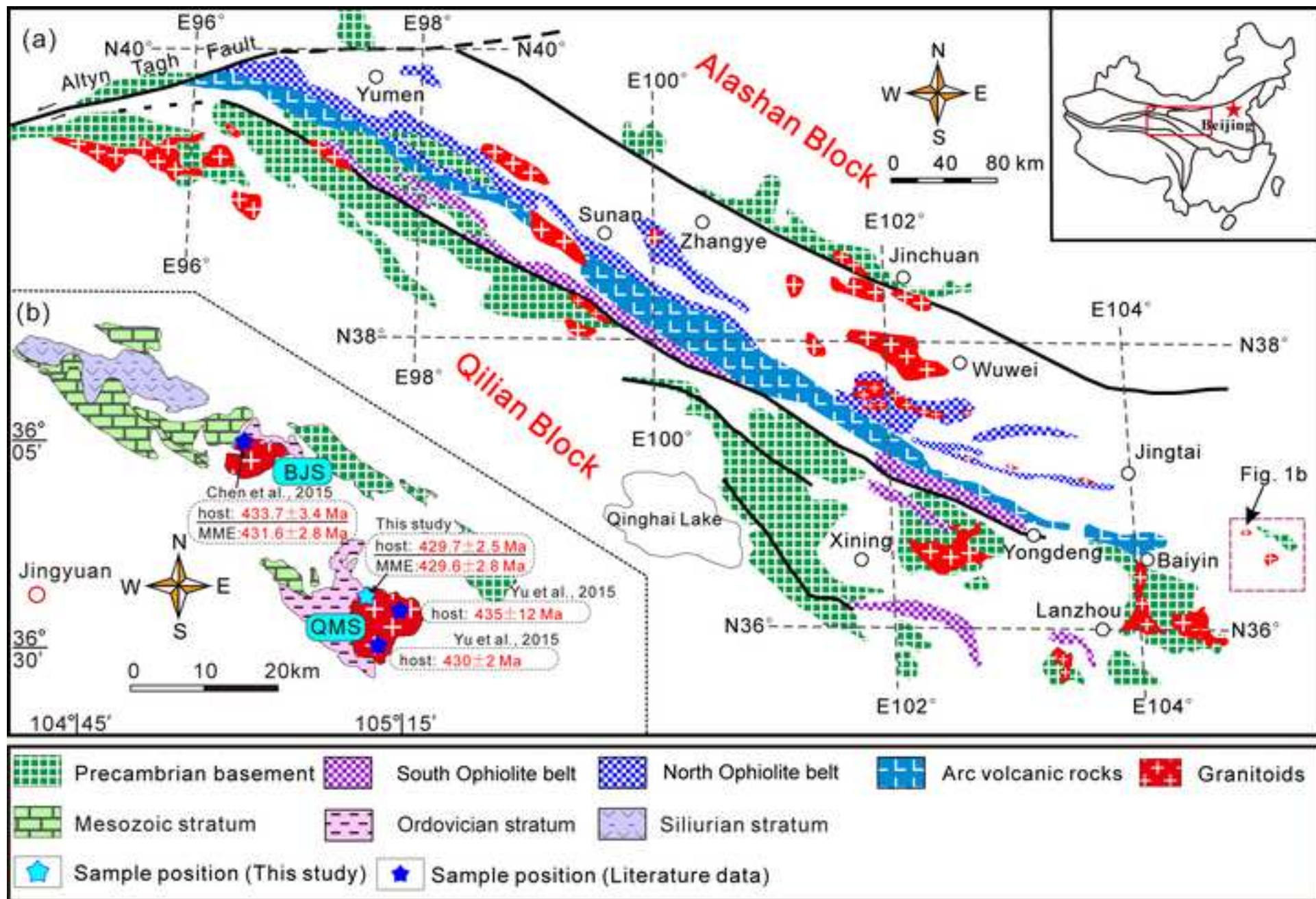


Figure 2  
[Click here to download high resolution image](#)

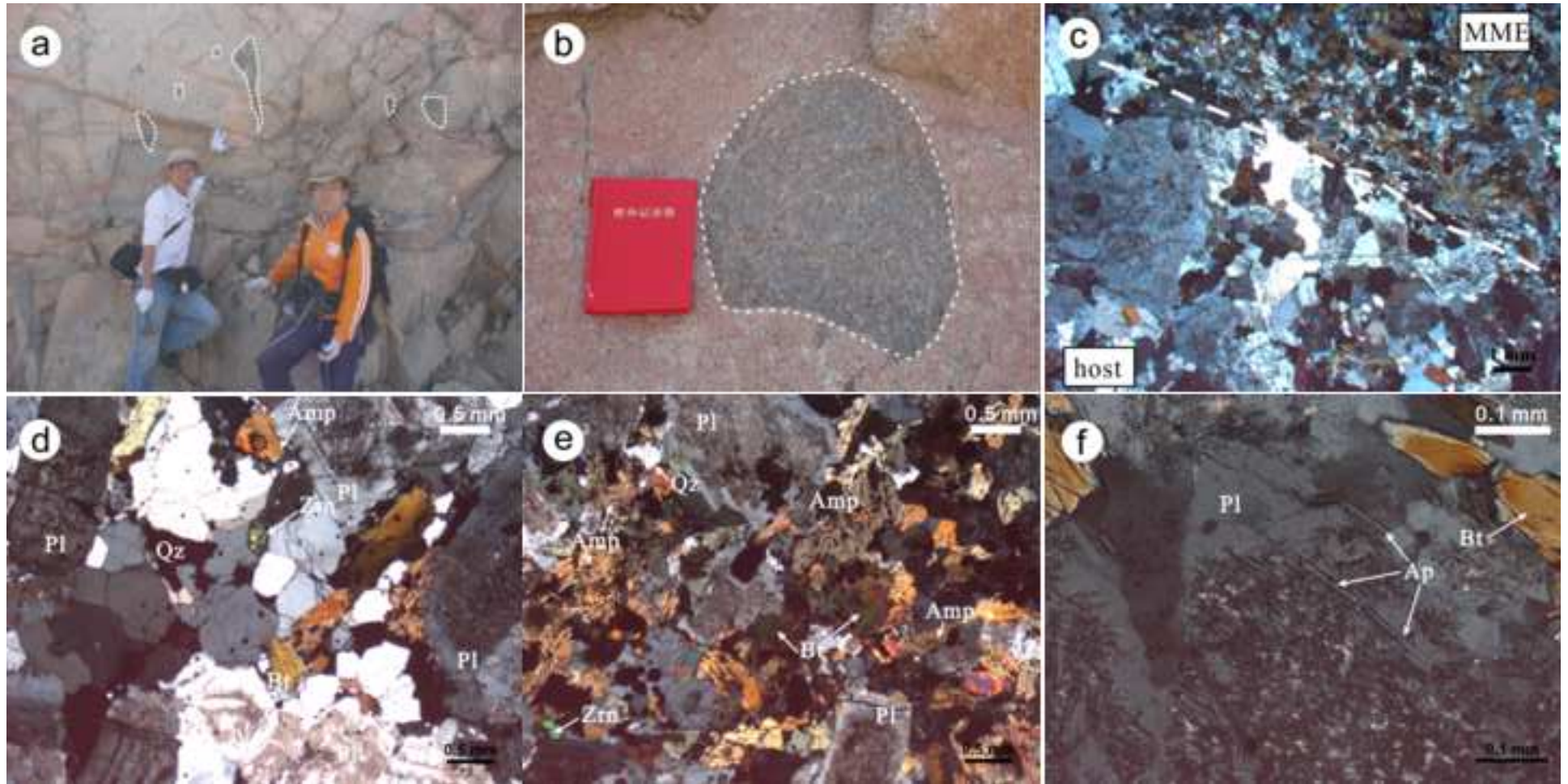


Figure 3  
[Click here to download high resolution image](#)

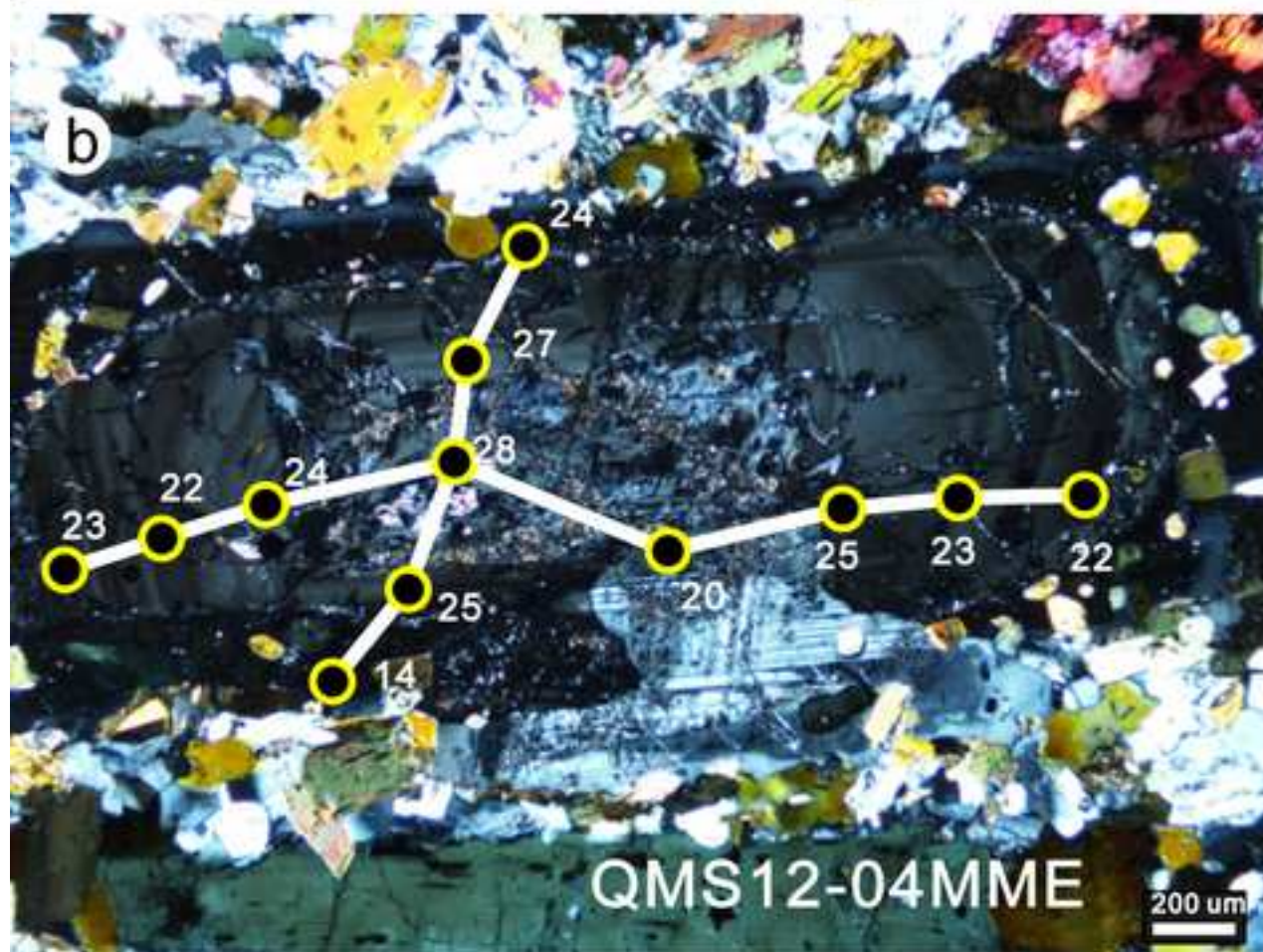
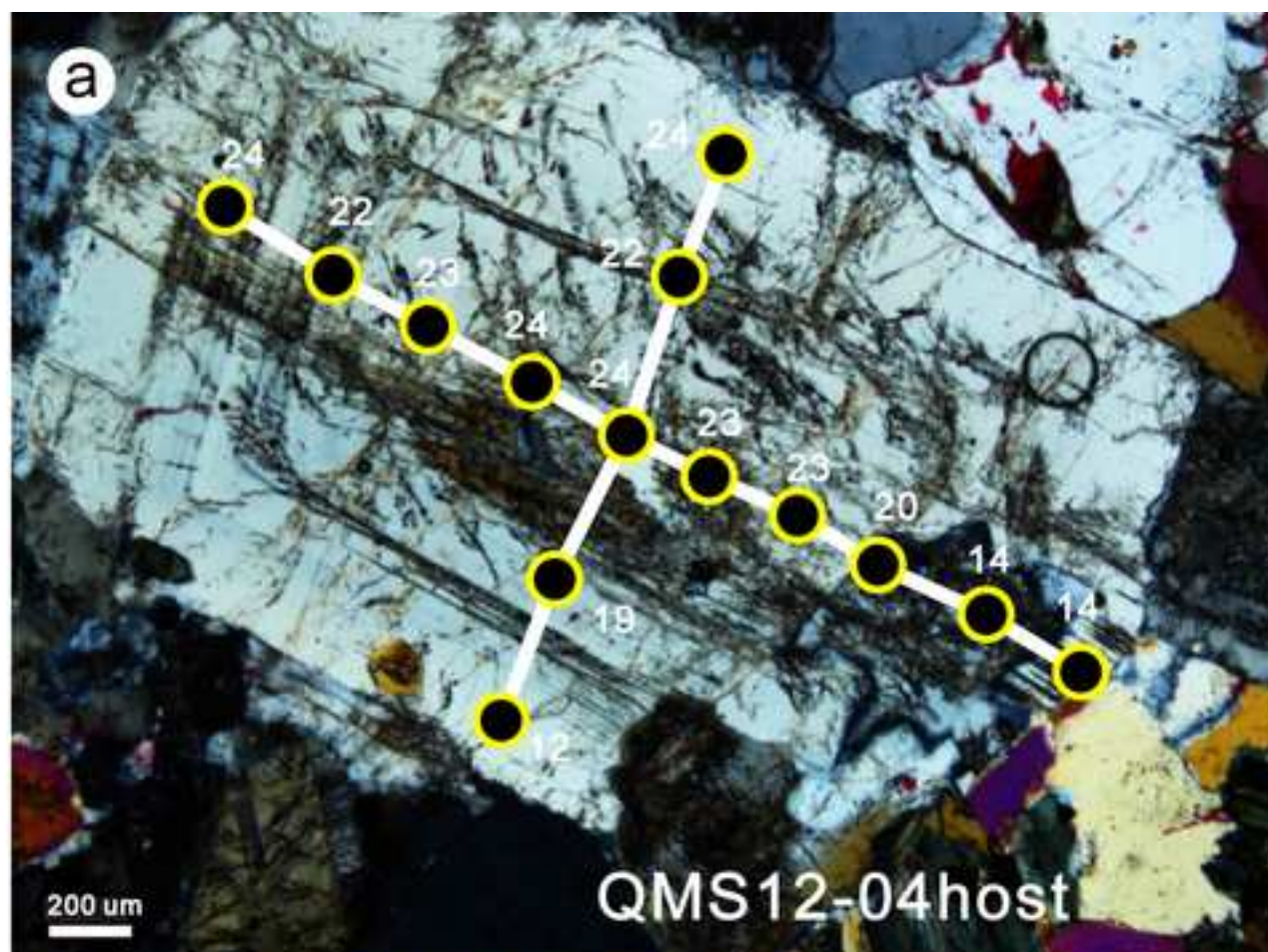


Figure 4  
[Click here to download high resolution image](#)

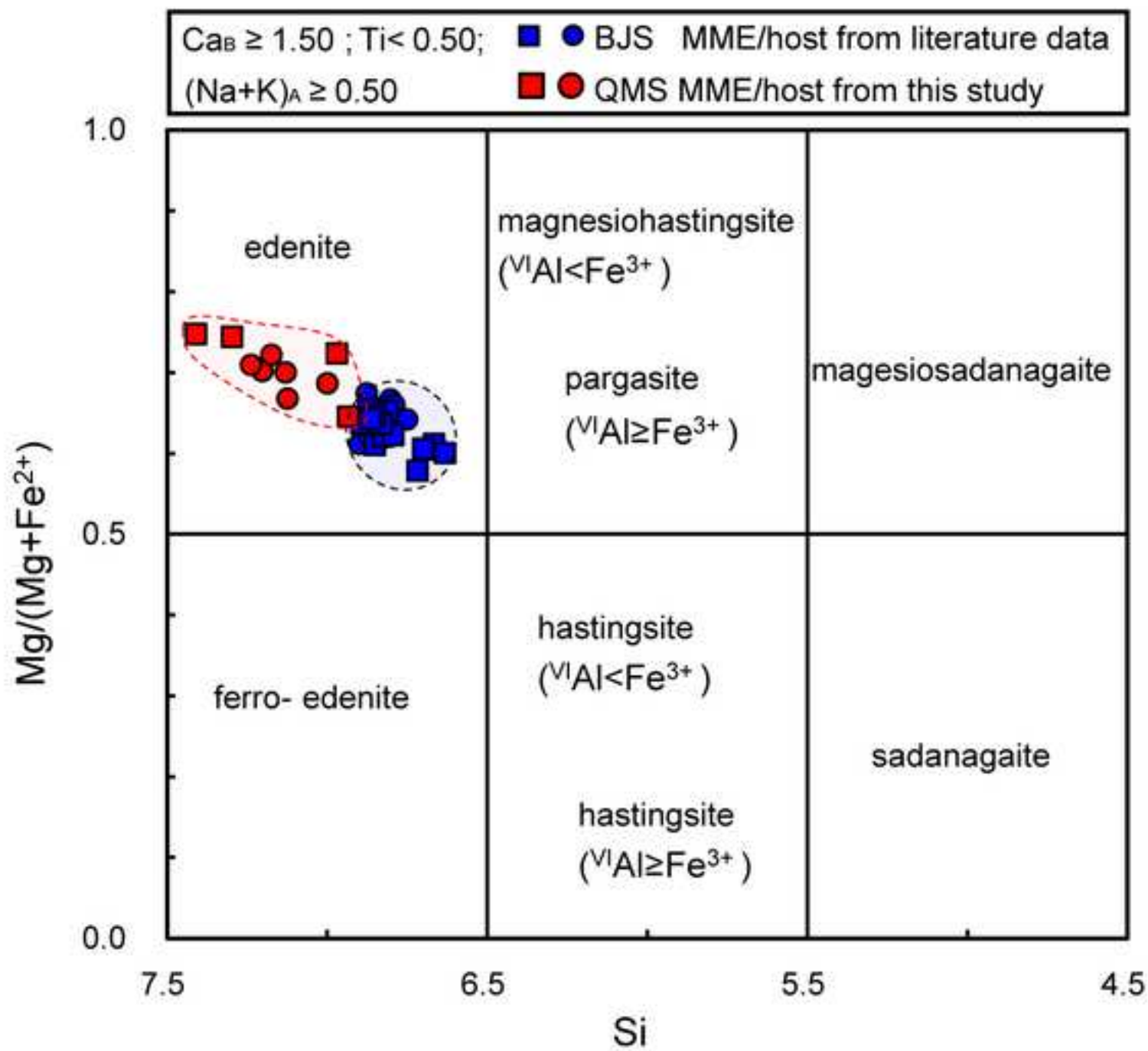


Figure 5  
[Click here to download high resolution image](#)

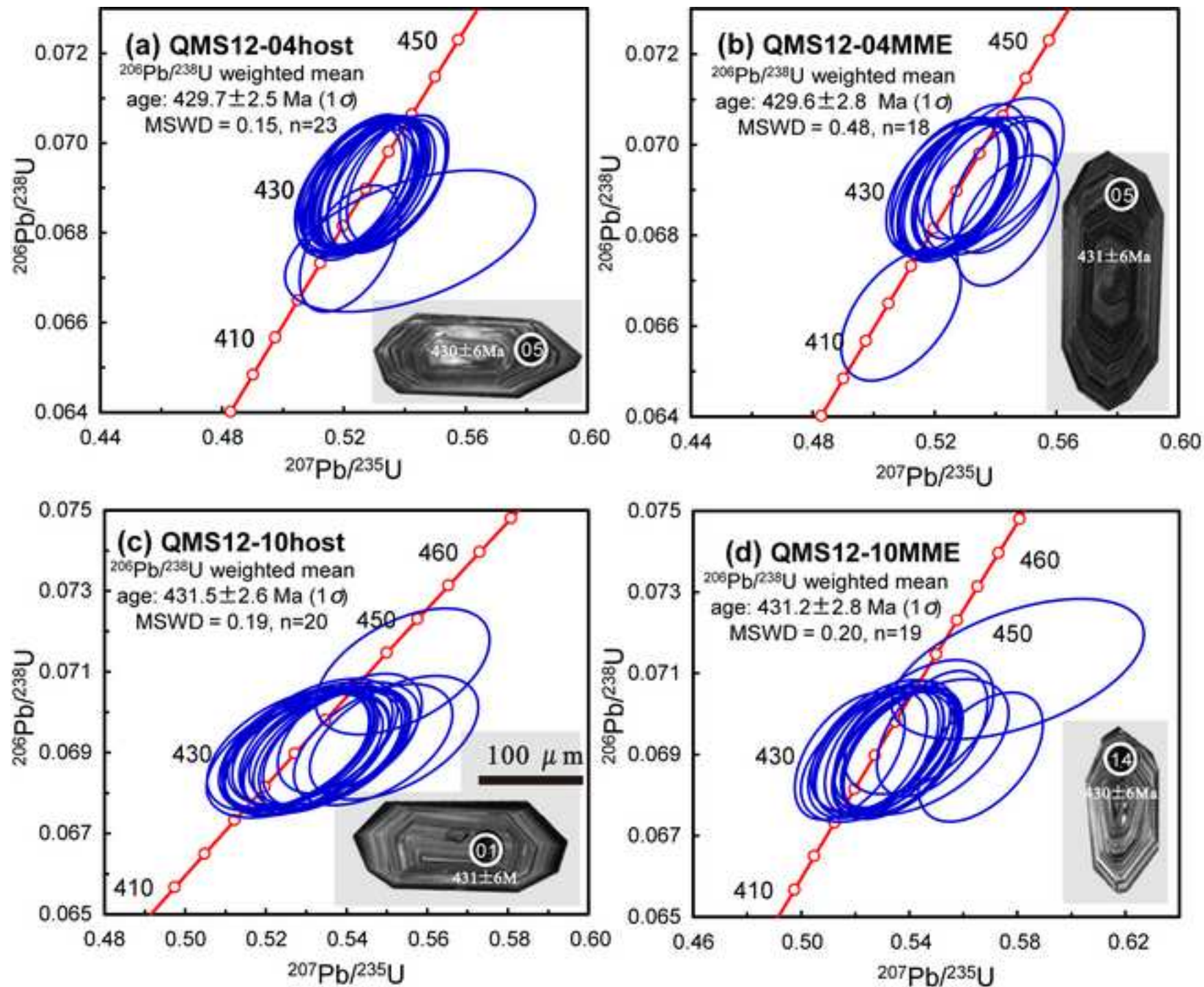


Figure 6

[Click here to download high resolution image](#)

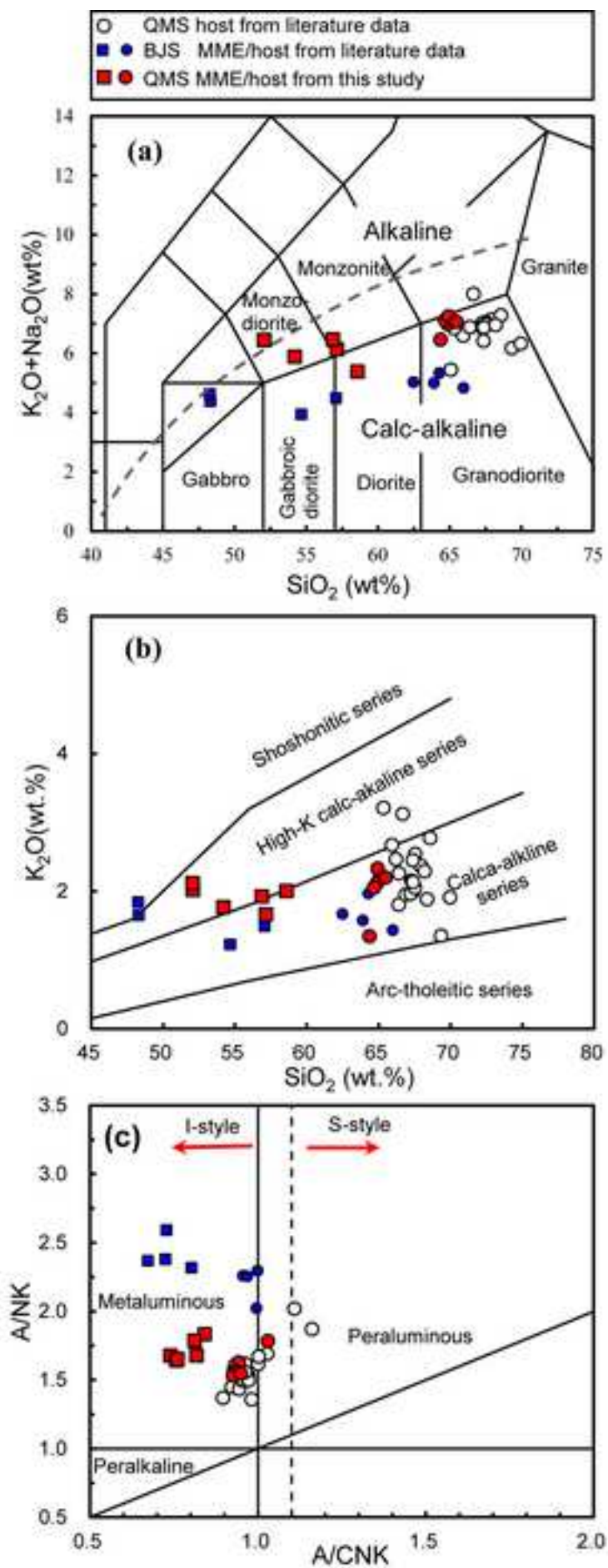




Figure 7  
[Click here to download high resolution image](#)

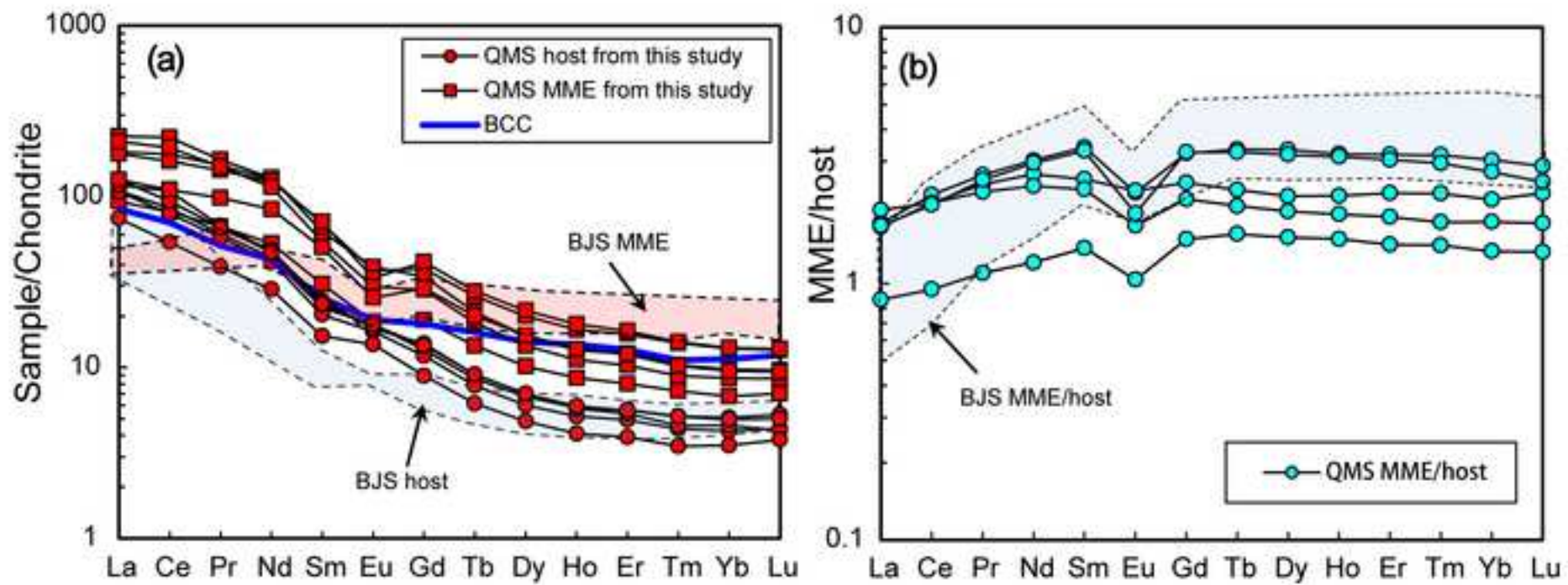


Figure 8  
[Click here to download high resolution image](#)

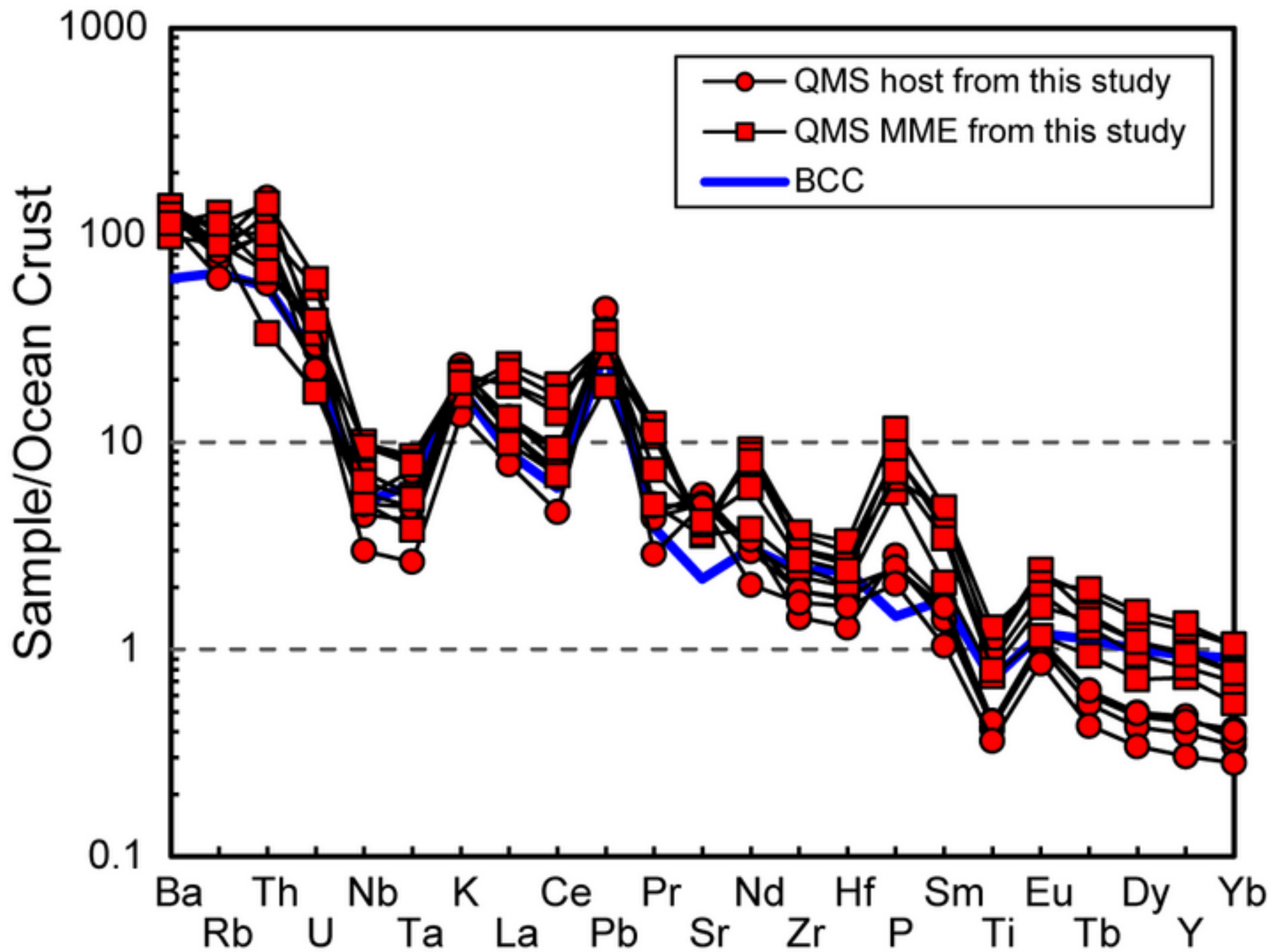


Figure 9  
[Click here to download high resolution image](#)

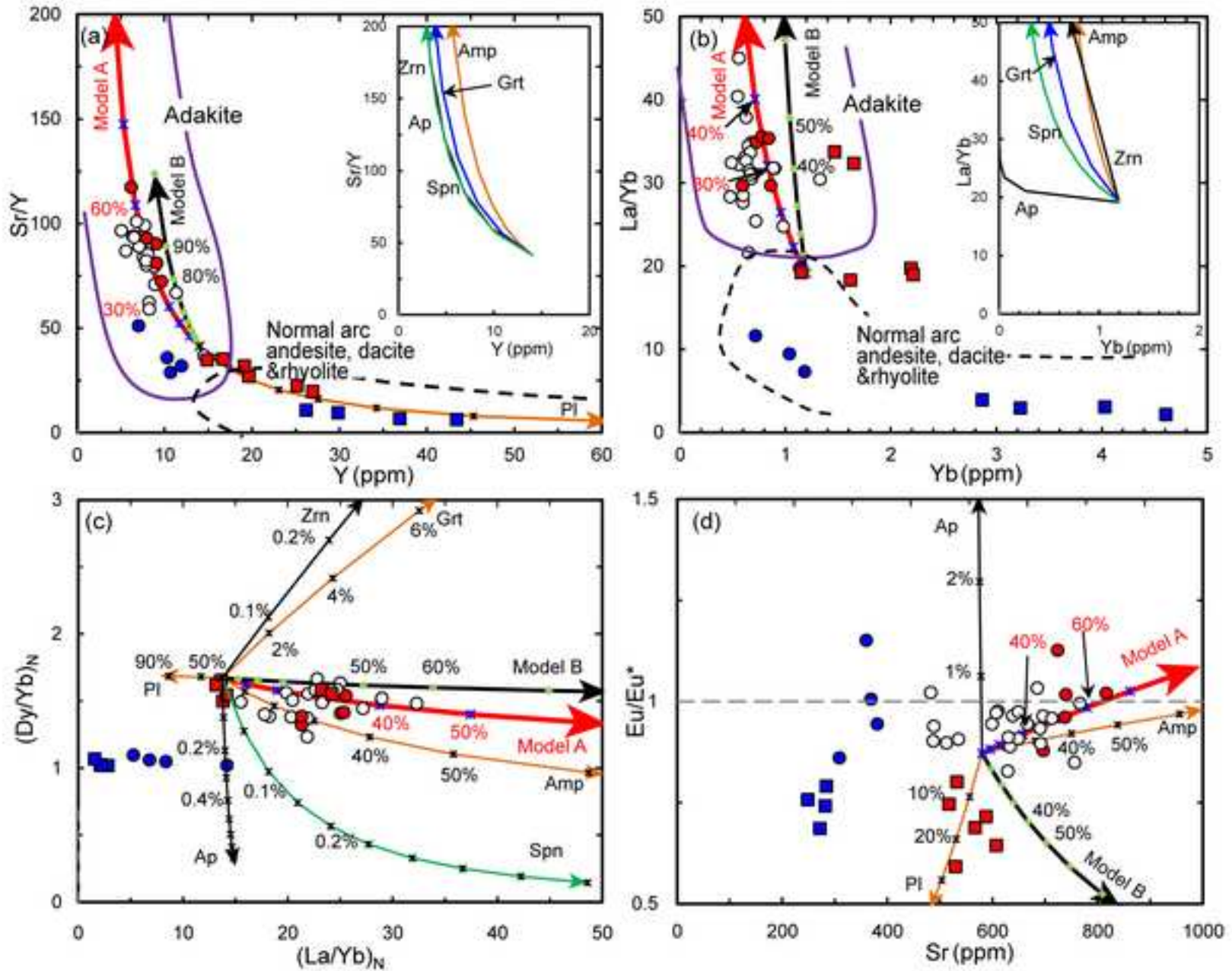
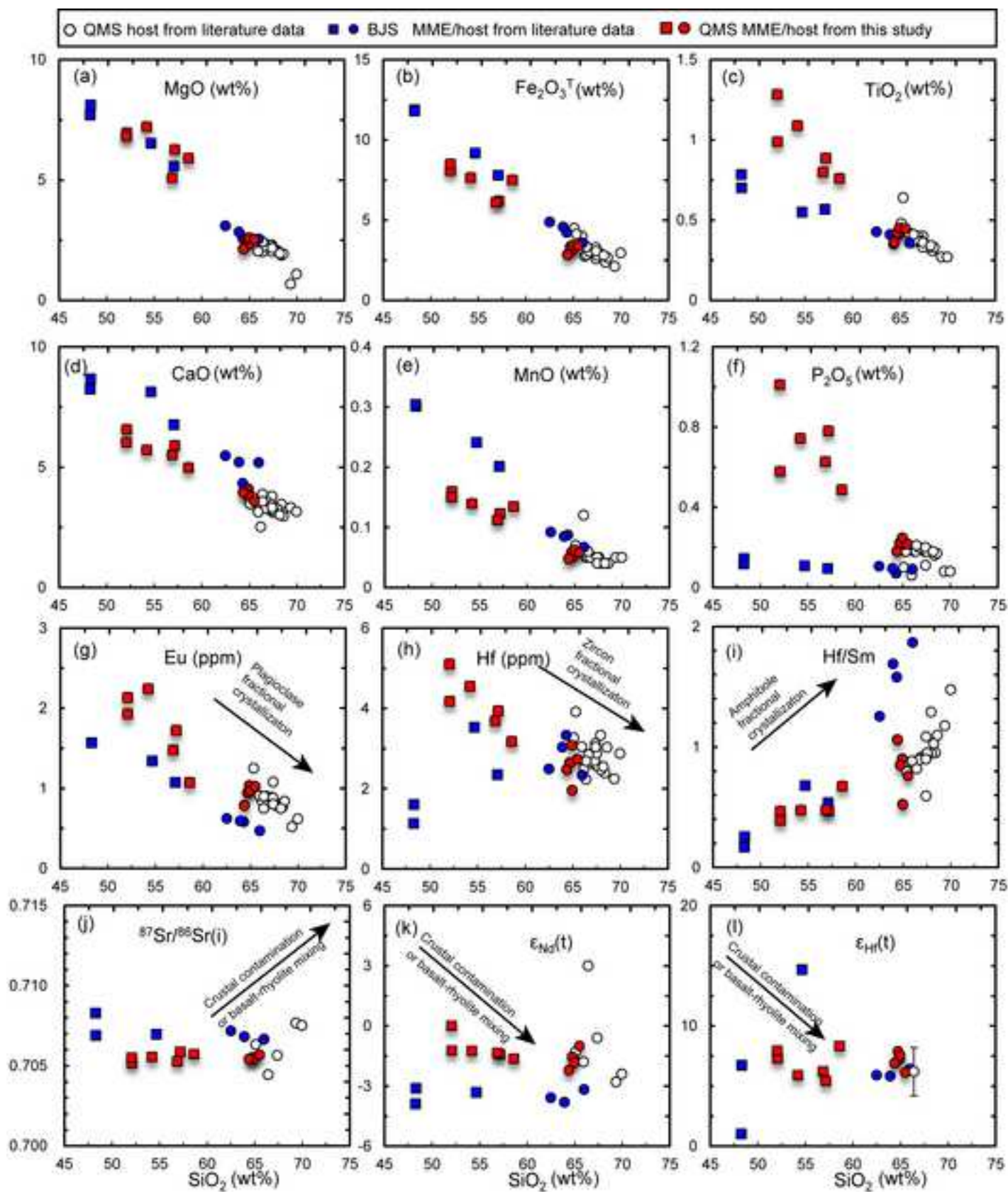


Figure  
[Click here to download high resolution image](#)



Figure

[Click here to download high resolution image](#)

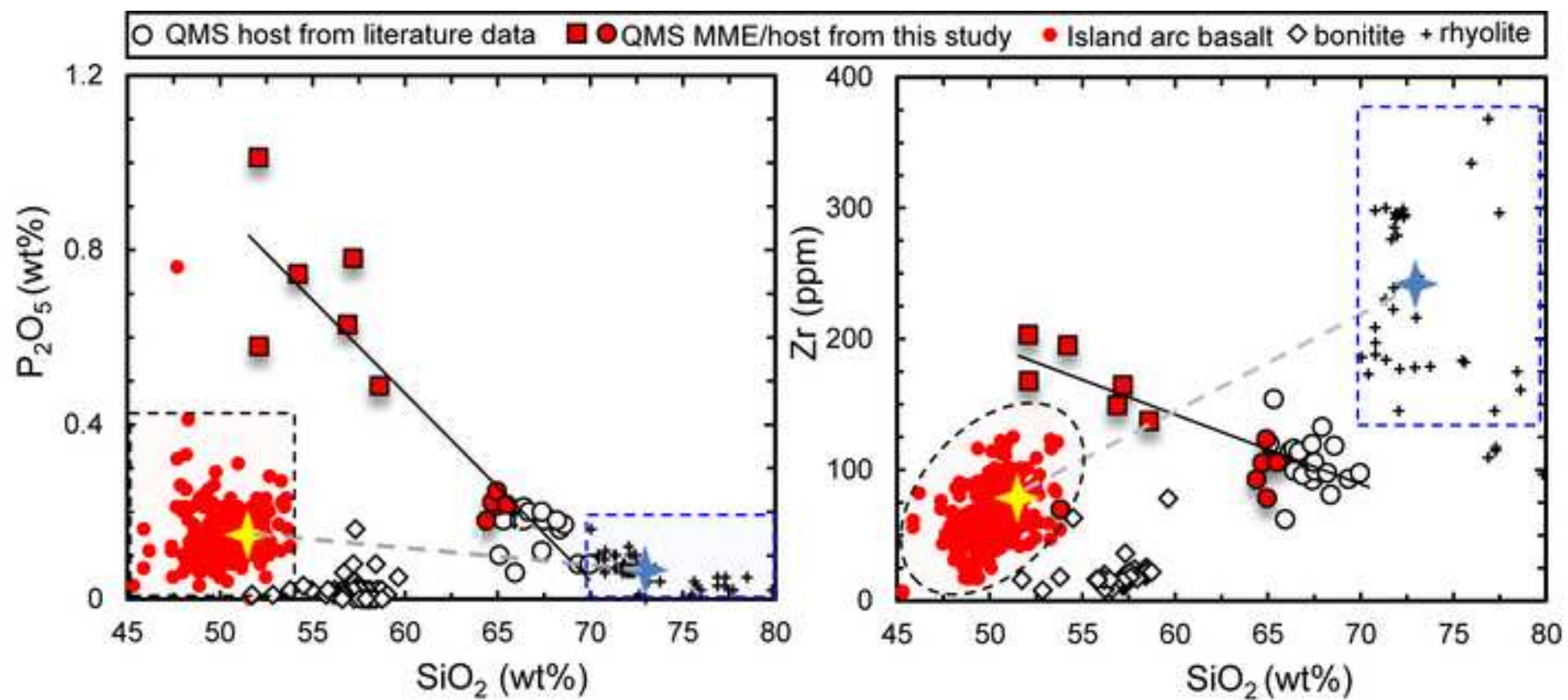
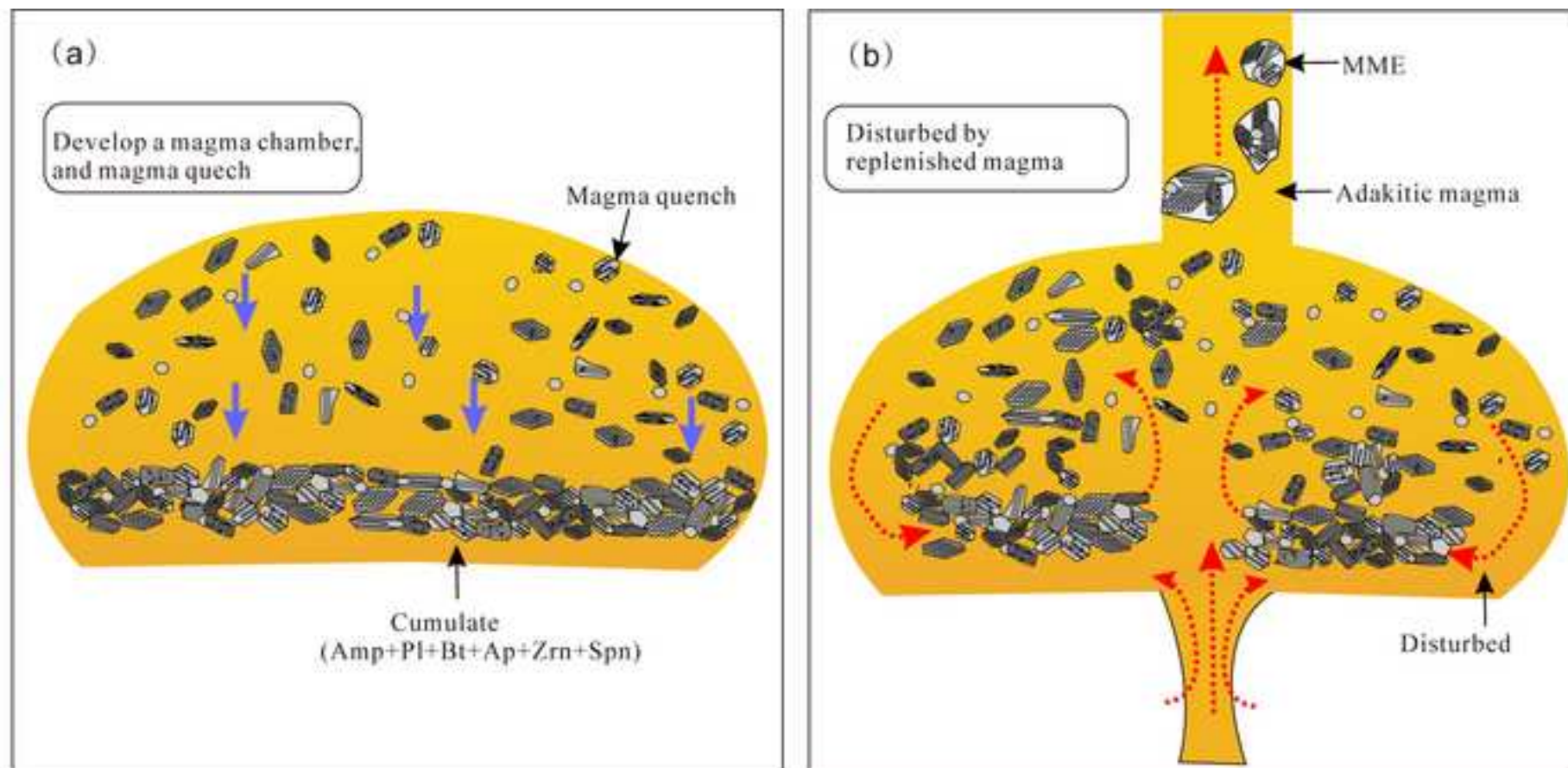


Figure 12

[Click here to download high resolution image](#)



Figure

[Click here to download high resolution image](#)

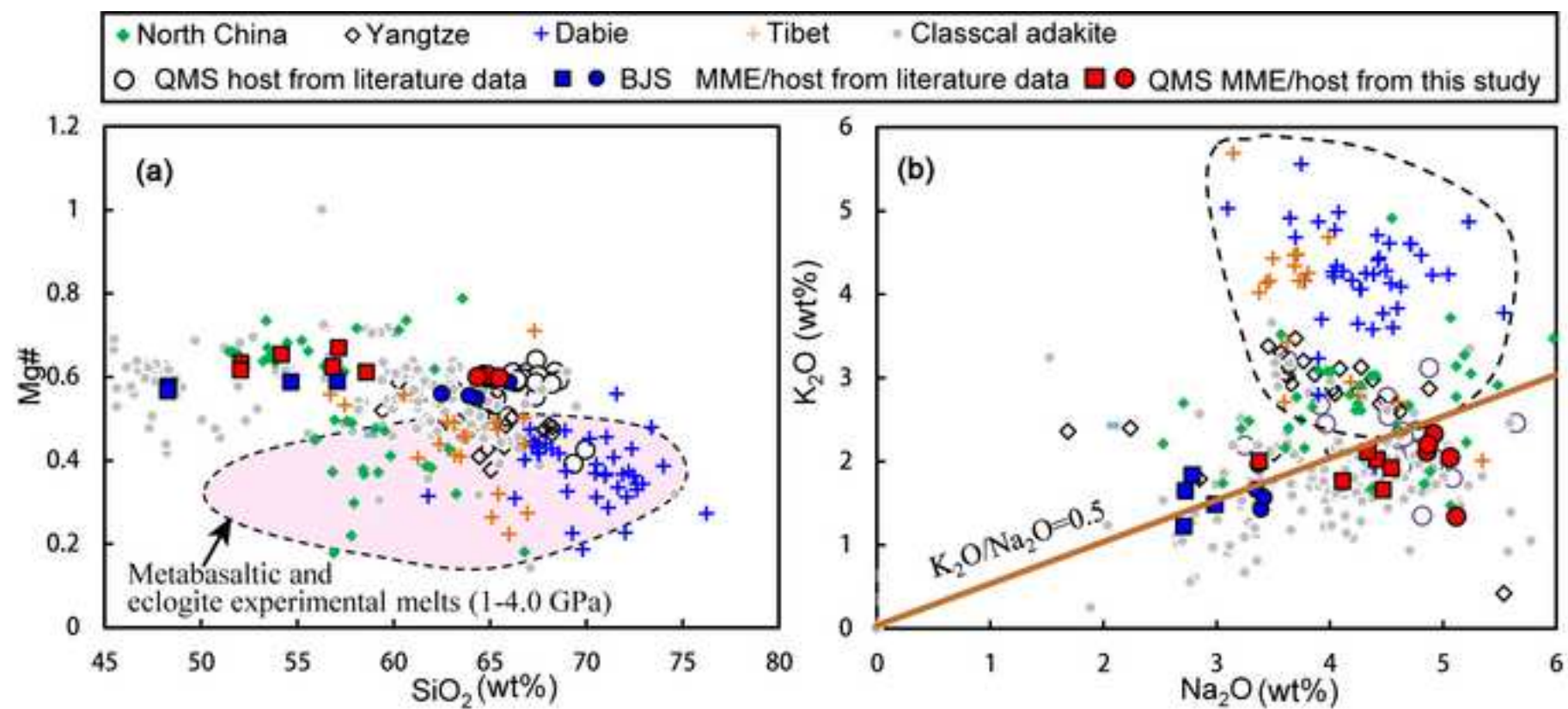


Figure 14

[Click here to download high resolution image](#)

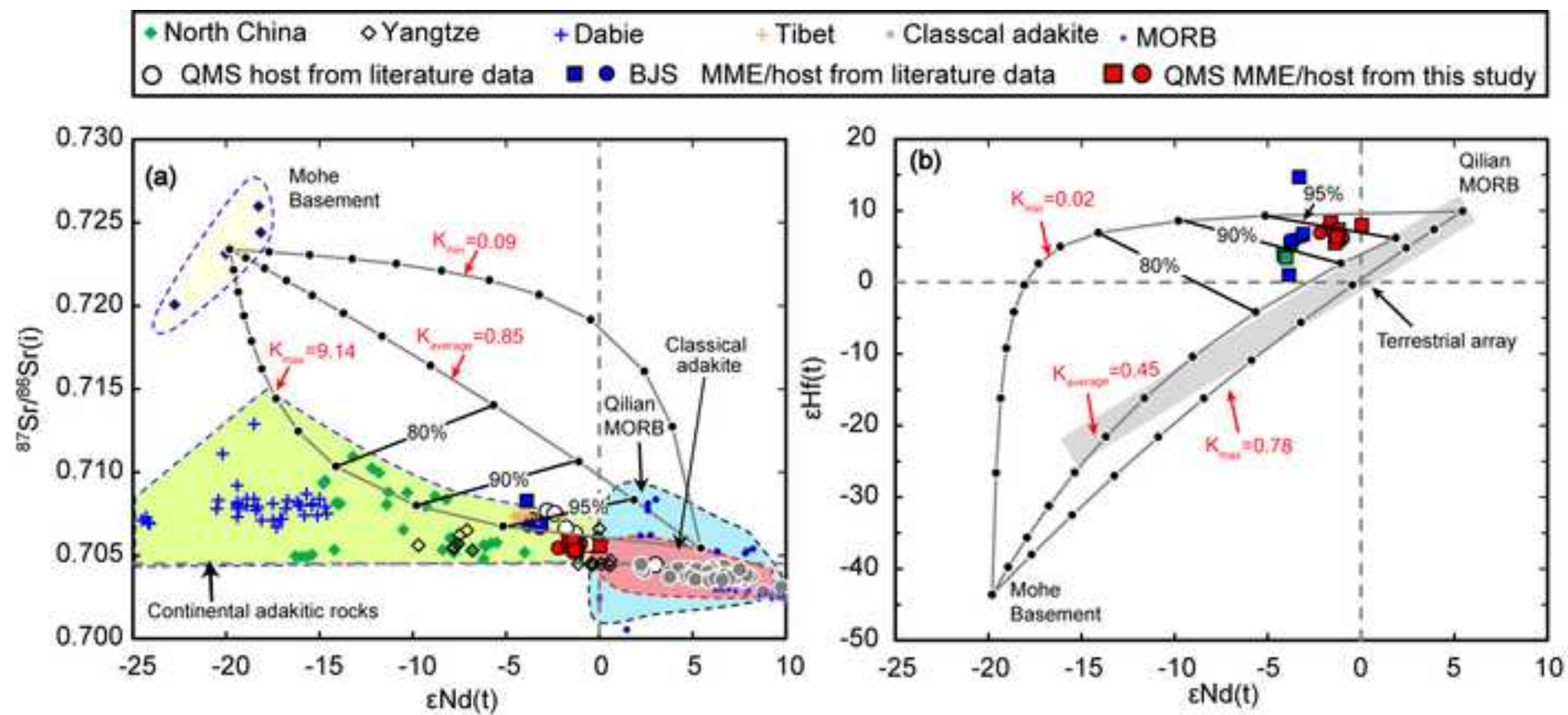
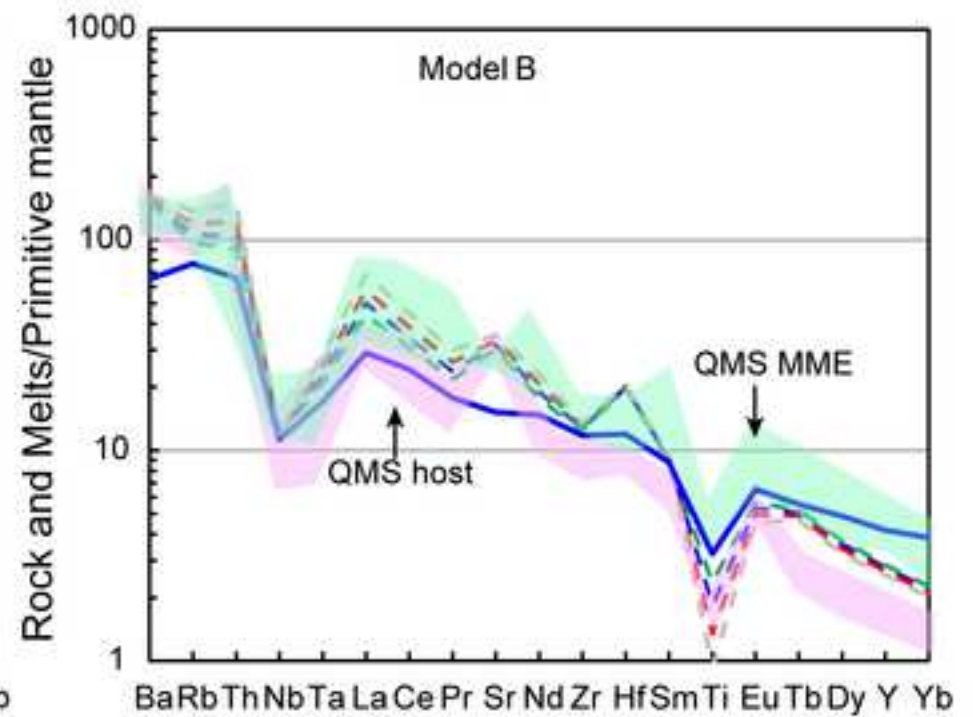
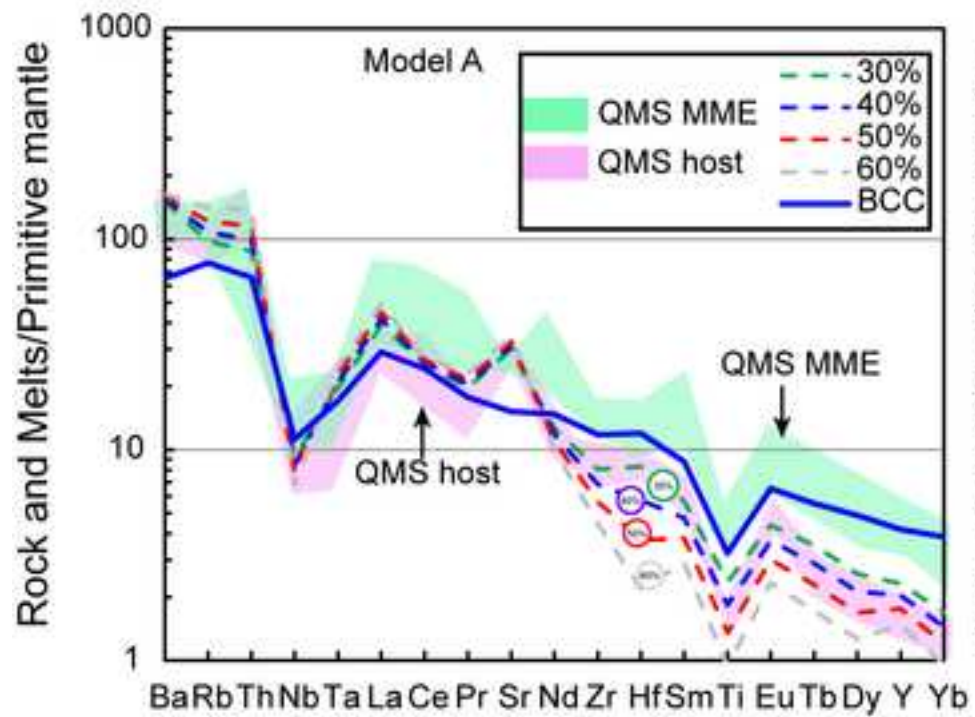


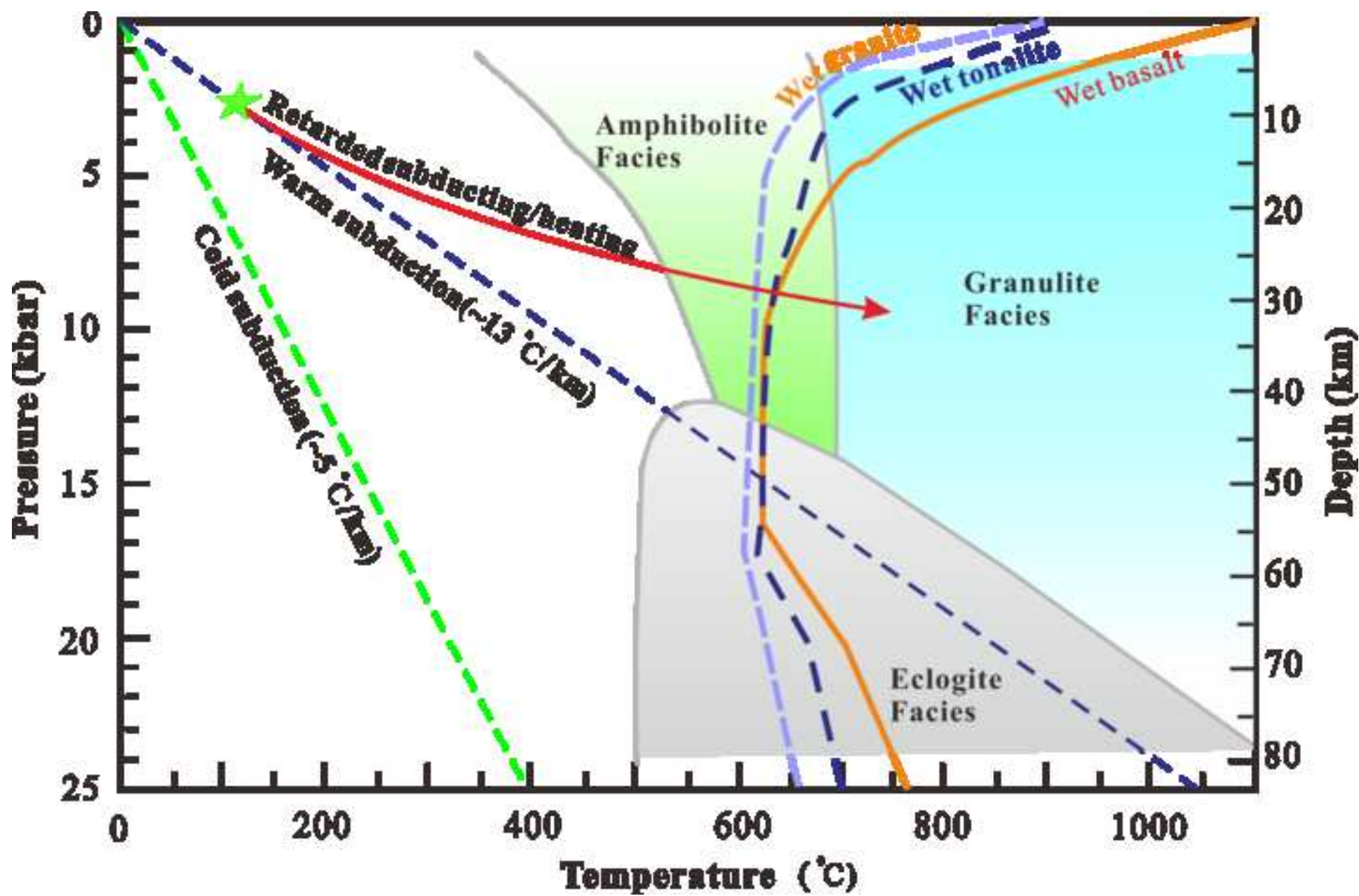


Figure 15

[Click here to download high resolution image](#)



Appendix Fig.S1  
[Click here to download high resolution image](#)



**Appendix tables**

[Click here to download Supplementary Interactive Plot Data \(CSV\): Appendix tables.xlsx](#)